9950 - 760

MODELING OF DIMENSIONAL STABILITY OF FIBER REINFORCED COMPOSITE MATERIALS

H. Thomas Hahn

A. Hosangadi

Final Report

Subcontract JPL-956011

June 1982

Department of Mechanical Engineering

and Materials Research Laboratory

Washington University

St. Louis, MO 63130

This work was performed for the Jet Propulsion Laboratory, California Institute of Technology, sponsored by the National Aeronautics and Space Administration under Contract NAS7-100.

ABSTRACT

A review has been made of various methods of predicting the expansion and diffusion properties of composite laminates. The analytical complexity and the lack of experimental data for short-fiber composites have been pointed out. However, it is concluded that the prediction equations for continuous-fiber composites can be applied to SMC composites as the effective fiber aspect ratio in the latter is large enough.

The effect of hygrothermal expansion on the dimensional stability of composite laminates has been demonstrated through the warping of unsymmetric graphite/epoxy laminates. The warping is very sensitive to the size of the panel, and to the moisture content which is in turn sensitive to the relative humidity in the environment. Thus, any long-term creep test must be carried out in a humidity-controlled environment.

Environmental effects in SMC composites and bulk polyester have been studied under seven different environments: RT/65% RH, RT/98% RH, RT/water, 75°C/65% RH, 75°C/98% RH, 75°C/water, and 100°C/steam. The SMC composites chosen are SMC-R25, SMC-R40 and SMC-R65. The maximum weight gain depends on temperature under high humidity environments while the diffusivity depends on relative humidity. In many environments moisture diffusion is not Fickian probably because of the material damage. The most frequent damage at 75°C is blistering while no visible damage occurs at room temperature. Small blisters are very thin and limited to the surface. When they burst open, the composite

loses a glossy appearance on the surface. These small blisters develop under all environments at 75°C in SMC composites, but they do not form in bulk polyester. Large blisters are much thicker and clearly visible to the naked eye. They develop most frequently at 75°C/water and 100°C/steam. The cracking at 100°C/steam in bulk polyester is much more severe than in the composites perhaps because of the reinforcing effect of fibers.

Although the main objective of this study was to characterize the dimensional stability of SMC composites, it has been found that there is a more urgent need to elucidate the degradation mechanisms under severe environments. A more reliable application of SMC composites hinges on our knowledge of environmental limits of these materials.

TABLE OF CONTENTS

LIST OF TABLES

LIST OF FIGURES

1.0 INTRODUCTION

The dimensional stability of structural materials is an important design consideration where environmental changes are encountered. The environmentally induced deformations lead to a distortion of structures and induce internal stresses. Thus, a comprehensive understanding of expansional characteristics is essential where a high degree of geometrical stability is required and where only low internal stresses can be tolerated.

One of the structures where good dimensional stability is of utmost importance is the solar collector. The efficiency of these collectors depends very much on the precise alignment; any perturbation of the alignment induced by environmental changes will lead to a decrease in efficiency.

Being relatively new as structural material, composites do not have sufficient design data base for expansional properties as compared with other conventional materials. The lack of design data is very serious especially for short fiber composites which are prime candidates for use in the solar collectors.

The objectives of the present work were thus twofold: (1) to develop an analytical model for the prediction of hygrothermal behavior of randomly oriented short fiber composites, and (2) to provide an experimental correlation of the model. The material chosen for study is sheet molding compound (SMC) composite.

Chapter 2 provides a summary of analytical methods for prediction of composite properties from constituent properties. Chapter 3 demonstrates the effect of residual stresses on dimensional stability through a study on warping of unsymmetric cross-ply laminates. The hygrothermal behavior of sheet molding compound (SMC) composites is discussed in Chapter 4.

2.0 ANALYTICAL BACKGROUND

2.1 Thermal Expansion

The typical thermal expansion properties of continuous fiber composites reported in the literature are listed in Table 1. The negative longitudinal coefficients of thermal expansion (CTE) reflect the shrinkage of graphite and Kevlar fibers with increasing temperature. The high anisotropy observed of all the unidirectional composites is responsible for residual stresses in the constituent plies of multidirectional laminates.

For transversely isotropic unidirectional composites with isotropic constituents the coefficients of thermal expansion are given by [1]

$$\alpha_L = \bar{\alpha} + \frac{\alpha_f - \alpha_m}{(1/k_f - 1/k_m)} \left[\frac{(3(1-2\nu_{LT})}{E_L} - \left(\overline{\frac{1}{k}}\right)\right] \quad (1)$$

$$\alpha_T = \bar{\alpha} + \frac{\alpha_f - \alpha_m}{(1/k_f - 1/k_m)} \left[\frac{3}{2K_T} - \frac{3\nu_{LT}(1-2\nu_{LT})}{E_L} - \left(\overline{\frac{1}{k}}\right)\right] \quad (2)$$

where

α = coefficient of thermal expansion

E = Young's modulus

k = bulk modulus

ν = Poisson's ratio

K = plane strain bulk modulus

sub f, m = fiber and matrix, respectively

sub L, T = longitudinal and transverse, respectively

Table 1. Typical thermal expansion coefficients

Composite	α_L μm/m/°K	α_T μm/m/°K
E-Glass/Epoxy	6.6	30.0
S-2 Glass/Epoxy	3.5	28.9
Boron/Epoxy	4.3	22.1
Graphite/Epoxy		
T300/5208	-0.27	24.7
AS/3501-5A	0	26.0
AS/3502	-0.56	21.7
Kevlar 49/Epoxy	-4.0	79.0

The over bar indicates a volume average,

$$\overline{(\ )} = v_f(\ )_f + v_m(\ )_m \tag{3}$$

where v_f and v_m are the volume fraction of fiber and matrix, respectively.

Equations (1) and (2) are valid regardless of fiber length as long as the appropriate composite moduli are used. Thus, the problem is reduced to the determination of the composite moduli E_L, K_T, and ν_{LT}. Various methods of predicting composite moduli are well summarized in [2,3]. A general method is briefly described below.

Consider a two phase composite. The composite stress and strain are related to the constituent stresses and strains respectively by

$$\overline{\sigma} = v_f\overline{\sigma}_f + v_m\overline{\sigma}_m, \qquad \overline{\varepsilon} = v_f\overline{\varepsilon}_f + v_m\overline{\varepsilon}_m \tag{4}$$

Here it is implicitly understood that the stresses $\overline{\sigma}$'s and the strains $\overline{\varepsilon}$'s are second-rank tensors. The appropriate constitutive relations are written as

$$\overline{\sigma} = C\,\overline{\varepsilon}, \qquad \sigma_f = C_f\varepsilon_f, \qquad \sigma_m = C_m\varepsilon_m \tag{5}$$

with the understanding that C's are fourth-rank stiffness tensors. By proper rearrangement of Eqs. (4) and (5) the composite stress can be written as

$$\overline{\sigma} = C_m\overline{\varepsilon} + v_f(C_f - C_m)\overline{\varepsilon}_f \tag{6}$$

Introducing the average strain influence tensor A,

$$\overline{\varepsilon}_f = A\,\overline{\varepsilon}, \tag{7}$$

one can easily show that

$$C = C_m + v_f(C_f - C_m)A \tag{8}$$

Thus, one only has to determine A since everything else on the right-hand side of Eq. (8) is given.

An analytical approach to determine A is to use Eshelby's method [4]. Here the fiber is treated as an ellipsoidal inclusion in an infinite homgeneous medium of stiffness C_m subjected to a uniform strain $\bar{\varepsilon}$ at infinity. The fiber strain ε_f is then obtained from the solution of the following equations:

$$C_f(\bar{\varepsilon}+\varepsilon') = C_m(\bar{\varepsilon}+\varepsilon'-\varepsilon^T), \qquad \varepsilon' = S\,\varepsilon^T, \qquad \varepsilon_f = \bar{\varepsilon}+\varepsilon' \tag{9}$$

Here S is known as Eshelby's tensor, ε^T is the stress-free strain tensor, and ε' represents the disturbance in the strain field resulting from the difference between C and C_f. Once A is obtained from Eqs. (9) and (7), it is substituted into Eq. (8) to determine C [5,6].

The foregoing method has been applied to short fiber composites in [7-10]. As A is obtained by solving the problem of a single fiber embedded in a infinite matrix, the resulting solution is good only for composites of low fiber volume content so that fiber-to-fiber interaction can be neglected. One method of remedying such a drawback is to replace the matrix by a homogeneous medium having the same properties as the composite. However, since the composite properties are not yet known, the final equation must be solved for the composite properties [11].

Although the aforementioned methods are analytically attractive, the results are difficult to use because the equations are complex. Especially in [11], the composite properties can only be determined numerically.

A frequently used semi-analytical method is based on the Halpin-Tsai equations [12]. The pertinent equations are

$$\frac{P}{P_m} = \frac{1+\xi\eta v_f}{1-\eta v_f} \tag{10}$$

$$\nu_{LT} = v_f\nu_f + v_m\nu_m \tag{11}$$

where

$$\eta = \frac{P_f/P_m - 1}{P_f/P_m + \xi} \tag{12}$$

$$\xi_{E_L} = 2\frac{\ell}{d}, \quad \xi_{E_T} = 2, \quad \xi_{G_{LT}} = \frac{1}{3-4\nu_m} \tag{13}$$

The variable P stands for any one of the elastic moduli, G is the shear modulus, and ℓ/d is the fiber aspect ratio.

Reference [11] gives a comparison between the results of a more exact analysis and those from the Halpin-Tsai equations for the longitudinal modulus E_L of E-glass/epoxy composite. It is concluded that a fiber aspect ratio of 100 is high enough for the corresponding short fiber composite to be treated as a continuous fiber composite. For glass fibers the nominal diameter is 13 μm. Therefore, the required minimum length is is the order of 1 mm. Since the current SMC composites are made with fibers 25 mm long, the equations for continuous fiber

composites are expected to be applicable even after allowing for the curved arrangement of fibers.

For continuous fiber composites the longitudinal strain does not change much from fiber to matrix. In this case, therefore, one can use the equations derived by Levin [13],

$$\alpha_L = \frac{\overline{E\alpha}}{E_L} - \frac{\overline{\alpha(1+\nu)}}{\nu_m - \nu_f}\left(\frac{\bar{E}}{E_L} - 1\right) \tag{14}$$

$$\alpha_T = \bar{\alpha} + \overline{\alpha\nu} - \alpha_L\bar{\nu} - (\bar{\nu}-\nu_{LT})\left[\alpha_m - \alpha_L + (\alpha_m-\alpha_f)\frac{1+\nu_f}{\nu_m-\nu_f}\right] \tag{15}$$

Here Eq. (15) was obtained by rearranging the original solution in [13]. Next, the composite moduli are given by [2,3,14,15]

$$E_L = \bar{E} + 4\left(\frac{\nu_f-\nu_m}{1/k_f-1/k_m}\right)^2\left[\left(\overline{\frac{1}{k}}\right) - \frac{1}{K_T}\right] \tag{16}$$

$$\nu_{LT} = \bar{\nu} + \frac{\nu_f-\nu_m}{1/k_f-1/k_m}\left[\left(\overline{\frac{1}{k}}\right) - \frac{1}{K_T}\right] \tag{17}$$

where

$$\frac{1}{K_T} = \frac{1}{\nu_f+\zeta\nu_m}\left(\frac{\nu_f}{K_f} + \frac{\zeta\nu_m}{K_m}\right) \tag{18}$$

$$\zeta = \frac{1 + (1-2\nu_m)K_m/K_f}{2(1-\nu_m)} \tag{19}$$

For most composites the second terms in Eqs. (16) and (17) are much smaller than the first terms. Therefore, the following approximate equations can be used for continuous fiber composites [16]:

$$\alpha_L = \frac{\overline{E\alpha}}{\bar{E}} \tag{20}$$

$$\alpha_T = \bar{\alpha} + \overline{\alpha\nu} - \alpha_L\bar{\nu} \tag{21}$$

Once the unidirectional properties are determined, the laminate properties can be predicted using the laminated plate theory [17]. In particular, when the fiber orientation is random in the laminate plane, the in-plane thermal expansion coefficient becomes [18,19]

$$\alpha_I = \frac{\alpha_L + (\alpha_L+\alpha_T)\nu_{LT}\,E_T/E_L + \alpha_T E_T/E_L}{1 + (1+2\nu_{LT})E_T/E_L} \tag{22}$$

whereas the thermal expansion coefficient in the thickness direction is given by [20,21]

$$\alpha_o = \alpha_T + \frac{(\alpha_T-\alpha_L)(\nu_{TT}-\nu_{LT}E_T/E_L)}{1 + (1+2\nu_{LT})E_T/E_L} \tag{23}$$

With α_L and α_T known from Eqs. (20) and (21), the in-plane and out-of-plane CTE of SMC panels can be calculated from Eqs. (22) and (23), respectively.

2.2 Swelling

Swelling of composite laminates can be predicted following the same procedure as for thermal expansion. For this purpose the swelling coefficient β is defined as

$$\beta = \frac{\varepsilon}{c} \tag{24}$$

where ε is the strain resulting from the moisture concentration c defined by

$$c = \lim_{\Delta V \to 0} \frac{\text{mass of moisture in } \Delta V}{\text{dry mass of } \Delta V} \tag{25}$$

Since both ϵ and c are dimensionless, so is β.

Unlike temperature, moisture concentration can vary from fiber to matrix even in an equilibrium state. Therefore, the moisture concentration in a composite is given by [17]

$$c = (c_m v_m s_m + c_f v_f s_f + v_v)/s \tag{26}$$

where s is the specific gravity and v_v is the void content.

For glass fibers we have $c_f = 0$. The resulting equations for swelling coefficients are (cf. Eqs. (20) and (21))

$$\beta_L = \frac{E_m s}{\bar{E} s_m} \beta_m \tag{27}$$

$$\beta_T = [(1+\nu_m) - \frac{E_m}{\bar{E}} \bar{\nu}] \frac{s}{s_m} \beta_m \tag{28}$$

where we have assumed no void content, $v_v = 0$. Note that the specific gravity of the composite is related to the specific gravities of the constituents by

$$s = v_f s_f + v_m s_m \tag{29}$$

The in-plane and out-of-plane swelling coefficients are now obtained by substituting β_L and β_T for α_L and α_T, respectively, in Eqs. (22) and (23).

In some composites and polymers swelling is negligible until a threshold moisture concentration is reached [22-24]. The existence of such threshold moisture concentration can lead to an almost bilinear relation between swelling and average moisture concentration in absorption tests [21]. For graphite/epoxy composites, the threshold moisture concentration is about 0.4%, whereas it is in the order of 1.5% for some epoxies [21,24]. In particular, Adamson [24] related the threshold moisture concentration to the free volume of epoxy. It remains to be seen whether or not a threshold moisture concentration exists in SMC composites.

2.3 Diffusion

The thermal conductivities of transversely isotropic composites are found in [2]:

$$k_L = v_f k_f + v_m k_m \tag{30}$$

$$k_T = k_m\left[1 + \frac{v_f}{k_m/(k_f-k_m) + (1-v_f)/2}\right] \tag{31}$$

On the other hand, based on a square arrangement Springer and Tsai [25] derived the following approximate equation for the thermal conductivity k_T:

$$k_T = (1-2(v_f/\pi)^{1/2})k_m + \frac{k_m}{B}\left[\pi - \frac{4}{(1-B^2 v_f/\pi)^{1/2}} \cdot \right.$$

$$\left. \tan^{-1}\frac{(1-B^2 v_f/\pi)^{1/2}}{1 + B(v_f/\pi)^{1/2}}\right], \qquad B = 2\left[\frac{k_m}{k_f} - 1\right] \tag{32}$$

The thermal conductivities of short-fiber composites have been predicted by Nomura and Chou [26]; however, no closed form solutions are available.

The moisture diffusivities can be analyzed similarly. Replacing the k's in Eqs. (30) and (31) or (32) by the diffusivities D's and noting that $D_f = 0$, we obtain

$$D_L = (1-v_f)D_m \tag{33}$$

$$D_T = \frac{1-v_f}{1+v_f} D_m \tag{34}$$

or

$$D_T = (1 - 2\sqrt{v_f/\pi})D_m \tag{35}$$

To a first order approximation the diffusion of moisture can be described by the Fick's equation [27]

$$\frac{\partial c}{\partial t} = D_{ij} \frac{\partial^2 c}{\partial x_i \partial x_j} \tag{36}$$

with D_{ij} independent of c.

For a thin, large plate immersed in an environment, diffusion can be assumed to be only one-dimensional through the thickness. Thus, for an SMC panel with fibers lying in the plane of the panel, Eq. (36) reduces to

$$\frac{\partial c}{\partial t} = D \frac{\partial^2 c}{\partial x^2} \tag{37}$$

where x is the thickness coordinate, and D is the transverse diffusivity.

The diffusivity D depends very much on temperature. The temperature dependence is conveniently expressed by an Arrhenius type of equation,

$$D = D_o \exp(-\frac{E_d}{RT}) \tag{38}$$

where E_d is the activation energy for diffusion [27].

The solution of Eq. (37) for a plate of thickness h is

$$\frac{c-c_o}{c_\infty-c_o} = 1 - \frac{4}{\pi} \sum_{j=0}^{\infty} \frac{1}{(2j+1)} \sin \frac{(2j+1)\, x}{h} \exp[\frac{-(2j+1)^2\pi^2 Dt}{h^2}] \tag{39}$$

where c_o and c_∞ are the initial and final uniform moisture concentrations, respectively. The average moisture concentration $\bar{c}$ throughout the volume, also called the moisture content, is given by

$$\frac{\bar{c}-c_o}{c_\infty-c_o} = 1 - \frac{8}{\pi^2} \sum_{j=0}^{\infty} \frac{1}{(2j+1)^2} \exp\ [- \frac{(2j+1)^2\pi^2 Dt}{h^2}] \tag{40}$$

If the lateral dimensions of the plate are not large enough compared with thickness, the diffusivity D in Eq. (40) may be taken as an effective diffusivity. For a rectangular SMC plate of width W and length L, D is related to D_L and D_T by (cf. [27])

$$D = D_T[1 + (\frac{h}{W} + \frac{h}{L}) \sqrt{\frac{D_I}{D_T}}\ ]^{1/2} \tag{41}$$

where D_I is the in-plane diffusivity,

$$D_I = \frac{1}{2}(D_L+D_T) \tag{42}$$

Equation (42) follows from the laminated plate theory and the assumption

of random in-plane arrangement of fibers in SMC.

The equilibrium moisture concentration depends mainly on the relative humidity (RH) through a power law [28]

$$c_\infty = a\left(\frac{RH}{100}\right)^b \tag{43}$$

where RH is in percent. For graphite/epoxy composites, a ranges between 0.015 and 0.020 and b is close to or greater than unity.

The actual diffusion may deviate from the ideal Fickian behavior. Many reasons for such deviation are discussed in [28,29].

The diffusivity may depend on moisture concentration [30] while the equilibrium moisture content changes with temperature [24,31]. Upon long-term exposure additional weight may be gained or lost. It is generally believed that the additional weight gain is associated with microcracking of the matrix and interface [32] while the weight loss is the result of leaching out of low-molecular weight materials [33]. In SMC composites the extraneous weight loss can be quite extensive at elevated temperatures [27].

Other factors affecting moisture diffusion are the applied stress and thermal cycling [34,35]. A tensile stress leads to an increase in the diffusion coefficient and moisture concentration. In fact, the same effect is observed in bulk polymers. Accelerated moisture diffu-

sion to a higher concentration can be caused by rapid thermal cycling to a temperature near the glass transition temperature.

Absorbed water plasticizes the matrix resin and lowers the glass transition temperature [22,36]. Severe damage is known to result from a combination of high moisture concentration and rapid thermal cycling above the glass transition temperature.

3.0 EFFECT OF HYGROTHERMAL EXPANSION ON DIMENSIONAL STABILITY: A DEMONSTRATION

3.1 Introduction

Although our main objective is to characterize the dimensional stability of SMC composites, the lack of control over the fiber arrangement in these composites makes it rather difficult to understand the basic mechanisms responsible for dimensional stability. Therefore, it is more instructive to demonstrate the presence of residual stresses and the effects these residual stresses have on dimensional stability and possible damage, using continuous-fiber composite laminates.

The inherent anisotropy in the expansional properties of unidirectional composites gives rise to residual stresses in multidirectional laminates. Immediately after fabrication, laminates are subjected to curing stresses because of the thermal expansion mismatch between plies with different fiber orientations. As the laminates are left in moist environment, they absorb moisture and swell. The swelling strains can annihilate the curing strains with the net result of reduced residual stresses.

The warping of unsymmetric laminates has been frequently used as a means of studying the dimensional stability of composite laminates [21,37-40]. The classical laminated plate theory is known to describe the warping of small panels fairly well [38]. However, large panels require the use of large-deflection plate theory [41].

Residual stresses naturally affect the first ply-failure stress, i. e., the stress at which the weakest plies fail [42]. Such effect manifests itself in the acoustic emission characteristic of laminates at room temperature after preloading. If the preloading is done at an elevated temperature, the corresponding Kaiser effect is not so conspicuous, indicating less damage caused by the preloading [43]. Residual stresses also exist in the form of interlaminar stresses [44] which may affect delamination.

In this chapter we present some experimental results on the warping of unsymmetric graphite/epoxy laminates, with a view toward a better understanding of the change of residual stresses resulting from long-term environmental exposure. The effect of residual stresses on ply failure is studied for a symmetric Kevlar 49/epoxy laminate.

3.2 Materials and Experimental Procedure

To study the size effect on the warping, a square $[0_4/90_4]_T$ panel was cured from T300/5208 graphite/epoxy prepregs following the manufacturer's suggested cure cycle. The nominal dimensions of this panel were 270 mm x 270 mm with a thickness of 1 mm. Shortly after fabrication, maximum deflections along the edges were measured using a cathetometer. The panel was then cut into four smaller pieces of equal size and again measurements were taken of the maximum edge deflections. The same procedure was repeated twice more until the

smallest panels had sides only one-eighth as long as those of the original panel. The nominal dimensions and numbering of all these panels are shown in Fig. 1.

Panels 1 and 4 were postcured at 177°C for 1 h, and panels 2 and 5 for 7 1/2 h. The resulting changes in weight and edge deflections were measured within a few days after fabrication.

For the study of the long-term exposure effect, eight 100 mm x 100 mm panels of $[0_4/90_4]_T$ stacking sequence were cured from T300/C69 prepregs. Three different cure cycles were employed. Cure cycle 1 was the standard cure, as shown in Fig. 2(a), and was used for panels 1-1, -2 and 3-1, -2. Cure cycle 2, Fig. 2(b), had slower cool down rate (1 C/min.) while cure cycle 3, Fig. 2(c), was distinguished by longer dwell time (2 h) at the initial cure temperature. Cure cycles 2 and 3 were used for panels 2-1, -2 and 4-1, -2, respectively.

Half of the panels were stored in a vacuum oven at 75°C while the other half were left in the laboratory environment. The maximum deflections at the center of the panels were measured periodically at room temperature. Concurrently measured were the weight changes.

The effect of residual stresses on ply failure was investigated using a $[0/90]_{2s}$ Kevlar 49/epoxy laminate. Specimens were 25 mm x 25 mm squares with a nominal thickness of 2 mm. These specimens were kept

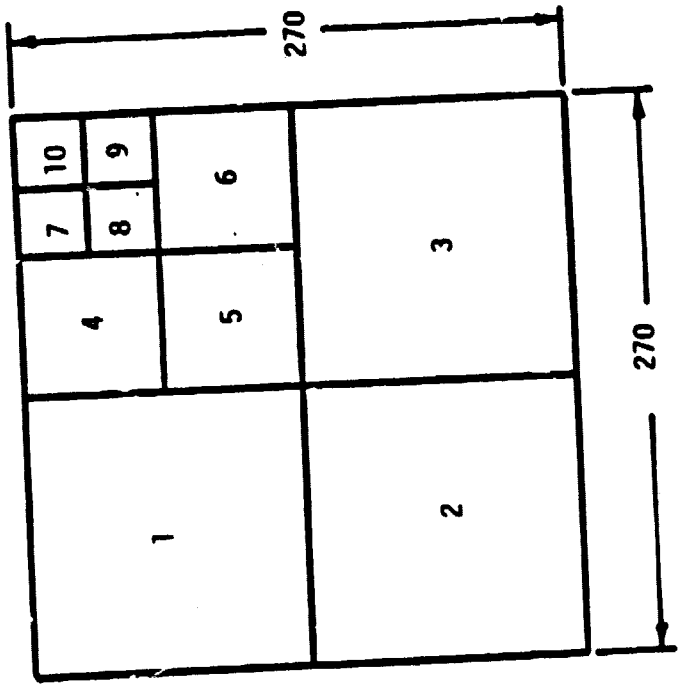

Fig. 1. Plate dimensions in mm, T300/5208

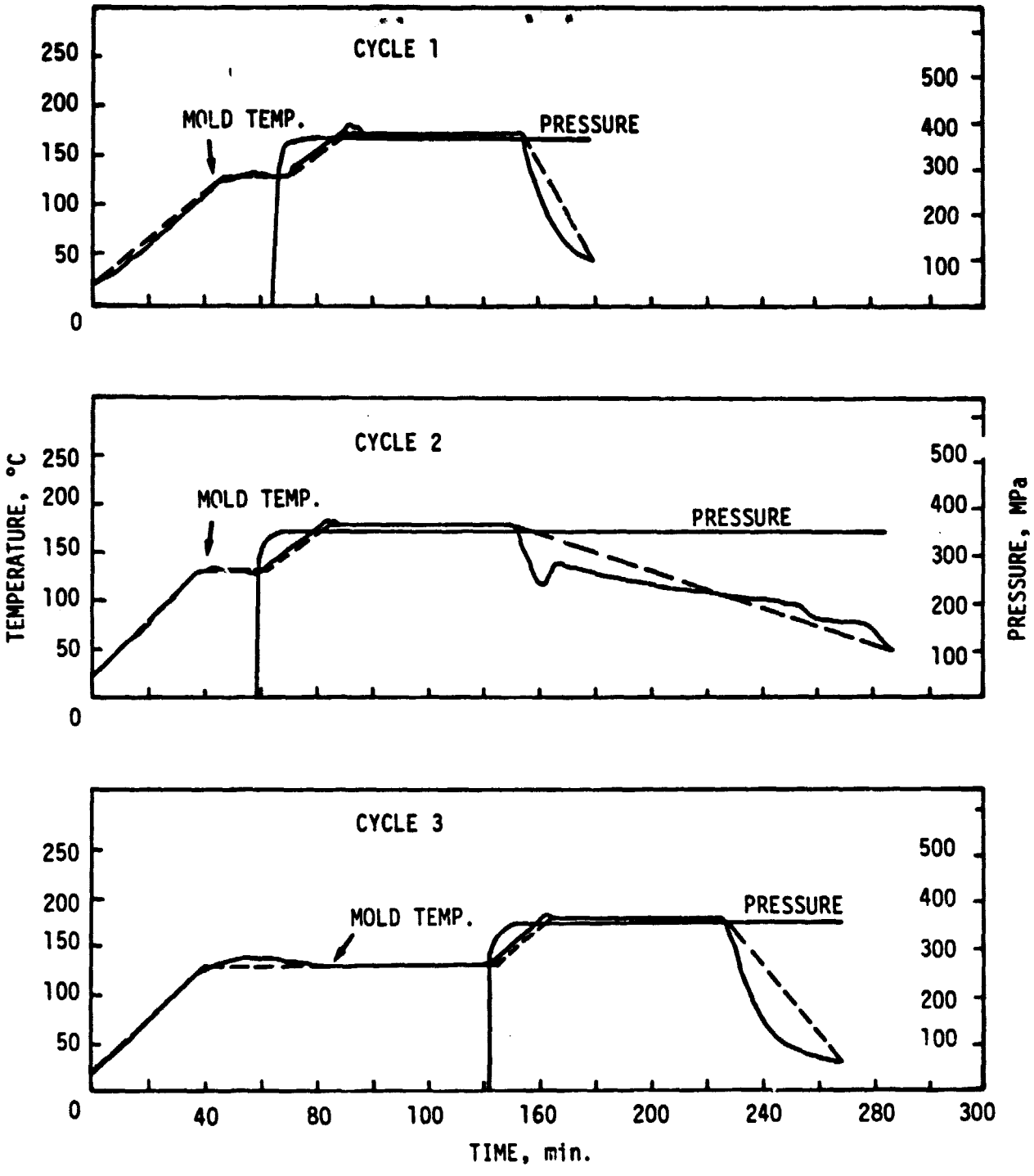

Fig. 2. Cure cycles for T300/C69

in a vacuum oven at 75°C. Periodic measurements of weight and of the number of cracks in the surface plies were taken at room temperature. A red dye penetrant was sprayed on the specimen surfaces to enhance the detectability. Weight measurements were taken on duplicate specimens to avoid the extraneous weight of the dye.

3.3 Results and Discussion

3.3.1 Surface Adsorption

Since weight was measured in the room environment, it increased during measurement as the specimen absorbed moisture. Figure 3 shows the weight gain during the first 30 minutes immediately after the specimen is taken out of the oven. Since the weight gain stabilizes much more quickly than predicted by the Fickian diffusion equation, it is the result of moisture adsorbed on the surfaces. The surface moisture concentration reached in about 30 minutes is 4×10^{-7} g/mm^2.

Figure 3 also indicates the possible range of error in weight change because it took 20-25 minutes to finish all the measurements.

3.3.2 Size Effect

Figure 4 shows the curvature calculated from the deflection measurements along the edges based on the assumption of circular

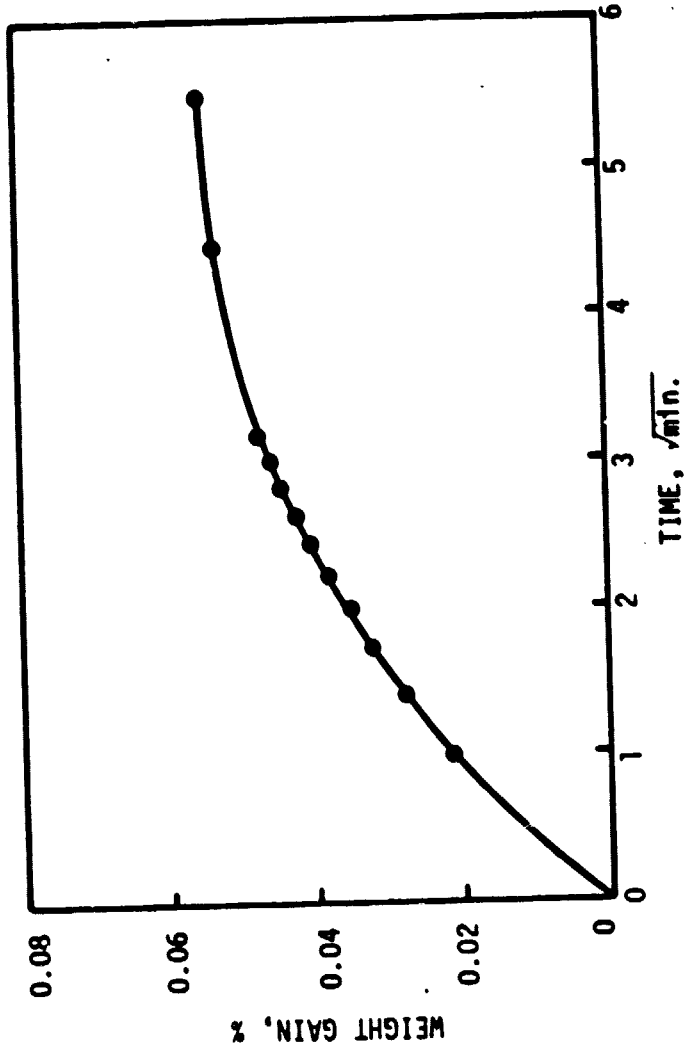

Fig. 3. Initial weight gain during measurement

deflection. For each pair of opposite edges an average curvature was calculated. Therefore, each panel had two curvatures, one positive and the other negative. Figure 4 shows only the magnitude of these average curvatures.

For the smallest plates the two curvatures are almost equal to each other and the warping is anticlastic. The next smallest plates are not saddle-shaped; one curvature is larger than the other. In Fig. 4 the larger curvatures are indicated by circles, and the smaller curvatures by triangles.

For the largest and next largest panels the smaller curvatures are almost zero; thus the warping is no longer anticlastic but cylindrical. Furthermore, the cylindrical warping is not stable because the curvatures can be interchanged by snapping back the plates. As the panel becomes larger, the smaller curvature decreases monotonically; however, the larger curvature reaches a minimum and then increases to a limiting value independent of the panel size.

The edges with zero curvature are not straight throughout their length. They are curved slightly over a length of 40 mm near each corner; the deflection at each corner is about 1.6 mm.

According to the classical laminated plate theory, the curvature for anticlastic deformation of $[0_4/90_4]_T$ panels is given by [17]

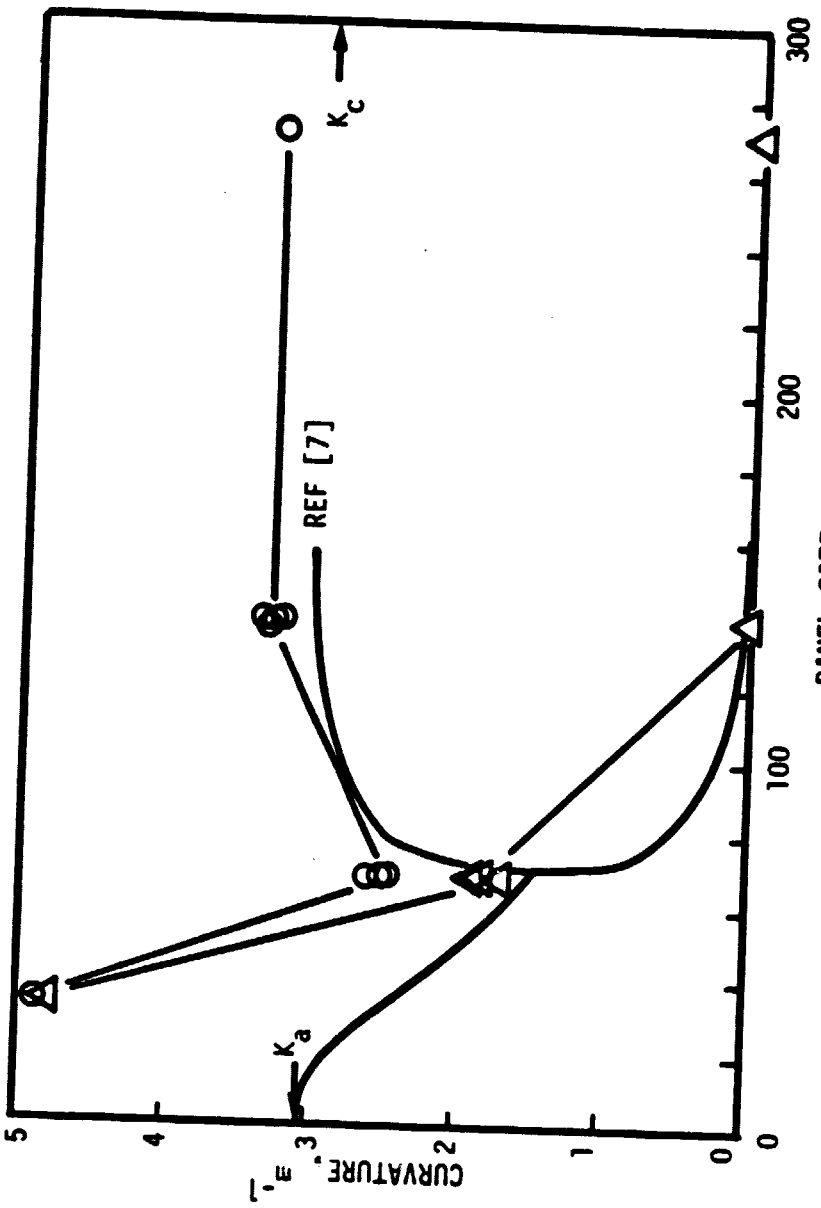

Fig. 4. Change of curvature with panel size, T300/5208

$$k_a = \frac{24}{h} K_a (e_L - e_T) \tag{44}$$

where

$$K_a = \frac{(1-\nu^2 E)E}{1 + 14E + (1-16\nu^2)E^2} \tag{45}$$

Here E and ν are the transverse-to-longitudinal modulus ratio and the major Poisson's ratio, respectively, of unidirectional plies. The e's are nonmechanical strains and h is the thickness of the panel. Note that unidirectional composite properties only are used in Eqs. (44) and (45).

The curvature for cylindrical deformation is obtained by setting one of the curvatures to be zero. The result is

$$k_c = \frac{24}{h} K_c (e_L - e_T) \tag{46}$$

where

$$K_c = \frac{[1 + (1-2\nu-\nu^2)E + (-\nu^2+2\nu^3)E^2]E}{1 + 15E + (15-16\nu^2)E^2 + (1-16\nu^2)E^3} \tag{47}$$

The curvatures k_a and k_c are calculated from the following material properties for T300/5208:

$E = 0.0569$, $\nu = 0.28$

$e_L = +16.4$ μm/m , $e_T = -3994$ μm/m

$h = 1$ mm

Note that e_L and e_T are the resulting thermal strains as the plate is cooled from the cure temperature of 177°C down to a room temperature of 21°C. The results for k_a and k_c are indicated by arrows in Fig. 4 at panel sizes equal to 0 and 300 mm, respectively.

Recently, Hyer [41] showed that the unstable warping of large panels can be explained by a large-deflection plate theory. In particular, the in-plane strains are given by

$$\varepsilon_x^o = \frac{\partial u}{\partial x} + \frac{1}{2}\left(\frac{\partial w}{\partial x}\right)^2$$

$$\varepsilon_y^o = \frac{\partial v}{\partial y} + \frac{1}{2}\left(\frac{\partial w}{\partial y}\right)^2 \qquad (48)$$

$$\varepsilon_{xy}^o = \frac{1}{2}\left(\frac{\partial u}{\partial y} + \frac{\partial v}{\partial x} + \frac{\partial w}{\partial x}\frac{\partial w}{\partial y}\right)$$

where u, v, and w are the displacements in the x, y, and z directions, respectively. Note that the x and y axes are in the plane of the laminate.

The displacements are assumed to be

$$u = cx - \frac{a^2x^3}{6} - \frac{abxy^2}{4}$$

$$v = dy - \frac{b^2y^3}{6} - \frac{abx^2y}{4} \qquad (49)$$

$$w = \frac{1}{2}(ax^2 + by^2)$$

The variational principle is then used to determine the unknown constants a through d. The results of Ref. [41] are shown in Fig. 4.

For small panels the results of Ref. [41] reduce to Eq. 44 whereas Eq. 46 provides a good approximation for large panels. The assumption used for the derivation to Eq. 46 leads to a nonzero moment along a pair of curved edges. Thus this equation should be used sufficiently away from the edges. It is not clear whether or not Eq. 46 is an asymptote

to the results of Ref. [41] for large panels.

The experimental results are greater than the analytically predicted especially for the smallest panels. It is possible that the deformation of these small panels is affected by the boundary regions. Also, the material properties used yield smaller curvatures than do those in Ref. [39].

As is clear by now, of utmost importance in the elastic analysis of residual stresses is the stress-free temperature. Usually the cure temperature is used as the stress-free temperature which is 177°C for the present graphite/epoxy. Within the framework of elastic behavior, the stress-free temperature can be determined by heating up a warped laminate and recording the temperature at which the laminate becomes flat. Figure 5 shows results from such tests where two panels of different sizes were used. Edge deflections are shown on the ordinate. Both laminates become flat somewhere between 180 and 190°C. However, an extrapolation of the data between 60 and 150°C indicates a stress-free temperature of 180°C. Therefore, the cure temperature of 177°C is believed to be a good candidate for the stress-free temperature for the T300/5208 composite. It should be noted that chemical shrinkage may increase the stress-free temperature above the cure temperature.

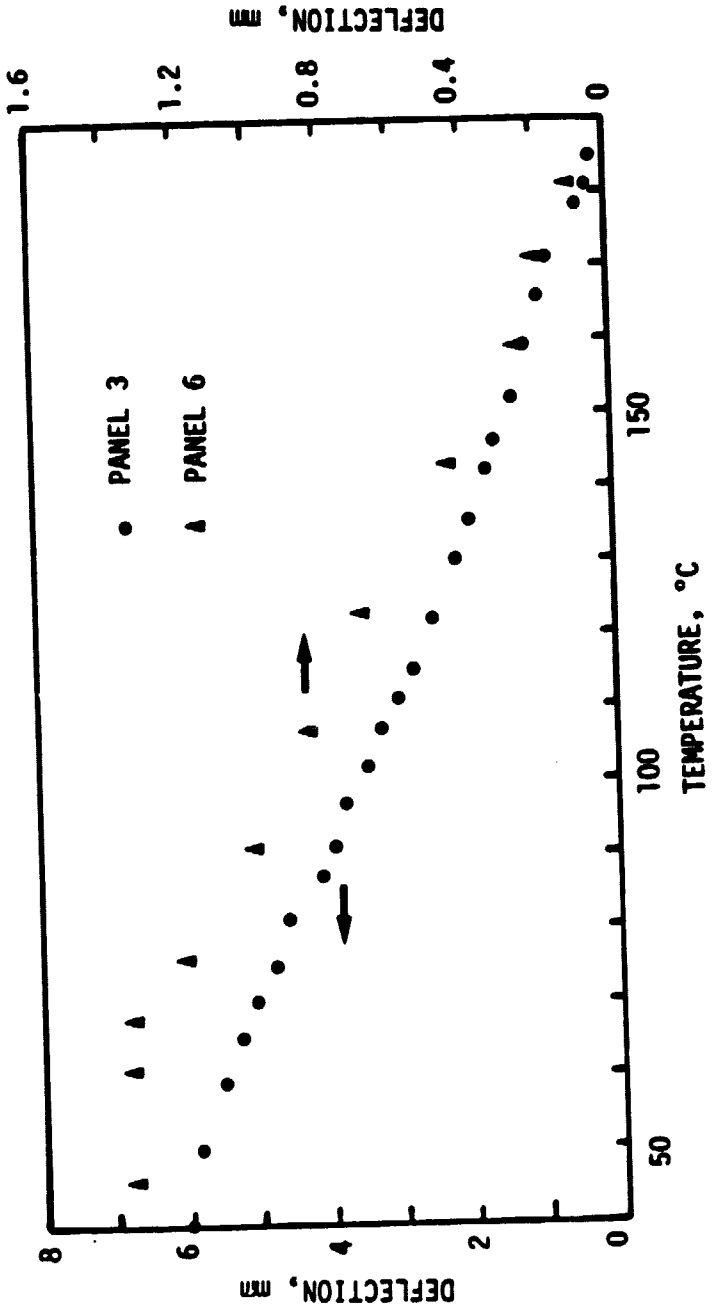

Fig. 5. Experimental determination of stress-free temperature

3.3.3 Effect of Postcure

The changes in curvature and weight after postcure are shown in Figs. 6 and 7. The larger panels, panels 1 and 2, reverse their curvatures both after 1-h postcure and after 7.5-h postcure. That is, the non-zero curvatures become zero, and vice versa, after postcure. The arrows indicate directions of change.

As for the smaller panels, the larger curvatures decrease or do not change much, Figs. 6 and 7. However, the smaller curvatures increase after postcure. As expected, more weight loss is observed in the 7.5-h postcure than in the 1-h postcure.

The reversal of curvatures in the larger panels indicates that the warping of these panels is unstable and that these panels become flat at the cure temperature. The weight loss and the increase in the maximum curvatures are believed to be caused by the moisture desorption during postcure.

3.3.4 Effect of Long-Term Exposure

The center deflections and weight losses of the panels stored in a vacuum oven at 75°C are shown in Fig. 8. Panels 1 ~ 3 are seen to lose about 0.54% of their initial weight while panel 4 loses only ~0.1%. The weight losses result from the desorption of the moisture that was

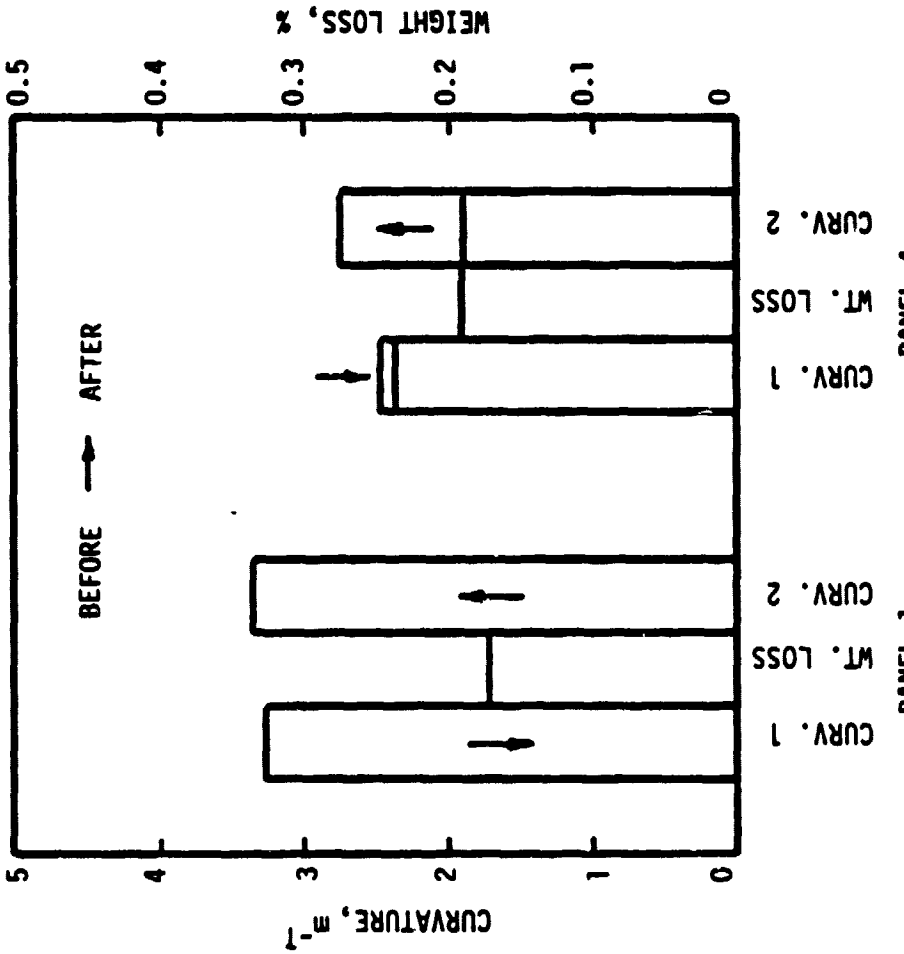

Fig. 6. Changes in curvature and weight after 1-h postcure, T300/5208

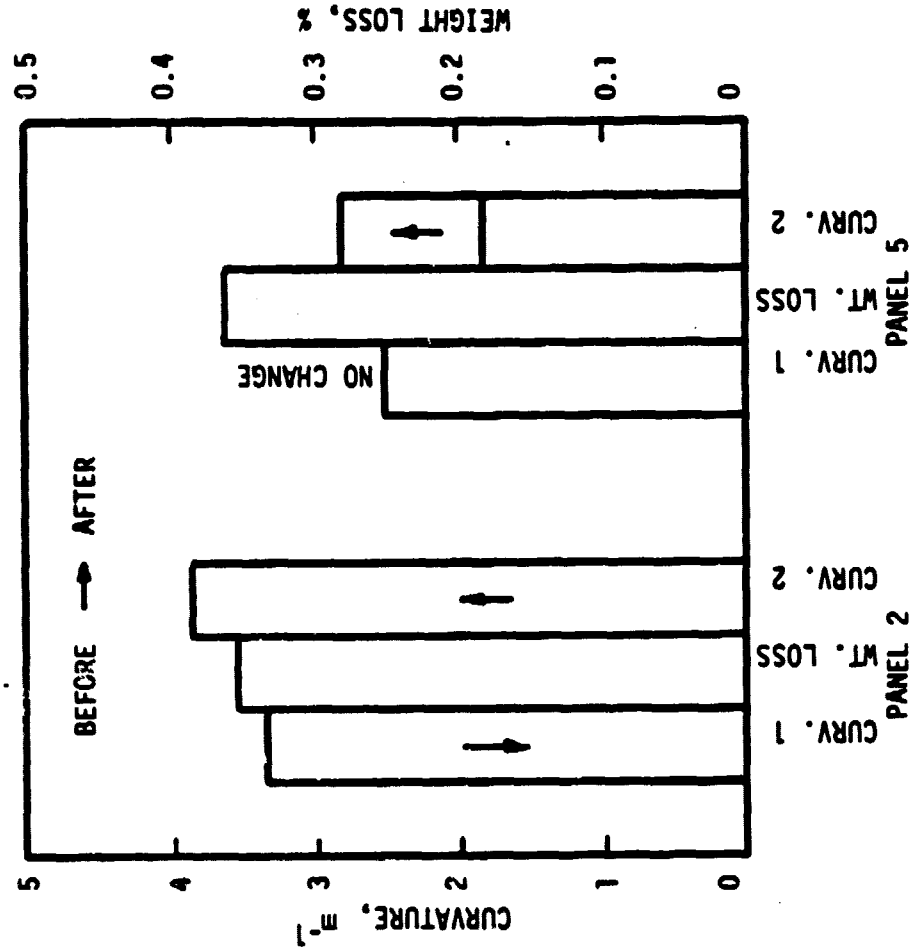

Fig. 7. Changes in curvature and weight after 7.5-h postcure, T300/5208

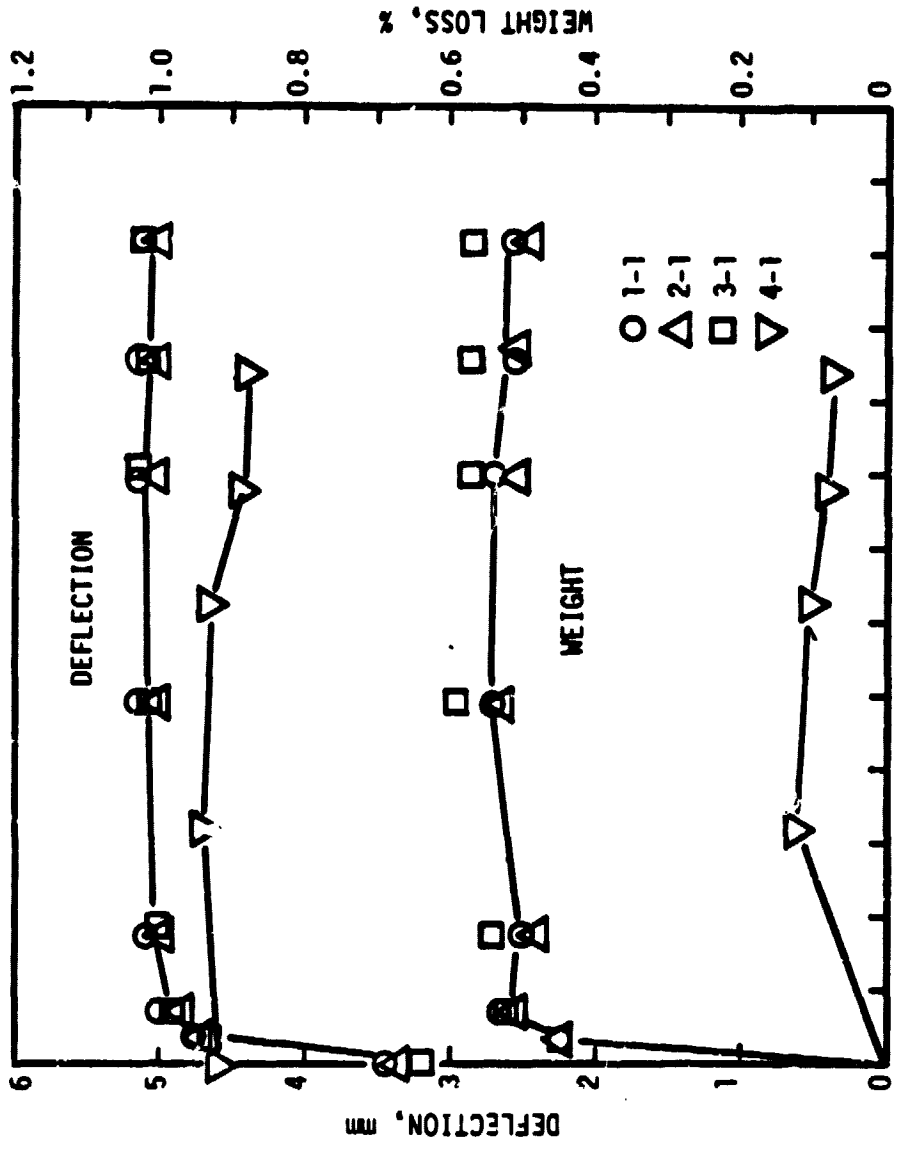

Fig. 8. Deflection and weight loss after various periods of preconditioning in vacuum at 75°C, T300/C69

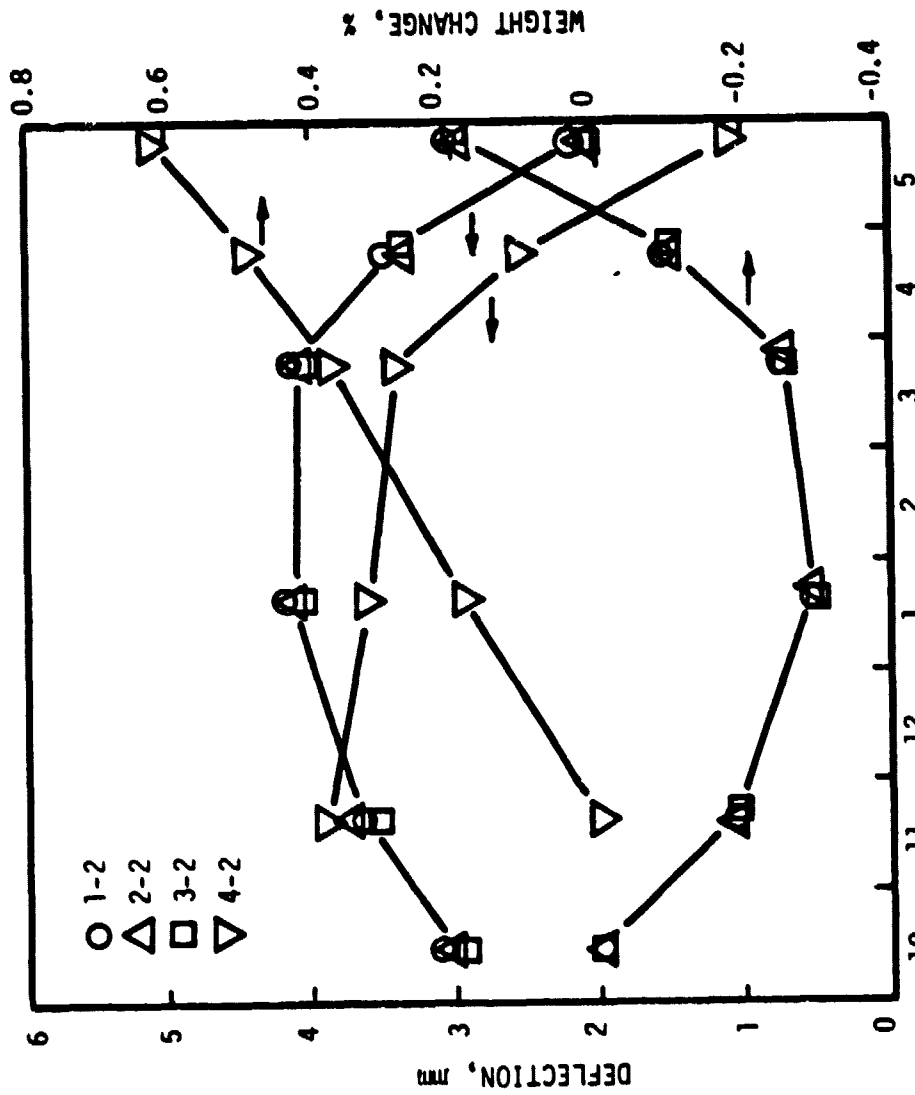

Fig. 9. Deflection and weight change in laboratory environment, T300/C69

present in the panels before conditioning.

The center deflections of panels 1 to 3 stand around 5 mm regardless of the period of conditioning. Since the deflections are caused by the residual stresses, we may infer from these data that the relaxation of residual stresses at 75°C is negligible within the time period studied. Also, the slow cool-down does not seem to have any effect on the deflection. The deflection of 5 mm observed when dry converts to a curvature of 4.0 m^{-1} for panels 1 to 3. This value is higher than those shown in Fig. 4.

The same type of data as in Fig. 8 are shown in Fig. 9 for the other group of panels that were left in the laboratory environment. The changes in weights reflect the variation of ambient relative humidity from month to month. Since panel 4 had much lower moisture content at the start of measurements, it continued to absorb moisture. In January the relative humidity hovered around 20% whereas it was about 74% in May.

3.3.5 Effect of Cure Cycle

Residual stresses at a given temperature will be minimized if cure is completed at the same temperature. For the graphite/epoxy panels, therefore, the cure cycle of Fig. 2(c) is preferred to that of Fig. 2(a) in reducing residual stresses if sufficient cure is achieved

at the initial cure temperature.

For 5208 resin the time to gel, t_{gel}, at a given hold temperature T is given by [45]

$$t_{gel} = 5.442550 \times 10^{-13} T^2 10^{3701.8/T} \tag{50}$$

where t_{gel} is in minutes and T in °K. On the other hand, the isothermal time to complete reaction, t_{CR}, is given by

$$t_{CR} = 3.187585 \times 10^{-17} T^2 10^{6229.77/T} \tag{51}$$

For any temperature history the fraction of gel is defined by

$$FG = \int_0^t \frac{dt}{t_{gel}} \tag{52}$$

Similarly, the fraction of complete reaction is

$$FC = \int_0^t \frac{dt}{t_{CR}} \tag{53}$$

In Ref. [45], FR and FC were evaluated numerically under the assumption of a stepwise increase in temperature. However, the integrals in Eqs. (52) and (53) can be given in closed form for any temperature change of constant rate.

If temperature is increased from T_o at a constant rate ϕ (°C/min.), i. e.,

$$T = \phi t + T_o \tag{54}$$

then Eqs. (52) and (53) can be reduced respectively to

$$FG = \frac{2.7575 \times 10^{8}}{\phi} \left(10^{-3701.8/T} - 10^{-3701.8/T_o}\right)$$

$$FC = \frac{2.7977 \times 10^{12}}{\phi} \left(10^{-6229.77/T} - 10^{-6229.77/T_o}\right) \qquad (55)$$

Consider now the three cure cycles in Fig. 2. For computational convenience these cycles are approximated by piecewise linear temperature histories as shown by broken lines. For each cure cycle, FG and FC are calculated and the results are shown as functions of time in Fig. 10.

For cycles 1 and 2 only about 20% of gelation takes place at 124°C while three times as much gelation is expected at the same temperature for cycle 3. For the latter, gelation is completed even before the final cure temperature is reached.

None of the three cycles is sufficient for complete reaction. The fraction of complete reaction at 124°C is negligible in all three cycles. Most of complete reaction takes place at 177°C with some occurring during cooldown. Thus, cycles 1 and 3 show the same fraction of complete reaction while cycle 2 shows the most.

The results of Fig. 10 are in qualitative agreement with the data on warping. That is, plate 4 shows the least amount of warping, but the difference is much less than what is predicted using 124°C as the stress-free temperature. The results of Figs. 8 and 10, however, prove

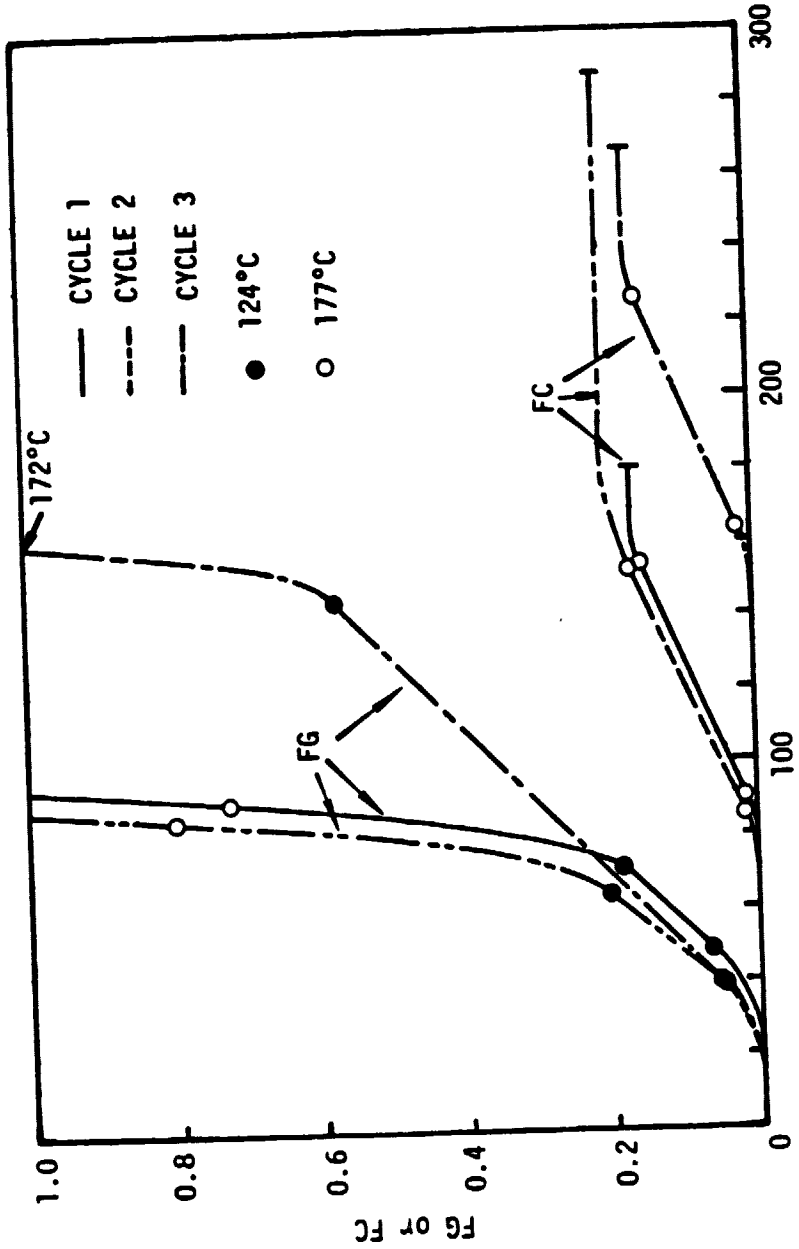

Fig. 10. Fraction of gel and fraction of complete reaction vs. time during cure

that residual stresses can be reduced by a prolonged gelation at a lower temperature.

3.3.6 Ply Failure

Residual stresses in composite laminates may exceed the unidirectional lamina strengths, causing failure of constituent plies. In symmetric cross-ply laminates having the same number of 0° and 90° plies, the transverse residual stress is calculated by using the laminated plate theory as

$$\sigma_T^R = \frac{1}{1 + E(1+2\nu)} E_T(e_L - e_T) \qquad (56)$$

where E_T is the transverse Young's modulus.

Figure 11 shows the average crack density in the surface plies of three $[0/90]_{2s}$ Kevlar 49/epoxy panels. The panels were initially left in the laboratory. They were then dried in a vacuum oven at 75°C, and weight losses and cracks were measured intermittently. The crack density generally follows the trend of the weight loss.

For the Kevlar 49/epoxy composite the pertinent material properties are [46]

$E = 0.0724$, $\nu = 0.34$

$E_T = 5.5$ GPa

The composite was cured initially for 4.5 h at 60°C and then for 3 h at 130°C. As a conservative estimate we choose the initial cure

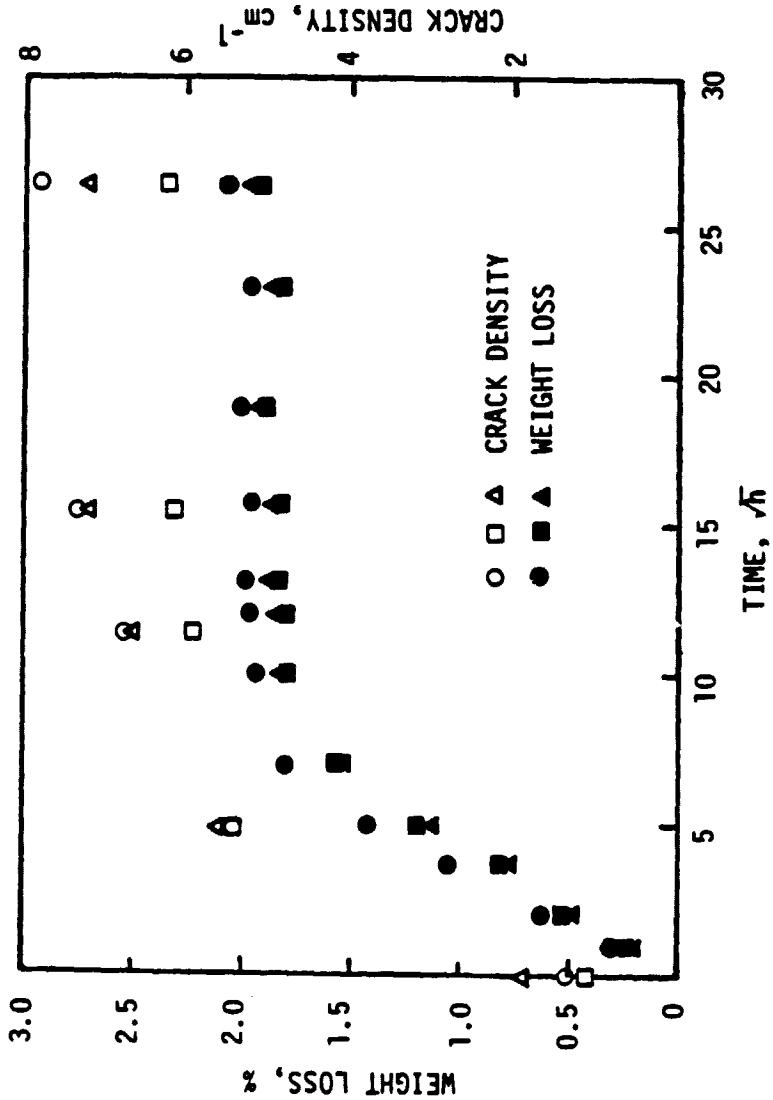

Fig. 11. Crack density vs. weight loss

temperature of 60°C as the stress-free temperature. The corresponding curing strains at a room temperature are then

$$e_L = 156\ \mu m/m\ , \quad e_T = -3081\ \mu m/m$$

The resulting residual stress from Eq. (56) is

$$\sigma_T^R = 15.9\ MPa$$

This stress is much higher than the transverse tensile strength of 8.9 MPa, and hence plies will fail along the fibers.

The reason for the crack density increasing with weight loss in Fig. 11 is that the residual stress increases as moisture leaves the panels. Absorbed moisture induces swelling which can annihilate the curing strains. However, since the panels were initially dry immediately after fabrication, the increasing crack density cannot be be explained by the elastic analysis alone. It is likely that a viscoelastic behavior and additional cure are responsible for such time-dependent behavior.

3.4 Conclusions

The residual stresses induced by fabrication and environmental exposure manifest themselves in the warping of unsymmetric laminates.

The type and amount of warping depend on the size of panels. Large panels exhibit cylindrical warping whereas small panels undergo saddle-shaped warping. The cylindrical warping is unstable in that

there are two stable deformed shapes. One shape can be snapped into the other by force, or by postcure at the cure temperature.

The relaxation of residual stresses in graphite/epoxy laminates at 75°C seems negligible up to a period of 220 days studied so far. The warping is very sensitive to ambient relative humidity because of the moisture absorption. A prolonged gelation at the initial cure temperature reduces residual stresses while postcure does not.

The residual stresses can be high enough to cause ply failure, as demonstrated in Kevlar 49/epoxy laminates. Such ply failures seem to be time-dependent.

4.0 HYGROTHERMAL BEHAVIOR OF SHEET MOLDING COMPOUND COMPOSITES

4.1 Introduction

Sheet molding compound (SMC) is a heterogeneous mixture of chopped reinforcing glass fibers, resin and filler, developed as an economical light-weight structural material. Fibers are nominally one inch long and distributed randomly, although not always straight, in plane.

Compared with the so-called advanced composites such as graphite/epoxy, the dimensional stability of SMC composites has not been understood well enough to allow more reliable and wider application. Therefore, the main objective of the present program was to characterize both experimentally and analytically the hygrothermal behavior of SMC composites.

4.2 Experimental Procedure

4.2.1 Materials

The sheet molding compound (SMC) composites chosen for study are SMC-R25, SMC-R40 and SMC-R65. SMC-R25 was obtained from B. F. Goodrich whereas the remaining two SMC's were supplied by Owens-Corning. Compositions of these three SMC composites are listed in Table 2. Note that there are two versions of SMC-R25.

Table 2. Compositions of SMC composites

SMC-R25C (Thickness 3.3 mm)

Function	Component	Manufacturer/Name	Weight Percent
Reinforcement	E-glass	PPG 516	25
Resin	Isophthalic unsaturated polyester	PPG 50271	18.6-17.2
Additive	Low profile thermoplastic	Union Carbide LP40A	10-11.5
Filler	Calcium carbonate	H. T. Campbell & Sons	43
Thickener	Magnesium oxide	Plasticolors Plastigel	0.72
Catalyst	t-butylperbenzoate	Aztec	0.29
Mold release	Zinc stearate	Fisher Scientific	1.15

SMC-R25W (Thickness 3.1 mm)

The same formulation but with addition of 0.375 wt % wetting agent KR 44S from Kenrich Chemical.

Table 2 (continued)

SMC-R40 (Thickness 3.8 mm)

Function	Component	Manufacturer/Name	Weight Percent
Reinforcement	E-glass	OCF 433 AE-113	40
Resin	Isophthalic polyester	OCF E987	54.5
Thickener	Magnesium oxide	Hatco Modifier M	2.7
Catalyst	t-butylperbenzoate	Lucidol	0.6
Mold release	Zinc stearate	Tennaco DLG-10	2.2

SMC-R65 (Thickness 4.5 mm)

The same matrix formulation but with 65 wt % E-glass.

Table 3. Composition of unidirectional panels

Function	Component	Manufacturer/Name	Weight Percent
Reinforcement	E-glass	OCF 433 AE-113	50
Resin	Isophthalic polyester	OCF E-987	45.40
Thickener	Magnesium oxide	Hatco Modifier M	1.44
Catalyst	t-butyl perbenzoate	Lucidol	0.46
Mold release	Zinc stearate	Tennaco DLG-10	2.70

To investigate the effect of fiber length, unidirectional composite panels were fabricated using the same ingredients as those in the SMC's. Two different lengths of fiber were used: 6 mm and 25 mm.

The fibers of desired length were first dried at 75°C in an oven. The base plate, the square mold and the cover plate were cleaned with acetone to remove grease, dirt and any other inert material. They were then uniformly coated with release agent Freekote 33 and dried in air. This facilitated easy removal of cured panel.

A thin wire mesh was positioned on the bottom plate, and fibers were aligned over this mesh. When all of the preweighed fibers were aligned uniformly to give a fairly constant thickness, another wire mesh was laid on top of the fibers. At this stage, the two wire meshes which sandwich the fibers were held on edges by clips.

The resin, initiator, mold release and thickener were mixed in exact proportions as listed in Table 3. The contents were thoroughly mixed and kept in a vacuum oven at room temperature to remove air bubbles generated while mixing. When all air bubbles were removed, the resin was slowly and evenly poured over the fibers. After half the content was used, the fiber-mesh assembly was flipped over, and the resin poured as before. After all the resin was poured, the container was weighed to obtain the exact amount of resin used.

The wire meshes were replaced by Teflon sheets, and the composite

was subjected to repeated press and release cycles for ~4 minutes in a hydraulic press to consolidate the fibers in resin and to remove air bubbles. The press platens were heated to ~40°C.

The composite was then removed from the press and cured at room temperature for at least 16 hours.

Bulk polyester panels were fabricated using the same proportions of thickener, initiator and mold release except for fibers as in the unidirectional composite. The panels were cured at room temperature for at least 16 hours.

Conventional specific gravity bottle method was used to obtain the actual specific gravities of composites. The mass contents of fiber were determined by burning off the matrix resin and weighing the residue. The measured values of specific gravity and fiber mass content are listed in Table 4.

In terms of mass contents m_f and m_m, the specific gravity of composites is given by

$$s = \frac{1}{m_f/s_f + m_m/s_m + v_v/s} \tag{57}$$

On the other hand, the fiber volume content is related to the fiber mass content by

$$v_f = m_f \frac{s}{s_f} \tag{58}$$

Table 4. Fiber and void contents

	R25C	R25W	R40	R65
Specific gravity				
Nominal	1.41	1.41	1.55	1.86
Measured	1.33	1.34	1.50	1.80
Fiber mass content, %				
Nominal	25	25	40	65
Measured	25	23	41	64
Fiber volume content, %				
Nominal	14	14	23	47
Measured	13	12	24	44
Void content, %				
Nominal	0	0	0	0
Measured	6.8	5.0	5.0	3.4

In Table 4 the nominal values of s and v_f were calculated from the nominal fiber mass contents under the assumption of no voids. On the other hand, the "measured" values of v_f and v_v were calculated from the actually measured values of m_f and s. The properties of E-glass fiber and polyester resin required in Eqs. (57) and (58) are listed in Table 5. It should be noted that the matrix resin of SMC-R25 composites contains a large amount of calcium carbonate, and therefore, some of the properties in Table 5 may not be applicable.

4.2.2 Moisture Diffusion and Swelling

The specimens chosen were 50 mm x 50 mm square plates. The nominal thicknesses of specimens are shown in Table 2.

Prior to environmental exposure, all the specimens were dried in a vacuum oven at 75°C. During drying, specimens were weighed after 1, 4, 9, 16, and 24 hours on the first day, and daily thereafter, Fig. 12. The drying was stopped after 36 days although SMC-R25 and polyester E987 had not reached equilibrium. The data in [27] show that equilibrium should be reached within 36 days for these composites. Therefore, the ever increasing weight loss is believed to be a loss of material other than moisture desorption.

After the preconditioning, three specimens each were subjected to the various environments listed in Table 6. Saturated salt solutions

Table 5. Properties of E-glass fibers and polyester resin

Property	Fiber (E-glass)	Matrix (polyester)
Young's modulus, GPa	72.35	2.80
Shear modulus, GPa	29.65	1.04
Bulk modulus, GPa	43.06	3.11
Poisson's ratio	0.22	0.35
Coefficient of thermal expansion, $\mu m/m \cdot K$	5×10^{-6}	95×10^{-6}
Density, 10^{-3} Kg/m^3	2.6	1.24

Table 6. Environments studied

Temperature	Relative humidity	Designation
Room temperature	65% RH	RT/65
	98% RH	RT/98
	Distilled water immersion	RT/water
75°C	65% RH	75/65
	98% RH	75/98
	Distilled water immersion	75/water
100°C	steam	100/steam

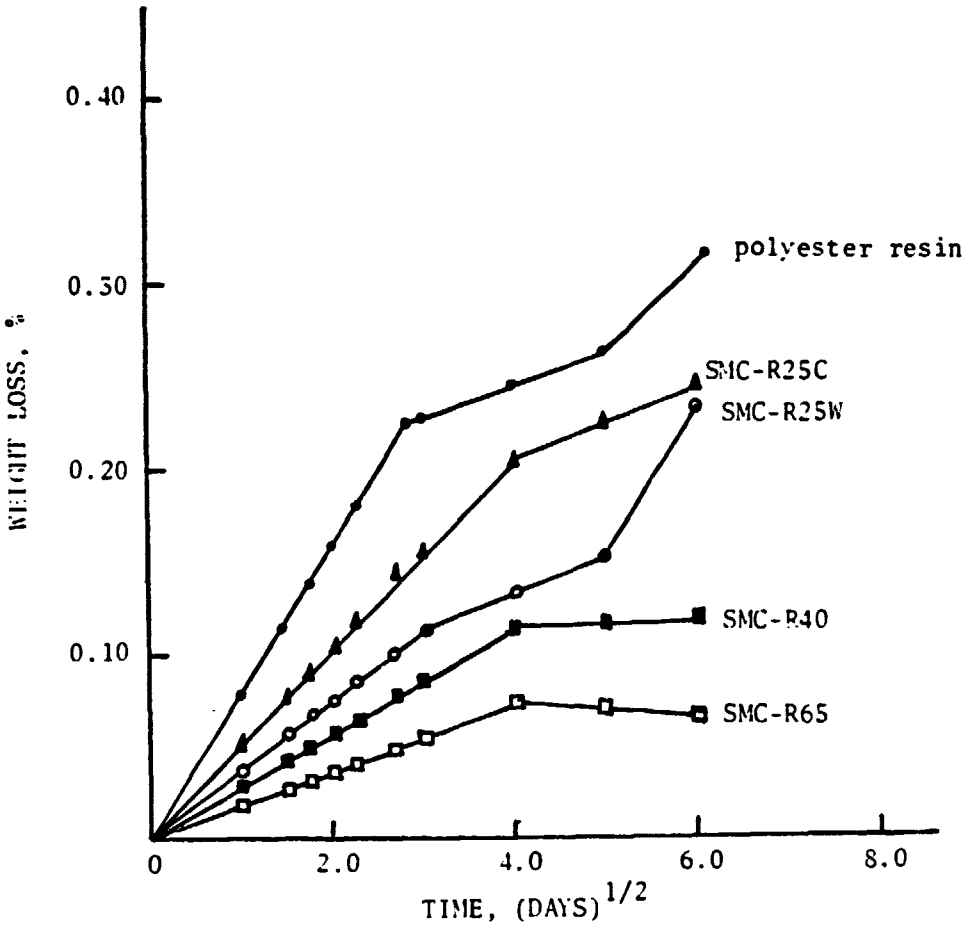

Fig. 12. Weight loss during preconditioning

of lead nitrate and magnesium nitrate were used to obtain relative humidities of 98% and 65%, respectively. At 75°C the 65% relative humidity could not be obtained; the actual value was 61%.

Both weight and dimensions of specimen were measured at room temperature at regular intervals based on $(\text{time})^{1/2}$. Before each measurement specimens were transferred into another chamber with the same relative humidity but at room temperature, and were allowed to cool down to room temperature. Specimens were then taken out one by one, and weight was measured on a Mettler balance with 10^{-4} gram accuracy, immediately followed by dimensional measurements using a caliper accurate up to 0.0005 in. The specimen was placed back in the original environmental chamber, so that it was not exposed to ambient condition for more than three minutes.

The measured weight was converted to the weight gain M by

$$M = \frac{\text{weight at time t}}{\text{dry weight after preconditioning}} - 1 \qquad (59)$$

The weight gain was monitored as a function of time, and the maximum value M_m was noted.

When specimens reached maximum weight gain, two out of three specimens were removed and dried in a vacuum oven at the same temperature to study the desorption behavior. One sample was left behind to monitor the long-term weight change.

4.2.3 Thermal Expansion

The thermal expansion curves for SMC, unidirectional and bulk polyester specimens were obtained on Orton automatic recording dilatometer. Specimen geometry of 2 in. by 1/2 in. by thickness with a tolerance of 0.001 in. was used. The coefficient of thermal expansion was measured in the thickness direction, also. In the thickness direction, the required 2-in. length of specimen was made up by using pre-calibrated glass rod. The thermal expansion was continuously recorded automatically on an x-y recorder against temperature. The small zone where the curve changes its slope was taken as the range of glass transition temperature, T_g.

4.2.4 Identification of Damage

Specimens were inspected visually for any sign of damage such as color change, blistering and void formation. After moisture absorption tests some specimens were cut and cross sections were examined on a Leitz-Panphot all-purpose optical microscope.

The change of attenuation due to environmental degradation was measured ultrasonically on a Sonoray 303B flaw detector with a 10 MHz transducer.

4.3 Results and Discussion

4.3.1 Absorption

The weight changes in SMC composites at various environments are shown in Figs. 13 through 19. The curves represent Eq. (40) with $\bar{c}$ as the weight gain. The maximum weight gain M_m was taken as the final equilibrium moisture concentration. The diffusivity was determined from the weight gain M_1 after the first day and the maximum weight gain M_m as

$$D = \frac{\pi}{16} \frac{h^2}{t_1} \left(\frac{M_1}{M_m}\right)^2 \tag{60}$$

where t_1 = 1 day = 86400 s. The values of M_m and D are listed in Table 7.

In every environment the weight gain reaches a maximum and then decreases. Also, the actual diffusion process is slower than predicted by the Fick's equation.

At room temperature, both R40 and R65 exhibit a fairly Fickian diffusion behavior until maximum weight gain is reached, Figs. 13-15. The most deviation from Fickian diffusion is observed for R25C and R25W.

Essentially the same type of behaviors is seen also at 75°C,

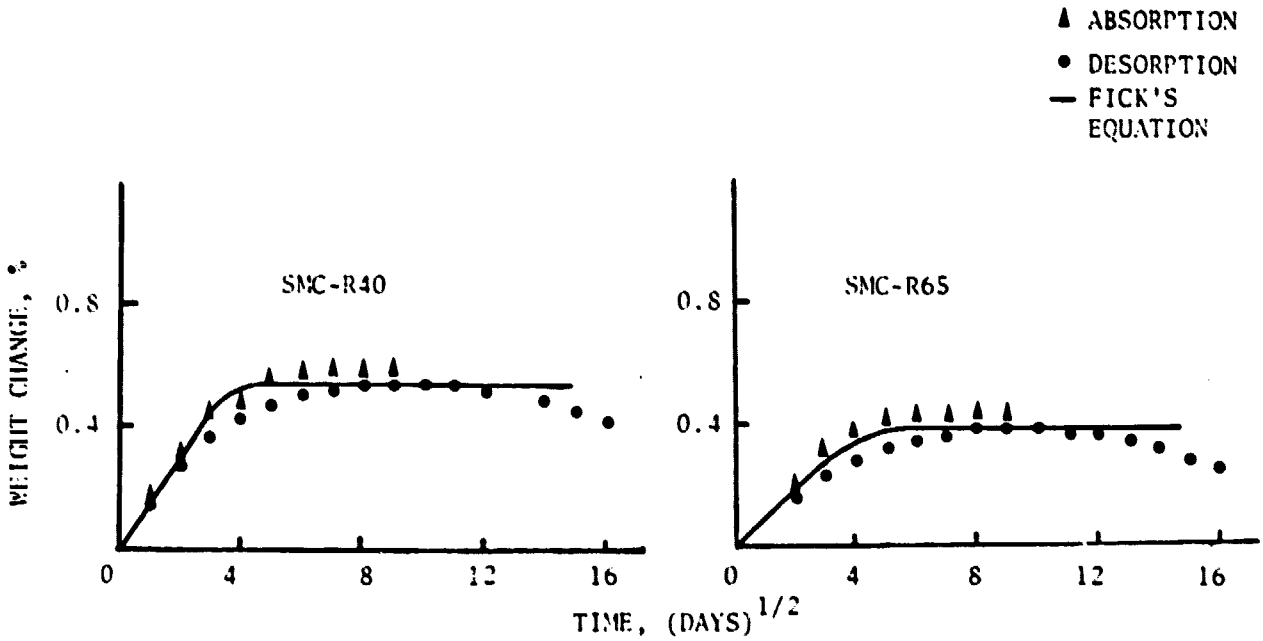

Fig. 13. Weight changes at RT/65% RH

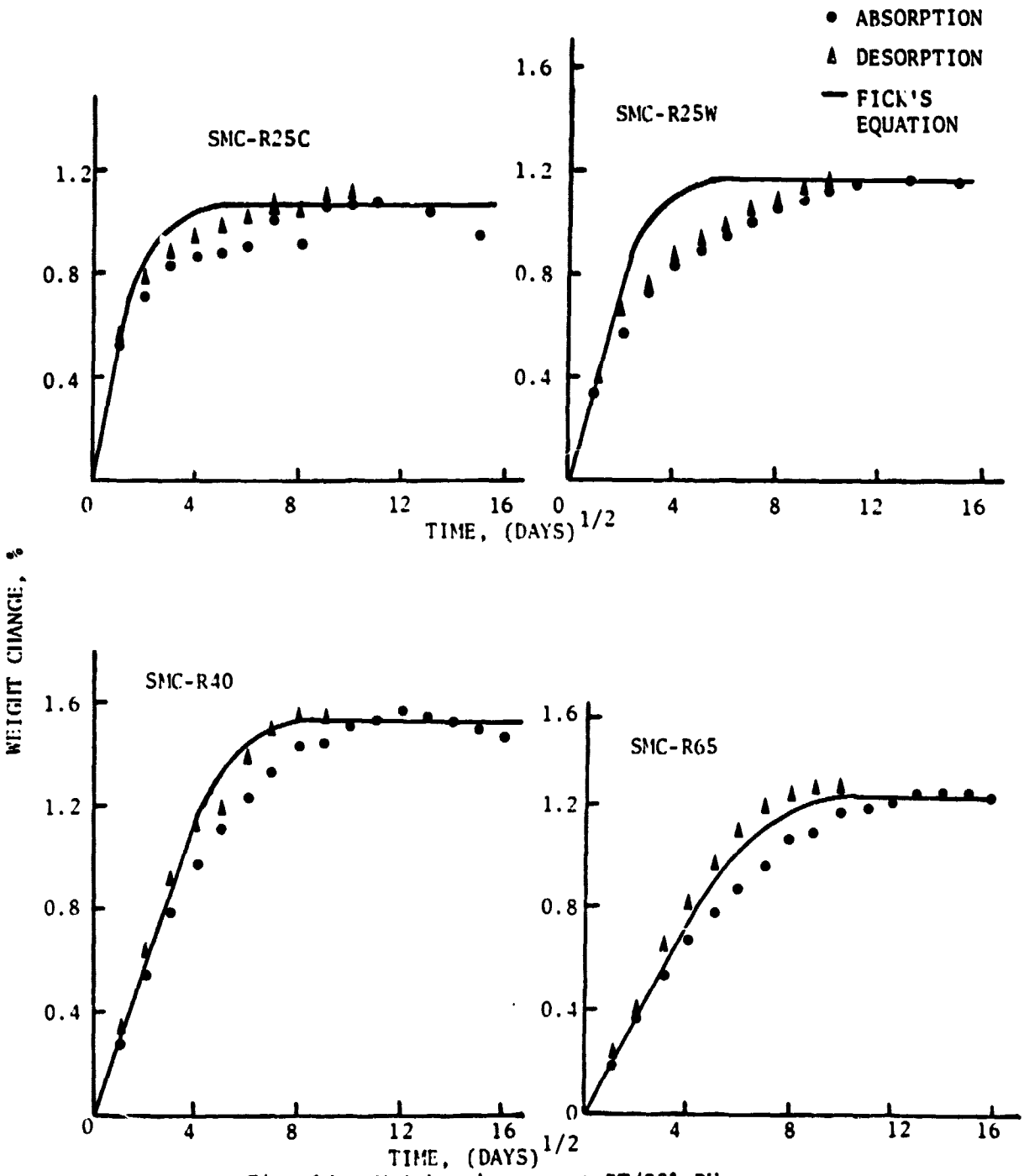

Fig. 14. Weight changes at RT/98% RH

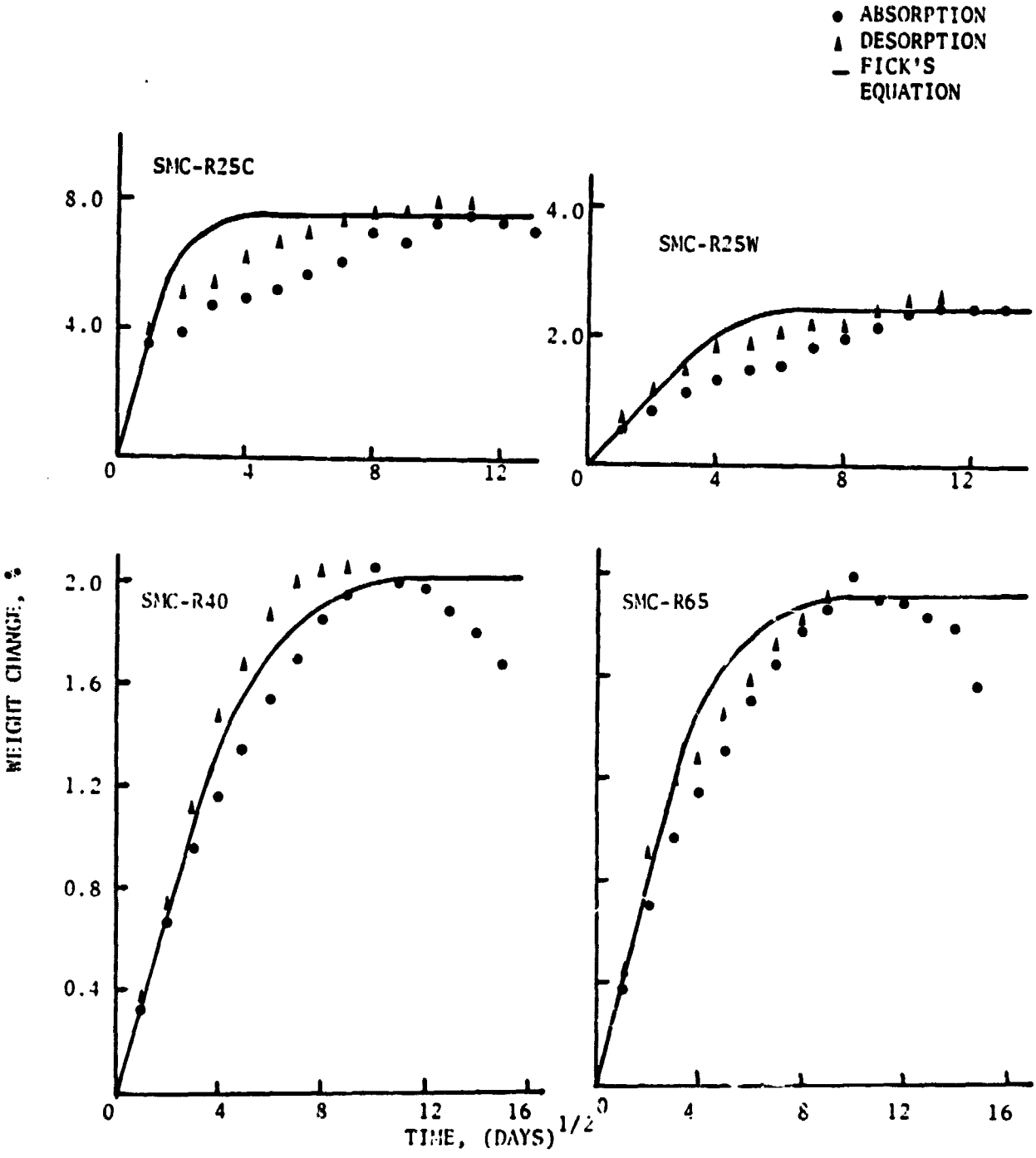

Fig. 15. Weight changes at RT/water

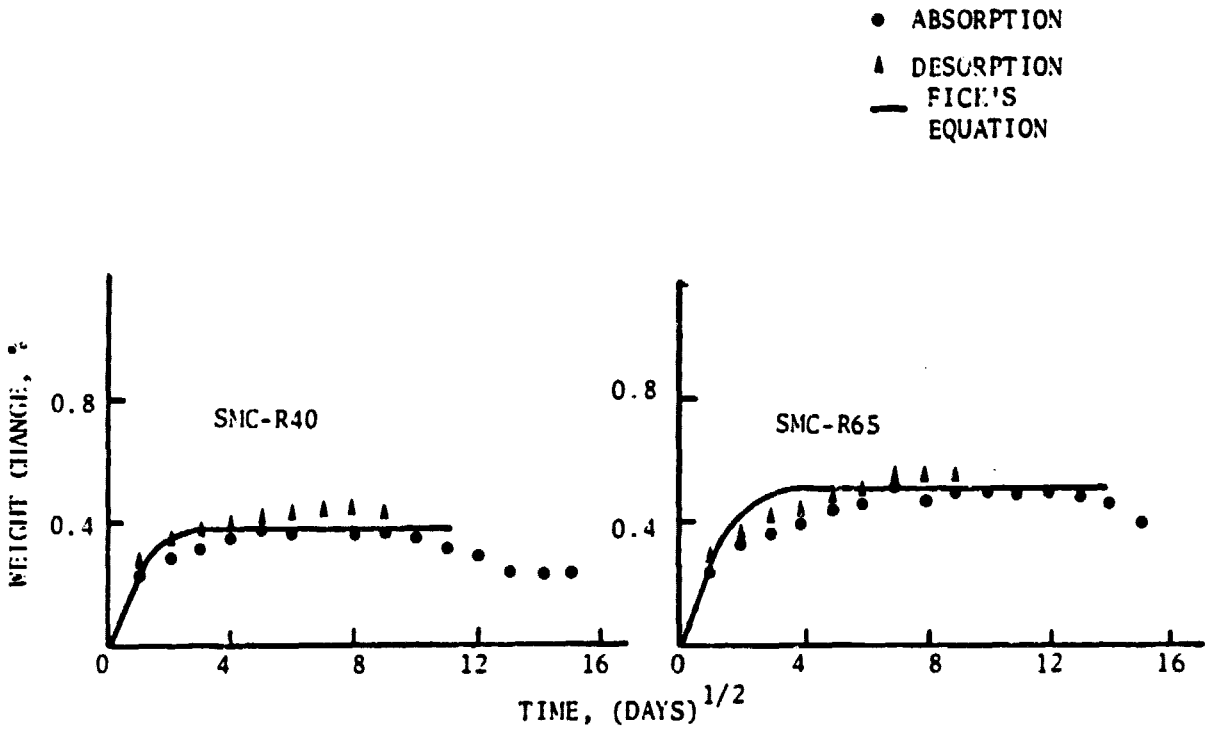

Fig. 16. Weight changes at 75°C/65% RH

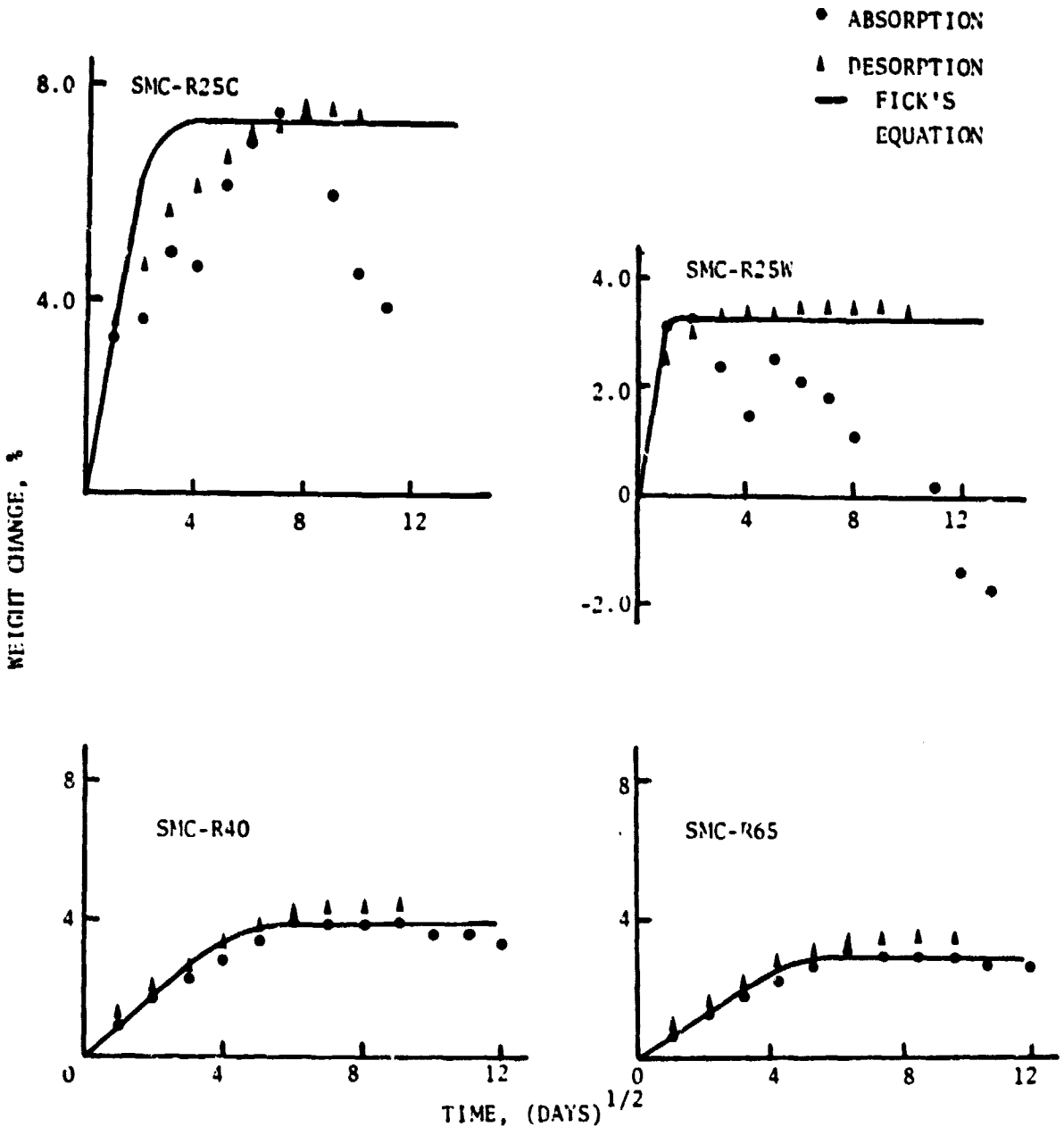

Fig. 17. Weight changes at 75°C/98% RH

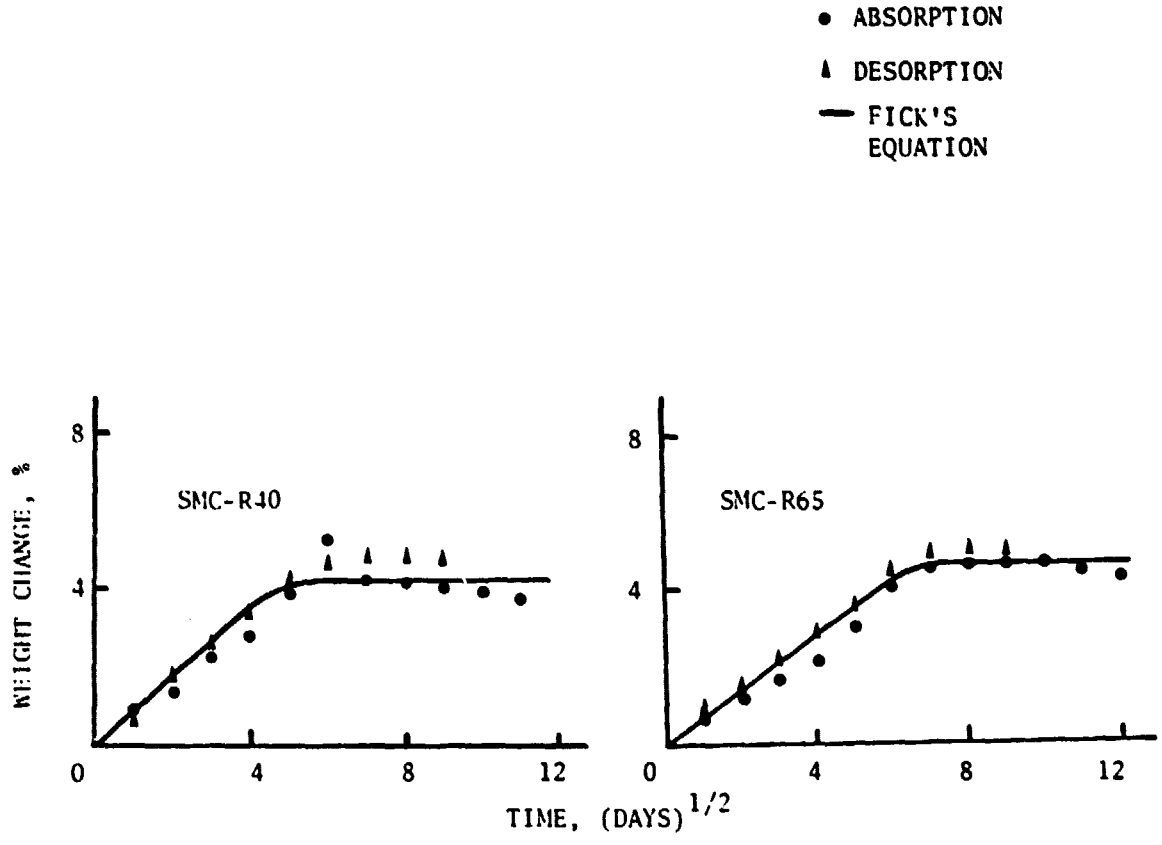

Fig. 18. Weight changes at 75°C/water

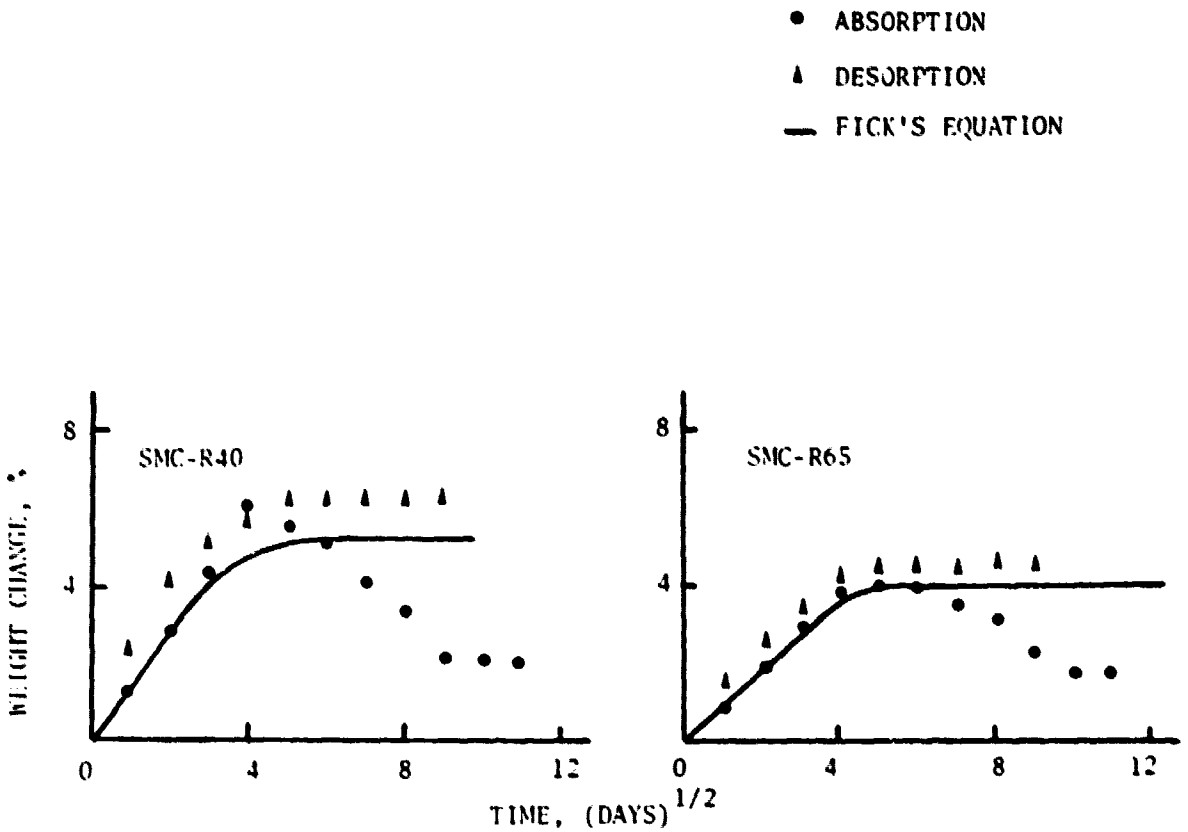

Fig. 19. Weight changes at 100°C/steam

Table 7. Maximum weight gain and diffusivity

Material	Environment						
	RT/65	RT/98	RT/water	75/65	75/98	75/water	100/steam
SMC-R25C							
Mm, %		1.08	7.5		6.82		
D x 10^6, mm^2/s		6.60	5.50		4.60		
SMC-R25W							
Mm, %		1.17	2.45		3.275		
D x 10^6, mm^2/s		2.60	1.10		20.0		
SMC-R40							
Mm, %	0.545	1.545	2.09	0.375	3.75	4.19	5.25
D x 10^6, mm^2/s	3.0	1.10	0.8	11.60	2.0	1.40	2.10
SMC-R65							
Mm, %	0.40	1.245	1.90	0.51	3.0	4.65	3.95
D x 10^6, mm^2/s	2.50	1.08	1.80	11.10	2.50	0.90	2.0
Polyester							
Mm, %	1.06	2.80	3.10	3.0	5.5	5.6	25.8
D x 10^6, mm^2/s	1.90	0.70	0.80	2.80	3.40	4.0	0.40

Figs. 16 through 18. The weight gain of R25C and R25W is extremely erratic at 75°C/98% RH. In the case of R25W the weight decreases below the initial dry value after about 100 days. Thus, R25C and R25W composites are believed to degrade faster than R40 and R65 composites. At 75°C/98% RH the weight gain in R40 and R65 slows down for a while and then speeds up as it approaches maximum.

The most deviation from Fickian behavior occurs at 100°C/steam. In some cases, e. g., R40 at 75°C/water and 100°C/steam, maximum weight gain appears as a sharp peak. Such behavior was usually associated with visible formation of blisters on specimen surfaces. When the blisters burst open, weight decreased. Therefore, sharp peaks were not taken as maximum weight gain.

Unlike SMC composites, bulk polyester follows the Fick's equation better at more severe environments, Fig. 20. At mild conditions such as RT/65% RH and 75°C/65% RH, weight gain is slower than predicted. However, at the remaining three conditions at 75°C the actual weight gain very closely follows the prediction.

The maximum weight gain M_m is shown in Fig. 21 against the fiber volume fraction at various environments. Also included in the figure are the data from [27]. For the composites studied in the present work, M_m in general increases with decreasing fiber volume content. However, such is not the case with the data from [27]. The reason is

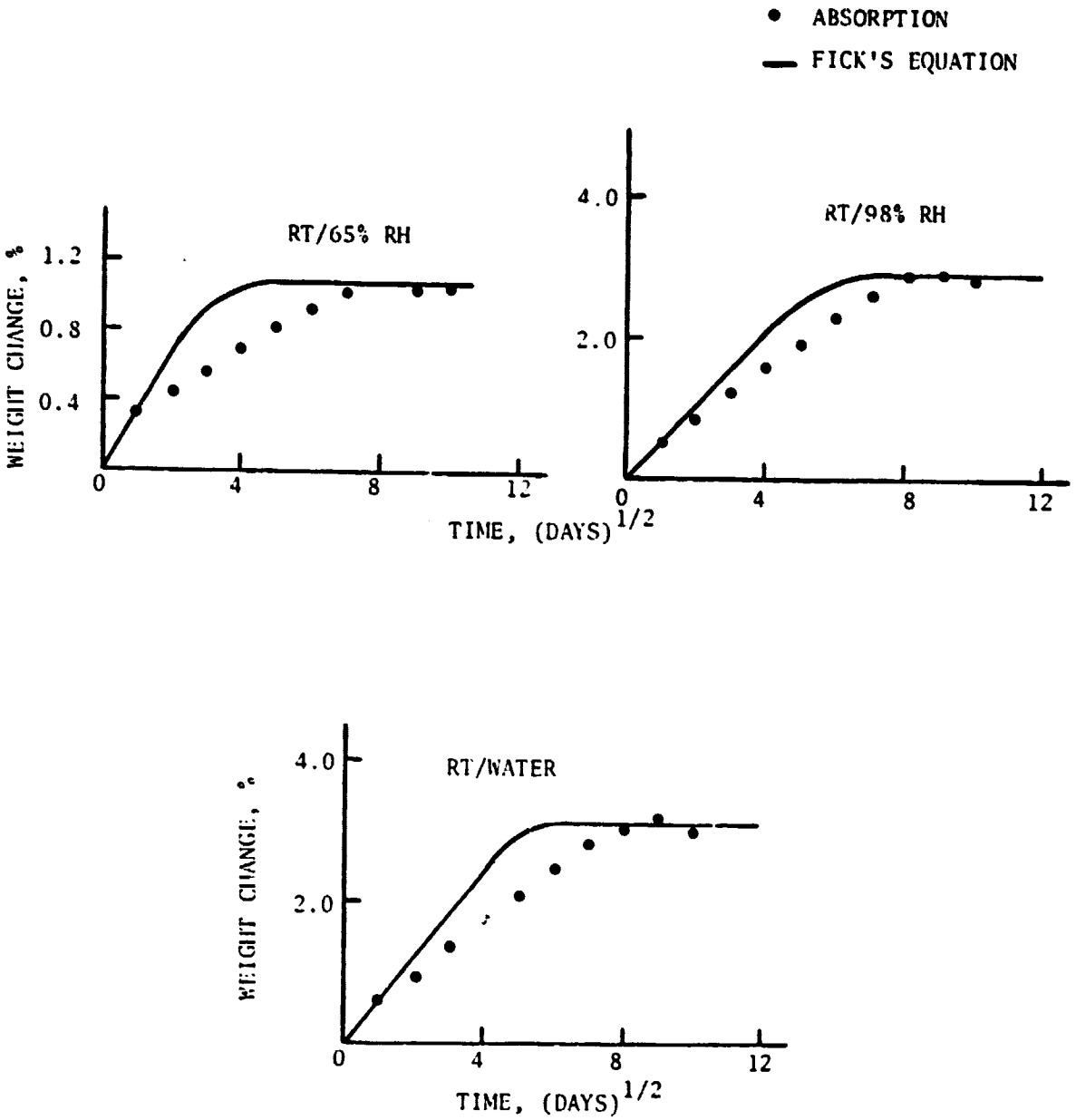

Fig. 20. Weight changes in bulk polyester

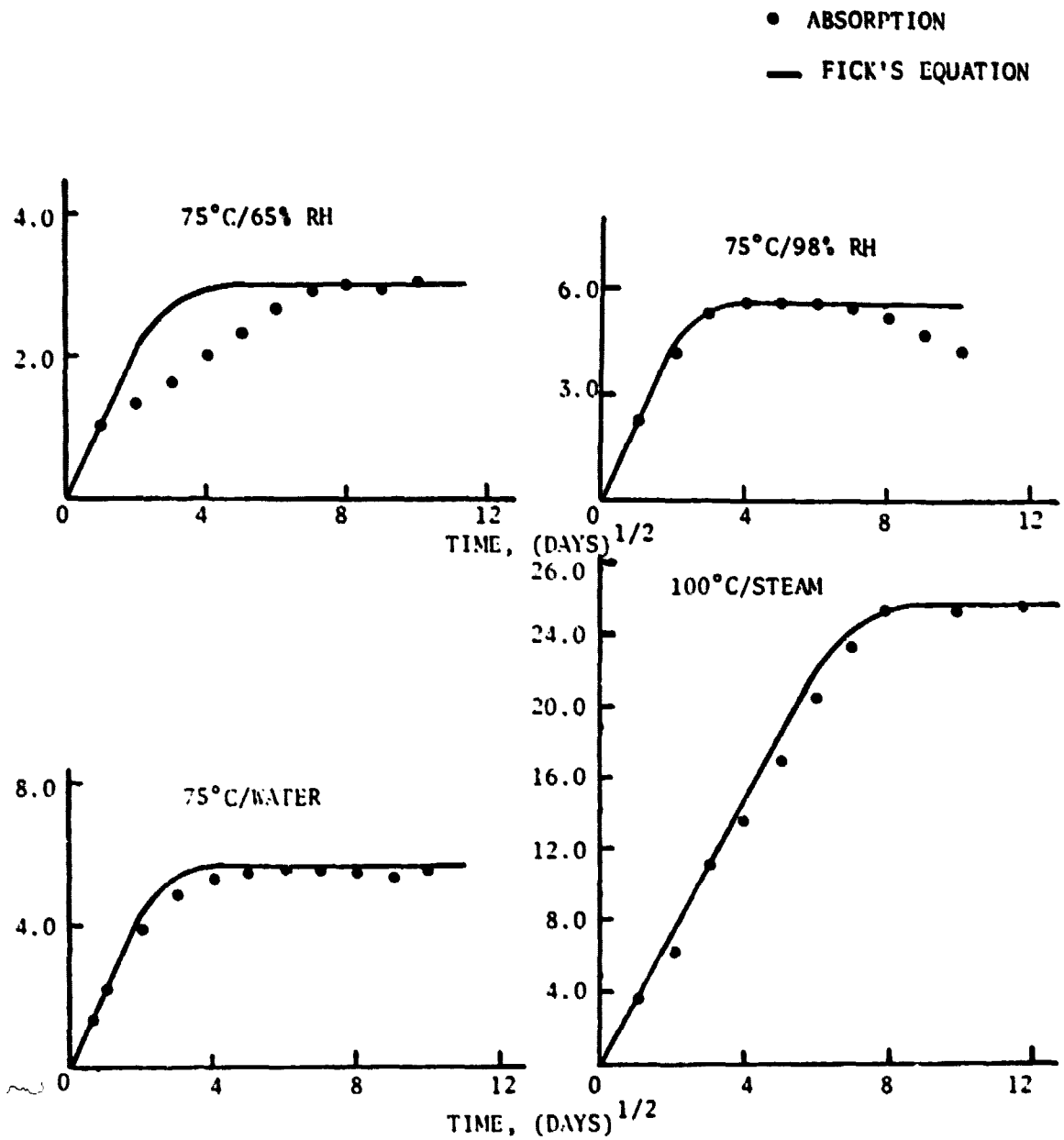

Fig. 20 (cont.). Weight changes in bulk polyester

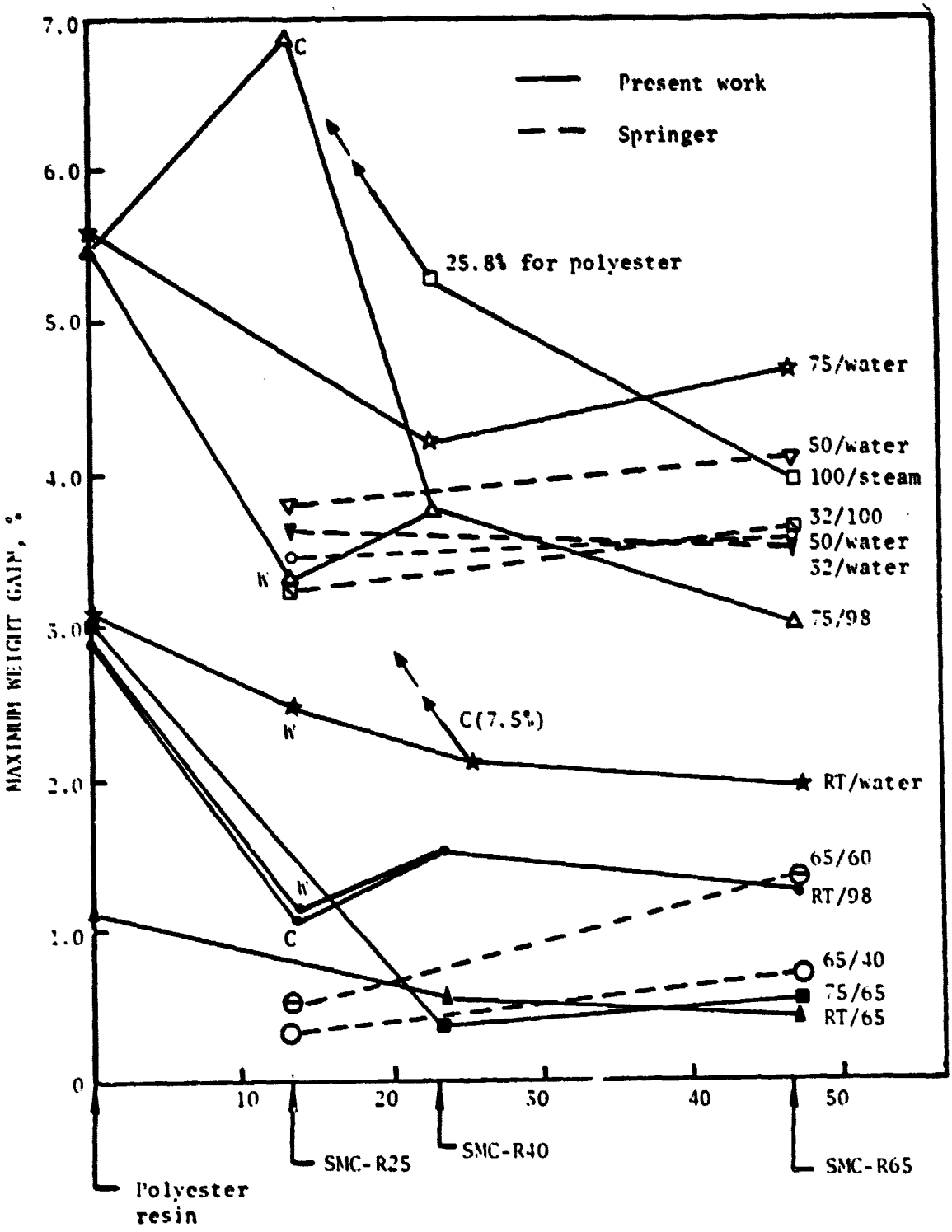

Fig. 21. Maximum weight gain vs. fiber volume content

that SMC-R25 composites contain a large amount of calcium carbonate, which is not believed to absorb as much water as polyester.

Exceptions are noted for SMC-R25 composites and at 75°C/water. It should be kept in mind that R25W and R25C have different matrix compositions than R40 and R60 do. At RT/98% RH both R25C and R25W show unexpectedly low weight gains. However, at RT/water and 75°C/98% RH conditions, R25C absorbs extremely large amounts of water whereas R25W behaves on or below par in comparison with R40 and R60. There are two differences between R25C and R25W. First, R25C has visible voids whereas R25W does not. Second, R25W has wetting agent KR 44S added to the matrix. Both differences are in support of better environmental stability of R25W.

At 75°C/water SMC-R40 shows a peak weight gain of 5.3% after 36 days. However, since this value was not in line with the other points before and after, a lower estimated value was used instead in Fig. 18. If the peak value is used, the maximum weight gain for R40 will be higher than for R65, thus conforming to the general trend of increasing weight gain with decreasing fiber volume content.

To check the effect of fiber reinforcement on maximum weight gain, the in situ maximum weight gain in the matrix was calculated from Eq. (26) with $c_f = v_v = 0$. The results are compared with the maximum weight gains in bulk polyesters in Fig. 22. The straight line in the figure

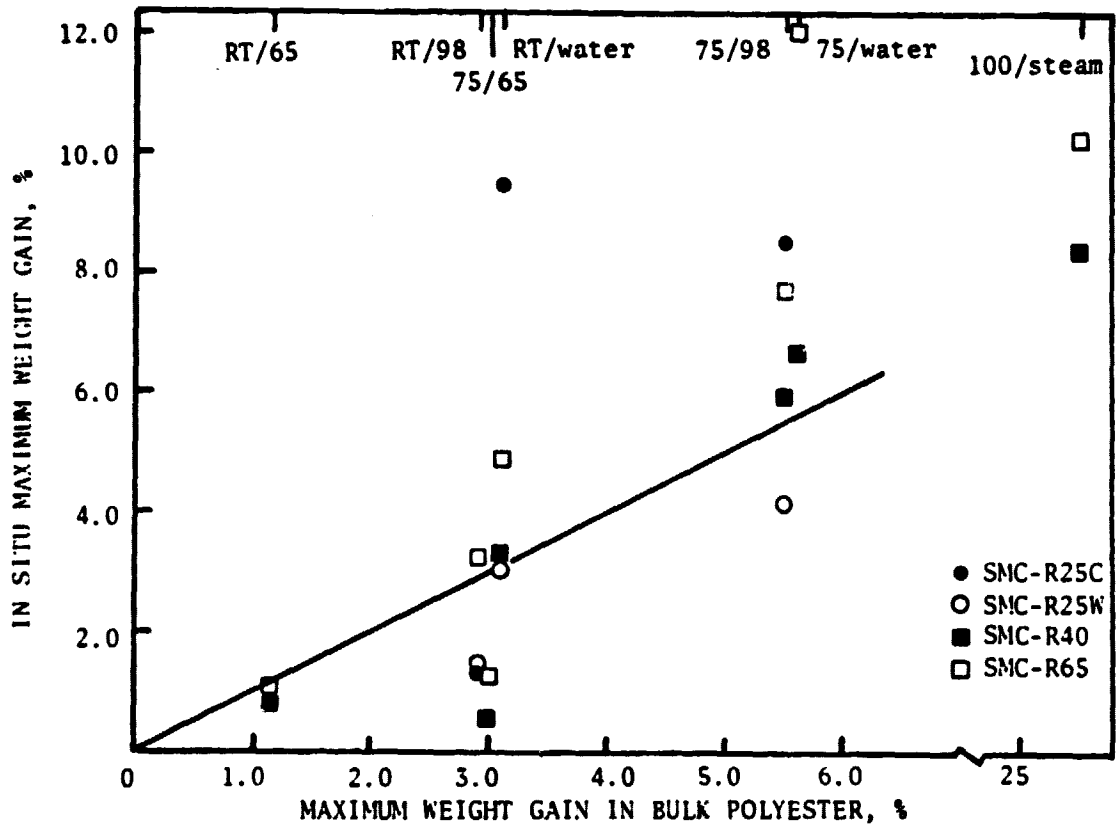

Fig. 22. In situ maximum weight gain in matrix

represents the equality between the in situ weight gain and the weight gain in bulk polyester. Since R25C and R25W have different matrix compositions, our discussion here is limited to R40 and R60 only.

The actual in situ weight gains are higher than predicted in high humidity conditions except at 100°C/steam. For some unknown reason the composites gain much less weight than expected at 75°C/65% RH. R65 has higher in situ weight gain than R40 in every environment tested. The difference is the largest at 75°C/water. It is possible that the increased interfacial area contributes to increased moisture absorption. The composites show much less weight gain than predicted at 100°C/steam. The bulk polyester specimens showed extensive cracking both outside and inside at this environment while the composite specimens did not show as much damage. Thus, the fibers seem effective in preventing damage. The less extensive cracking is credited for lower weight gains in the composite specimens.

Relations between maximum weight gain and relative humidity are shown in Fig. 23. Here the water immersion data are plotted at 100% RH for convenience. At 65% RH maximum weight gain is fairly independent of temperature for both composites, but not so for polyester. At 98% RH and in water maximum weight gain increases substantially with temperature. Such behavior is contrary to the behavior of graphite/epoxy composites which usually show equilibrium moisture content decreasing with increasing temperature [24,31].

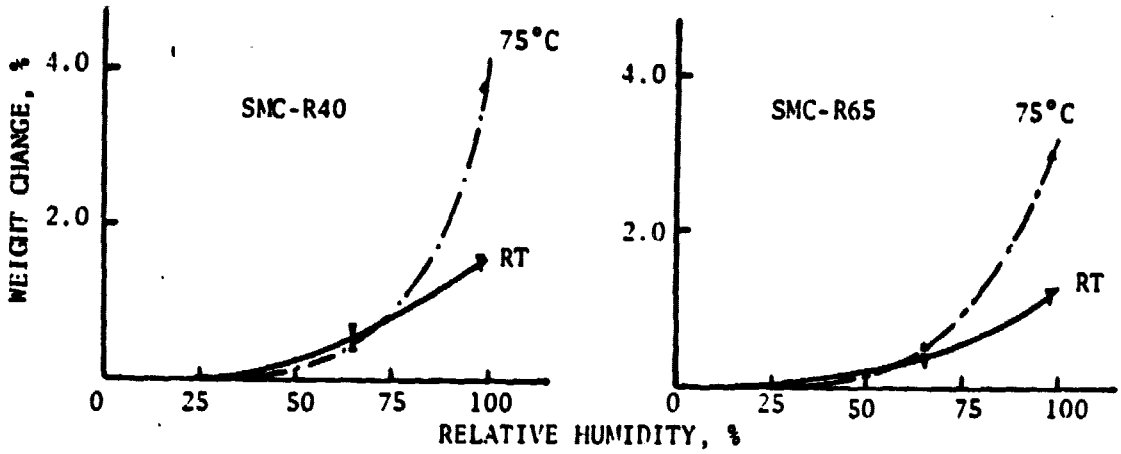

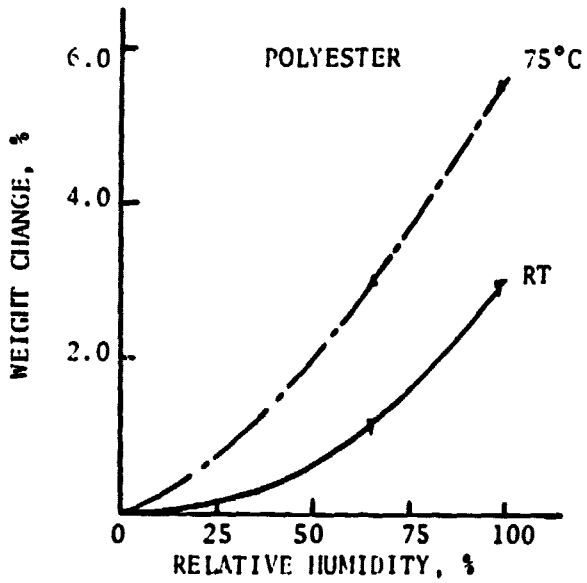

Fig. 23. Maximum weight gain vs. relative humidity

The maximum weight gain data at 65 and 98% RH were used to determine the parameters in Eq. (43). The resulting values of a and b are listed in Table 8, and the corresponding equations are shown as curves in Fig. 23.

To check the temperature dependence of diffusivity as indicated by Eq. (38), the results for D in Table 7 are shown in Fig. 24 against the inverse of temperature.

Both R40 and R65 have comparable diffusivities except in water where R65 shows an erratic behavior. A reference to Fig. 21 reveals that R65 has an unusually high weight gain at 75°C/water. Since diffusivity is inversely proportional to the square root of maximum weight gain (cf. Eq. (60)), a lower value will result at 75°C/water. Note that bulk polyester shows much less dependence of diffusivity on relative humidity.

4.3.2 Desorption

To study desorption behavior two specimens were taken out of each environmental chamber and placed in a vacuum oven at the same temperature. The weight gains of these specimens at the start of desorption tests were near their respective maximum values.

The weight loss during desorption is defined as the difference between the current weight gain and the weight gain at the start of

Table 8. Parameters describing relation between maximum weight gain and relative humidity

Material	Temperature, °C	
	RT	75
SMC-R40		
a, %	1.6253	4.1956
b	2.5353	5.601
SMC-R65		
a, %	1.3156	3.2714
b	2.7618	4.3114
Polyester		
a, %	3.0344	5.6661
b	2.2506	1.4745

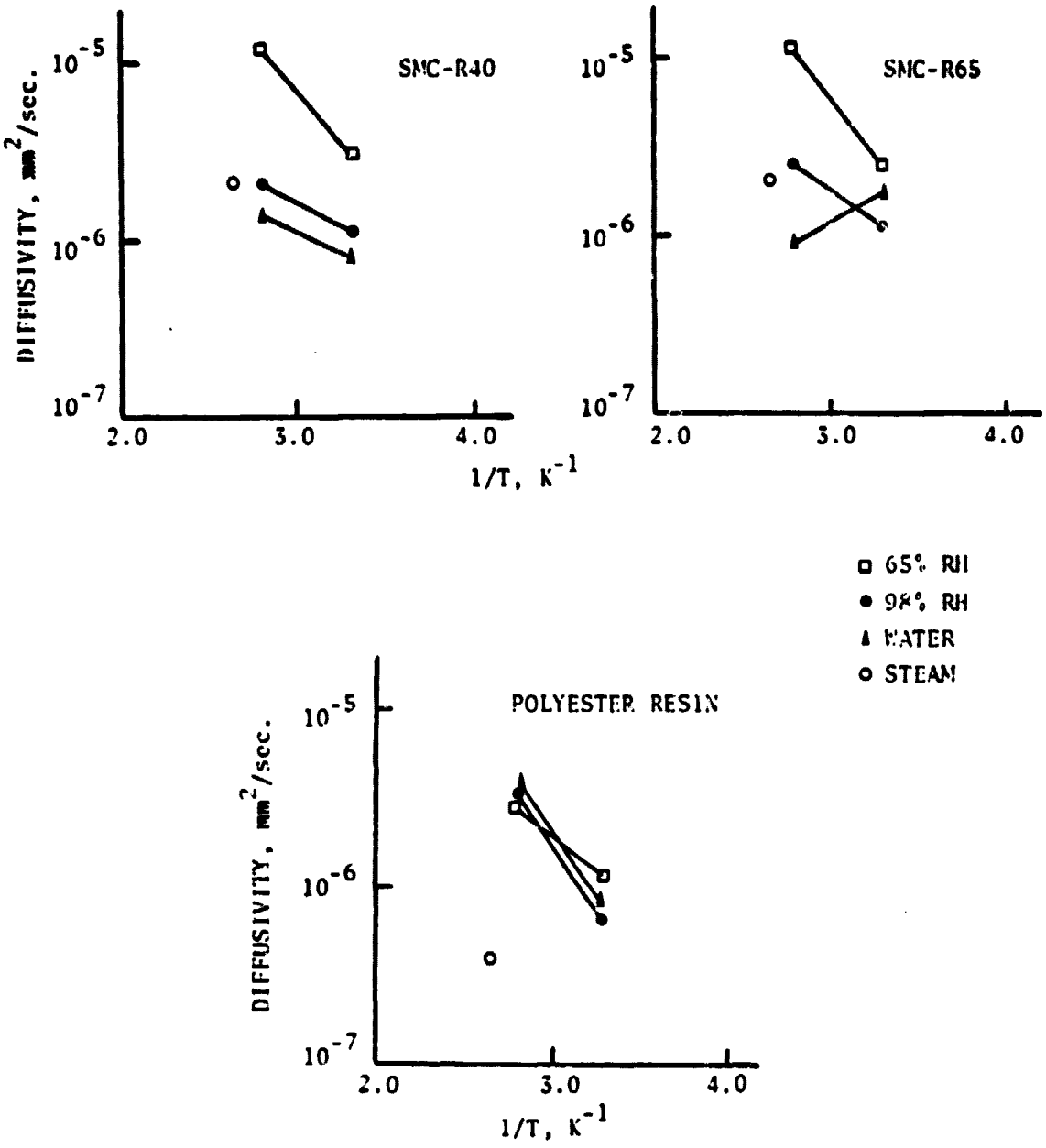

Fig. 24. Diffusivity vs. temperature

desorption. The measured weight losses are compared with the corresponding weight gains during absorption in Figs. 13 through 20.

All desorption curves fairly closely follow the respective absorption curves up to the points of maximum weight gain. Yet the desorption curves are always above the absorption curves, resulting in a permanent loss of material after a complete moisture cycling. The permanent losses of mass are listed in Table 9. These values would have been higher if desorption tests had been performed on those specimens that already showed a decrease in weight gain in absorption tests. The relatively small amounts of mass loss indicate that not much material is lost during absorption before a maximum weight gain is attained.

The most material loss occurs at the most severe environment, i. e., 100°C/steam. Among the remaining environments those that give higher weight gains are also responsible for higher material losses. On the whole, SMC-R40 loses more material than SMC-R65 while SMC-R25C is more susceptible to material loss than SMC-R25W. The difference between R40 and R65 is plausible because the lost material is expected to be mostly from the matrix phase. As discussed earlier R25W is more stable environmentally than R25C. However, the difference in material loss is surprisingly small.

Table 9. Permanent loss of material (%) in desorption

Environment	Material				
	SMC-R25W	SMC-R25C	SMC-R40	SMC-R65	Polyester
RT/65			0.045	0.03	
RT/98	0.03	0.03	0.02	0.07	
RT/water	0.30	0.50	0.45	0.13	
75/65			0.08	0.05	
75/98	0.125	0.30	0.50	0.30	
75/water			0.60	0.15	
100/steam			2.9	1.40	

4.3.3 Swelling

Both thickness and in-plane swelling strains were measured during absorption, and the results are shown in Figs. 25 and 26. The in-plane strains were measured in two perpendicular directions parallel to the edges. However, only one set of measurements are shown in Fig. 26 because the two directions are indistinguishable and also because there was no consistent difference between the two sets.

Most of the swelling data are quite erratic in thac any consistent trend cannot be found easily. Composites can swell or contract with moisture absorption. Also swelling can be abruptly followed by contraction within the time scale used.

The three environments at RT and the 75°C/65% RH environment are mild in that no sign of damage is visible on specimens surfaces under these environments. The remaining three environments are severe for the present material systems because they lead to visible degradation of material.

In the thickness direction, R40 and R60 composites contract under the mild environments, while they swell under the severe environments, Fig. 25. No dimensional change is observed in all cases until some minimum amount of water is absorbed. The threshold weight gain depends on the type of environment as well as the type of composite. However, R25 composites swell under all the environments tested.

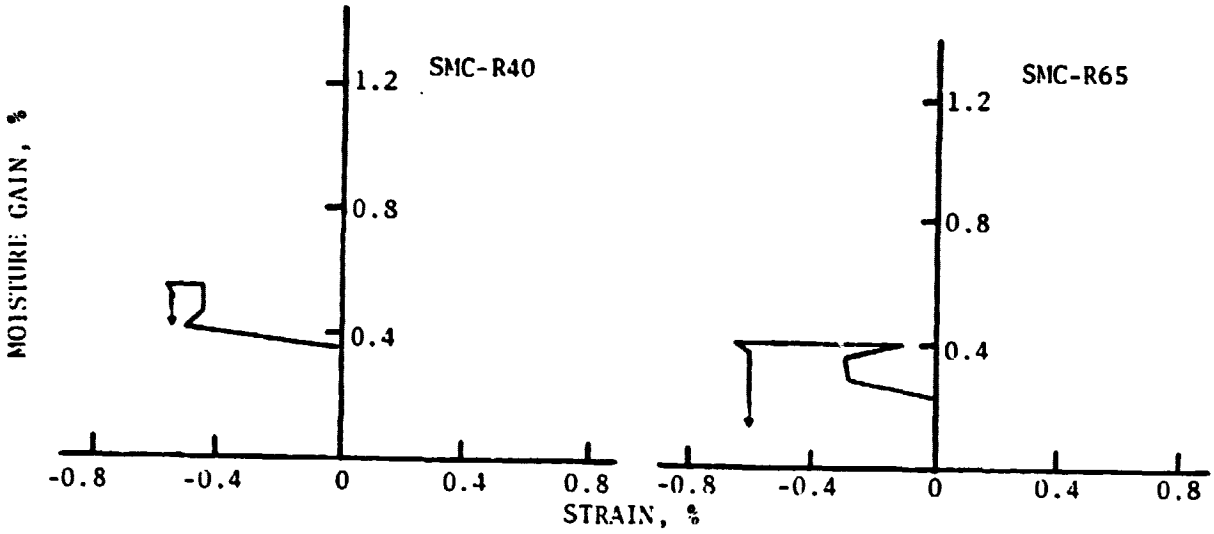

Fig. 25(a). Swelling strains in thickness direction at RT/65% RH

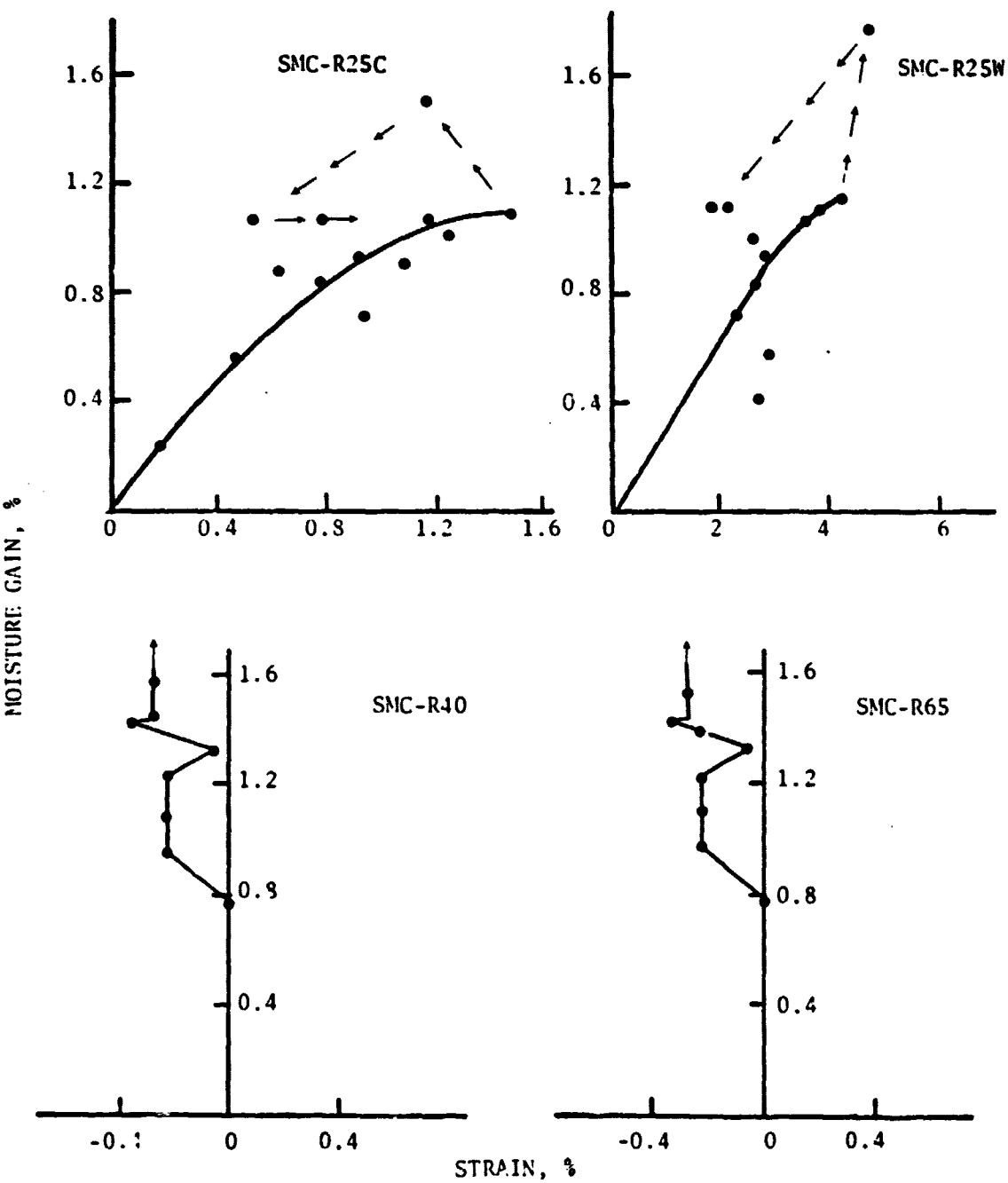

Fig. 25(b). Swelling strains in thickness direction at RT/98% RH

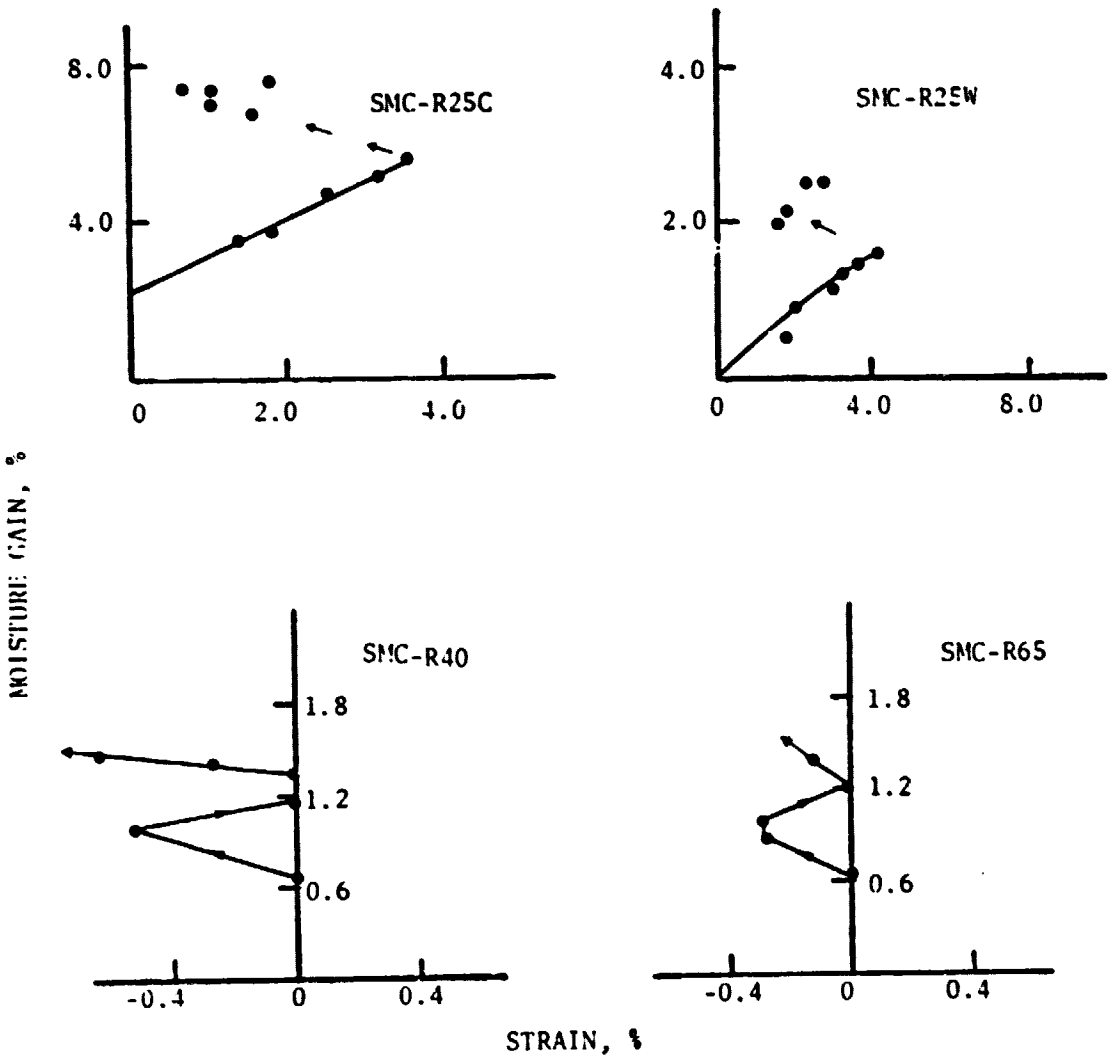

Fig. 25(c). Swelling strains in thickness direction at RT/water

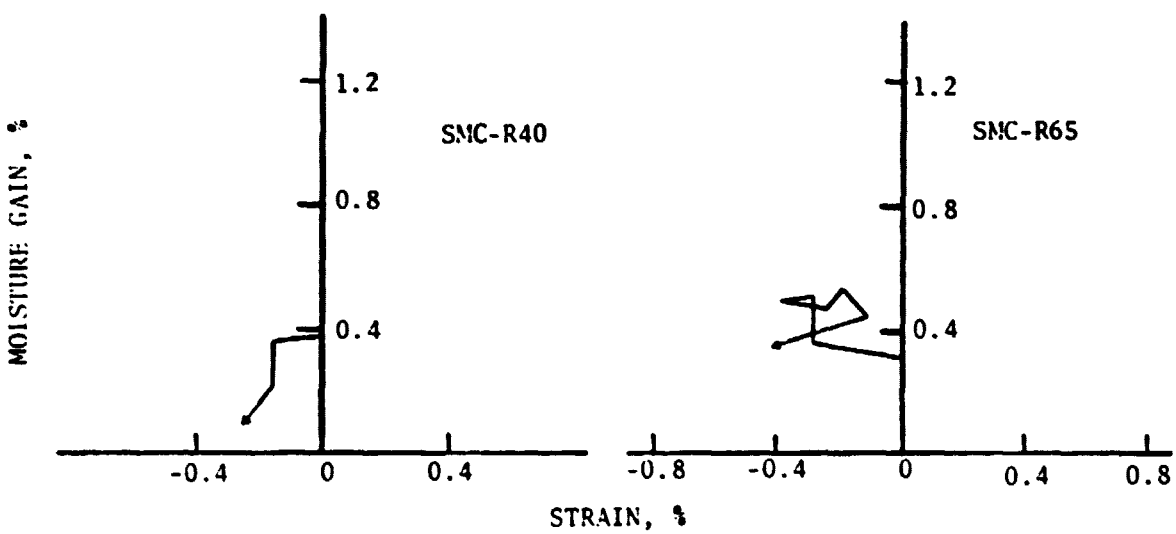

Fig. 25(d). Swelling strains in thickness direction at 75/65% RH

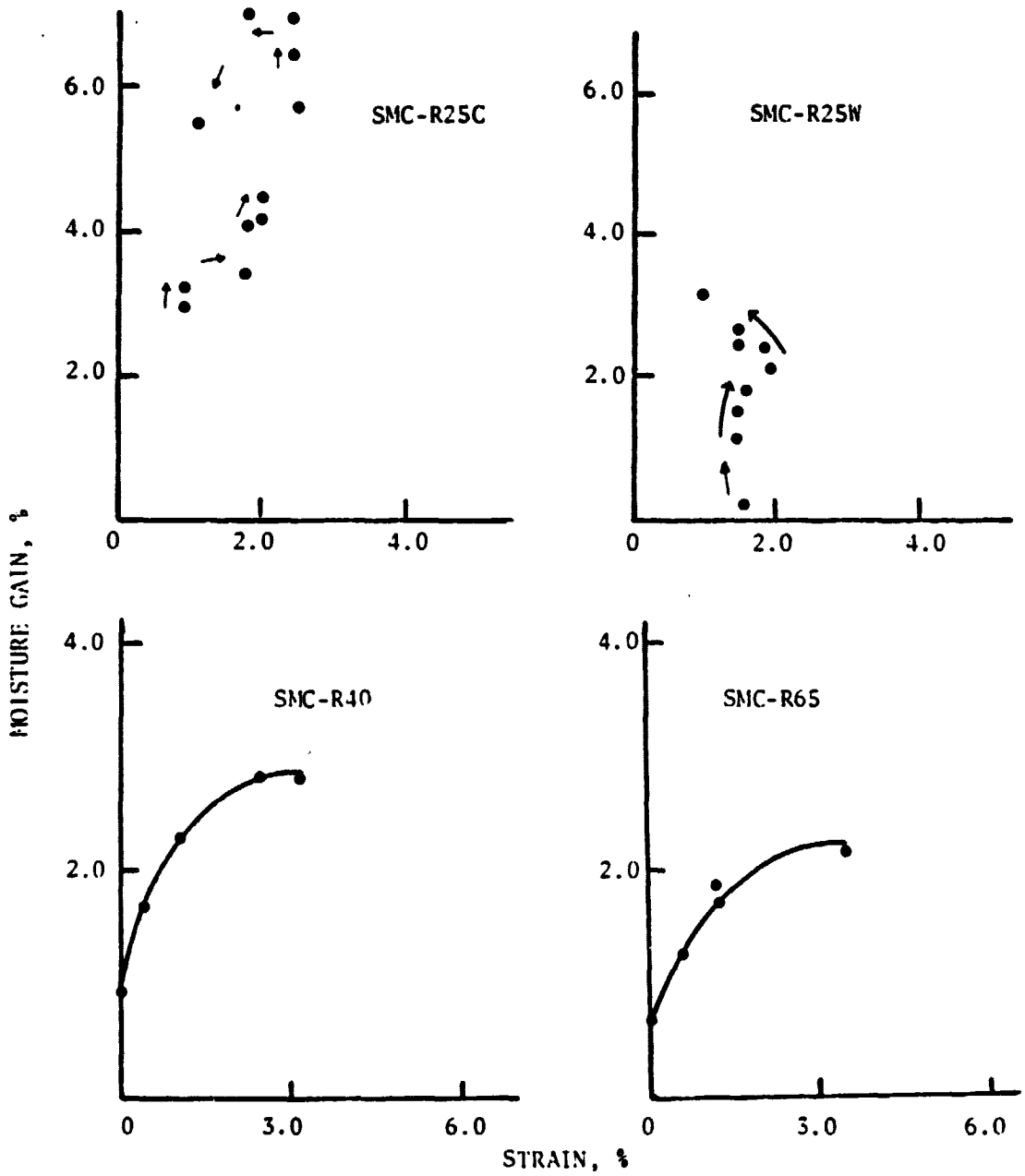

Fig. 25(e). Swelling strains in thickness direction at 75/98° RH

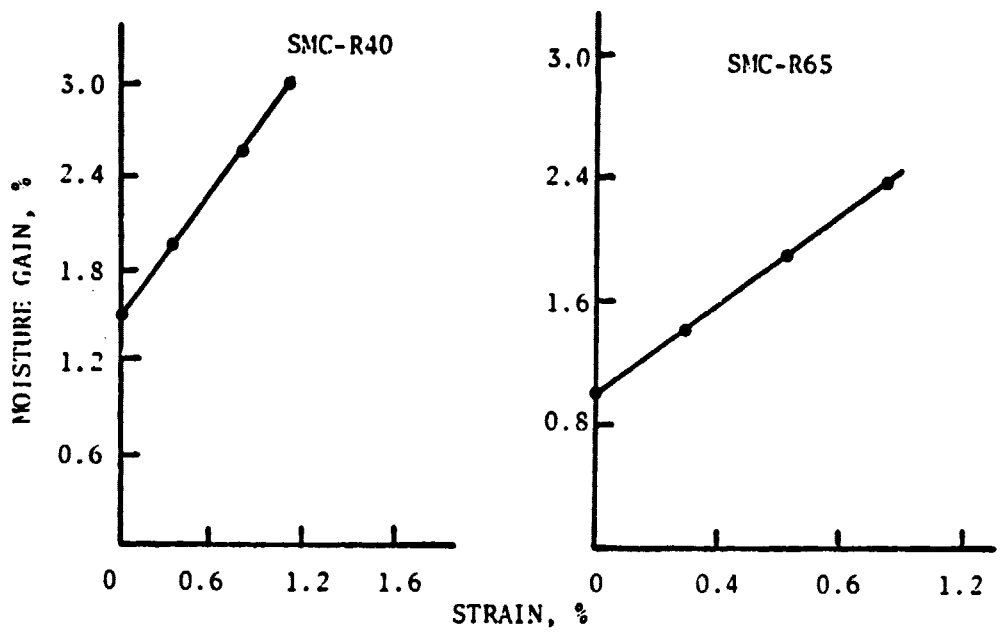

Fig. 25(f). Swelling strains in thickness direction at 75/water

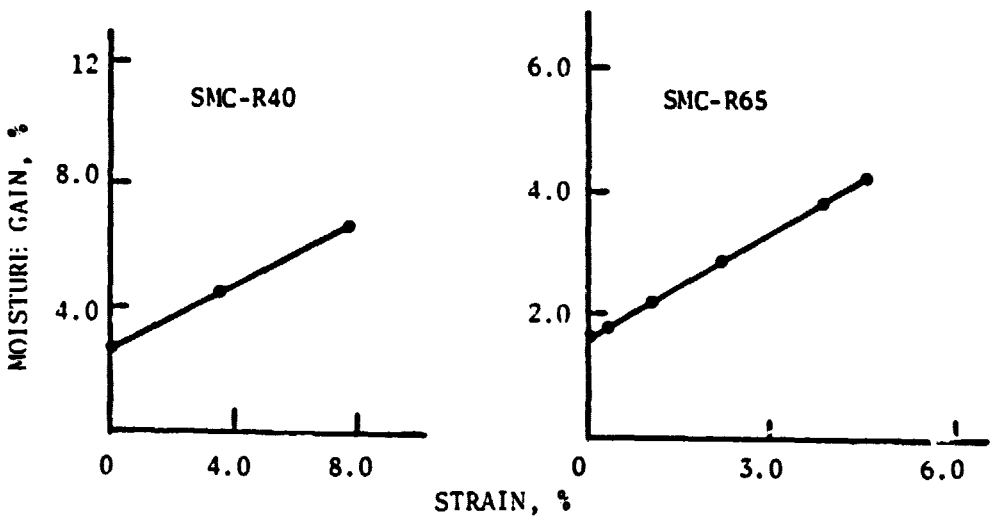

Fig. 25(g). Swelling strains in thickness direction at 100/steam

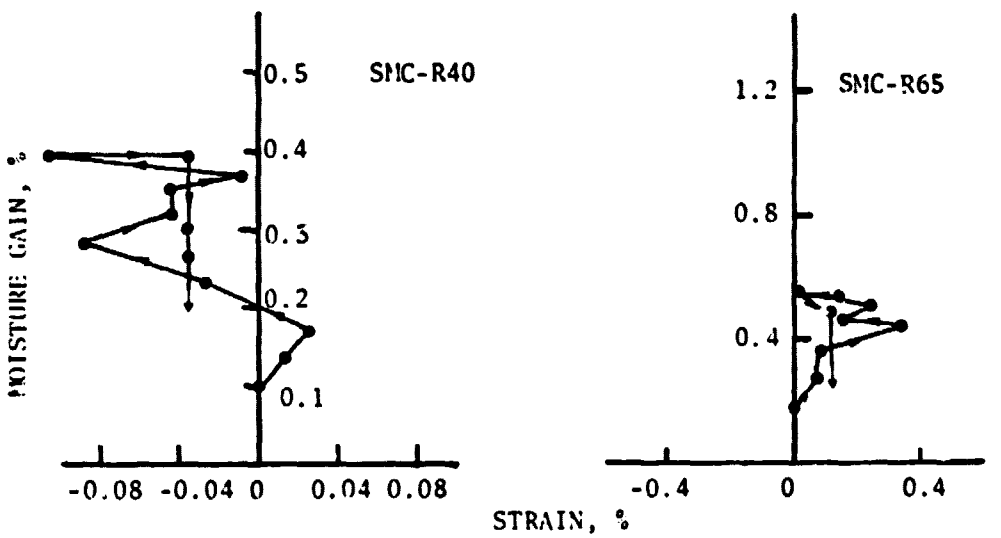

Fig. 26(a). Inplane swelling strains at RT/65% RH

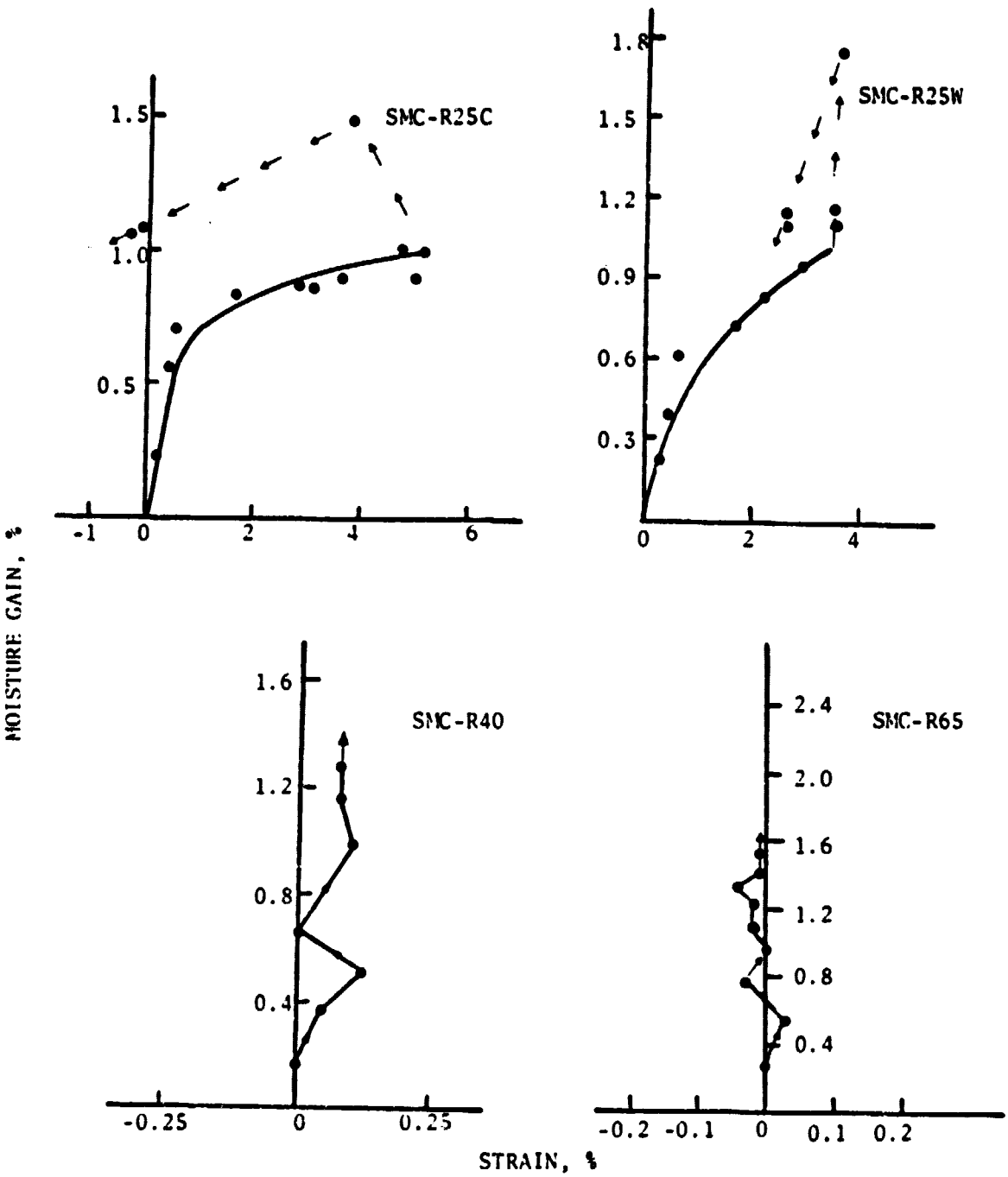

Fig. 26(b). Inplane swelling strains at RT/98% RH

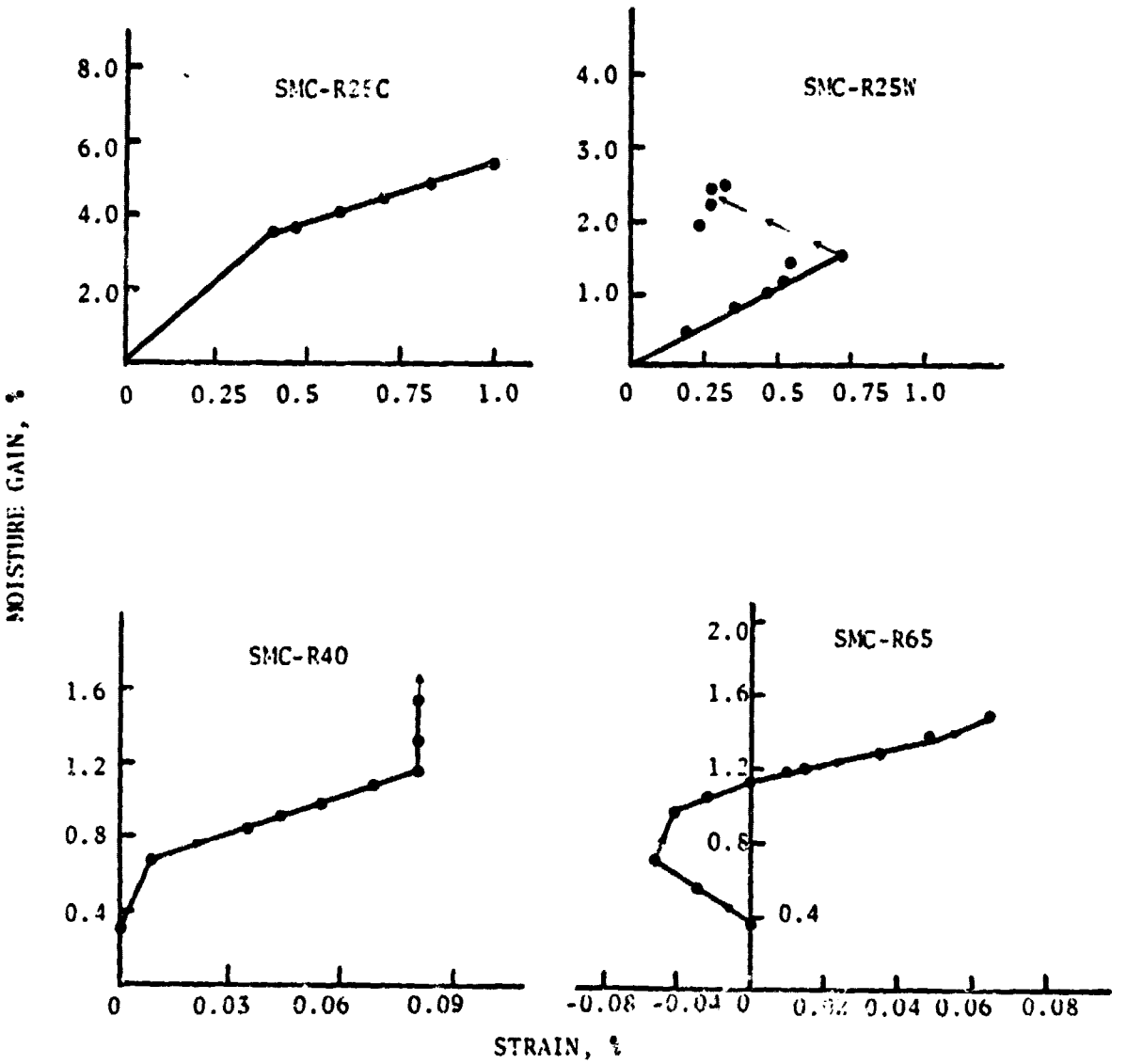

Fig. 26(c). Inplane swelling strains at RT/water

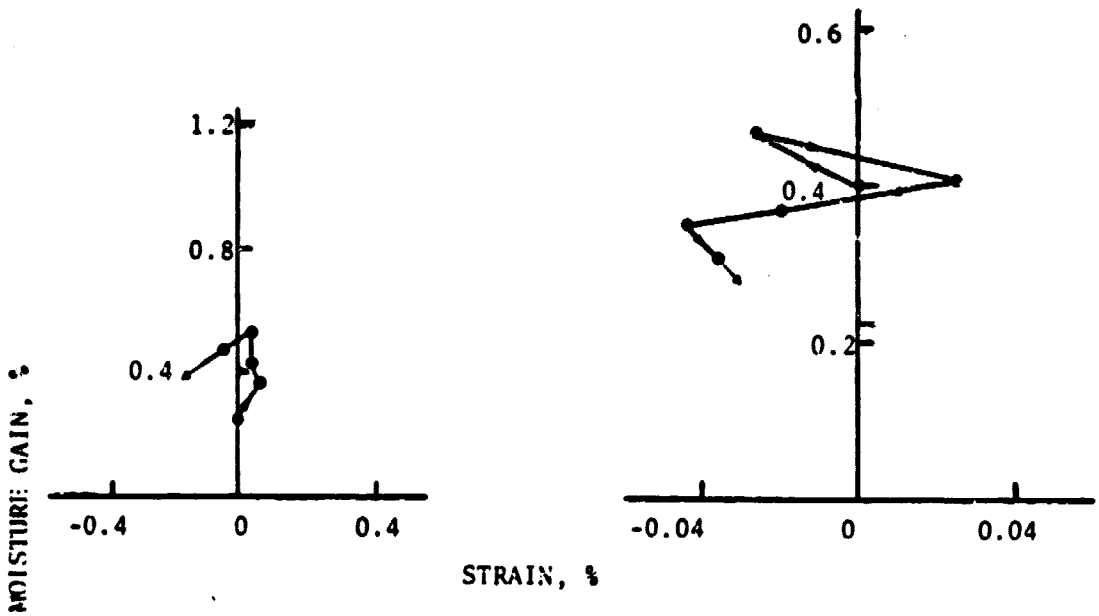

Fig. 26(d). Inplane swelling strain at 75/65% RH

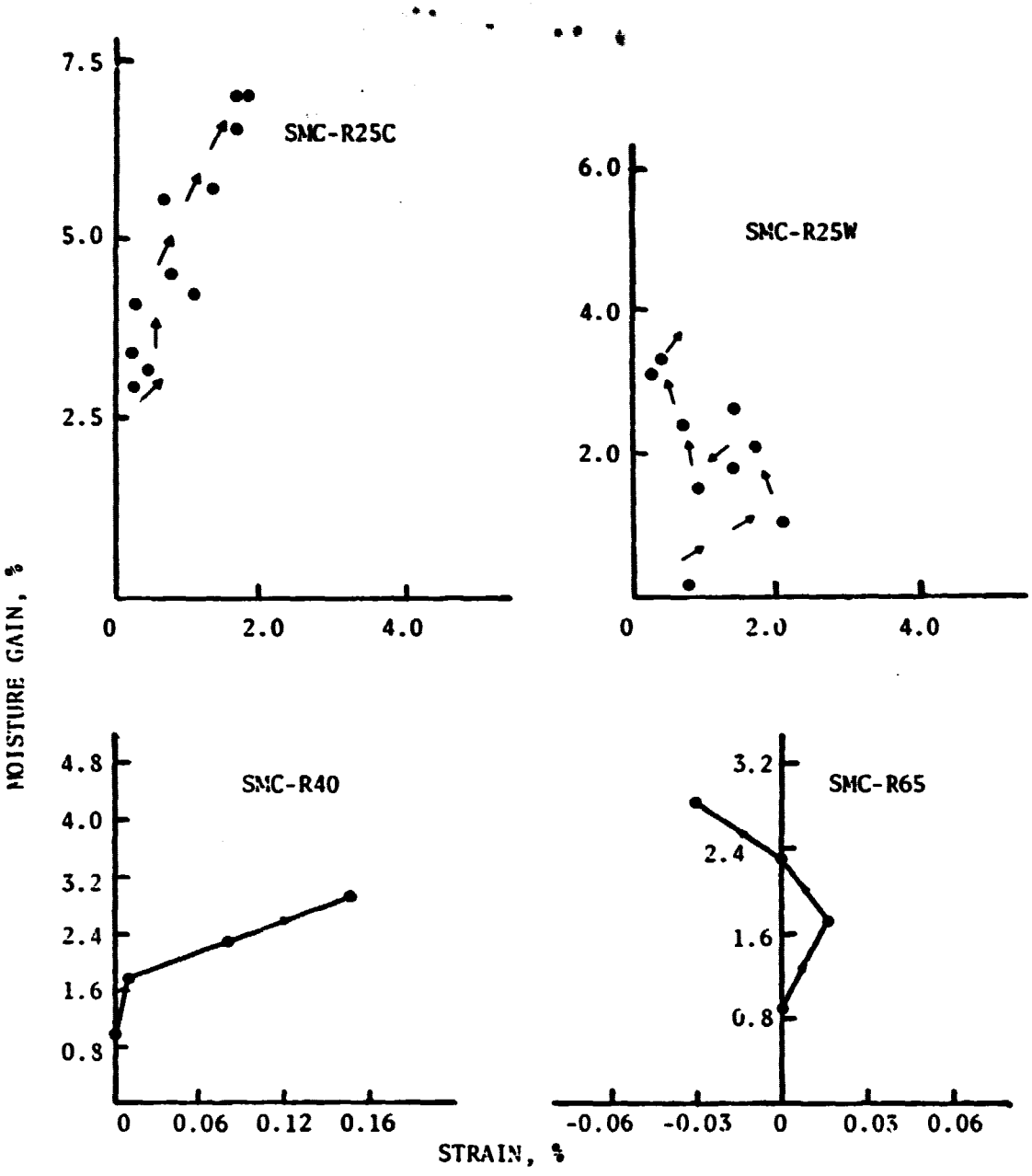

Fig. 26(e). Inplane swelling strains at 75/98% RH

C-2

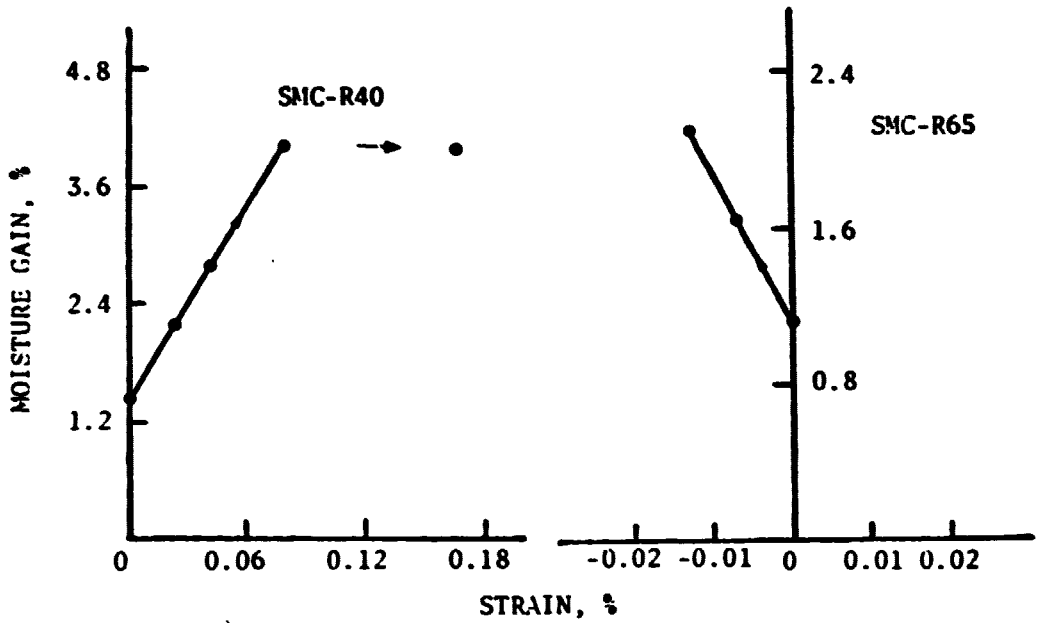

Fig. 26(f). Inplane swelling strains at 75/water

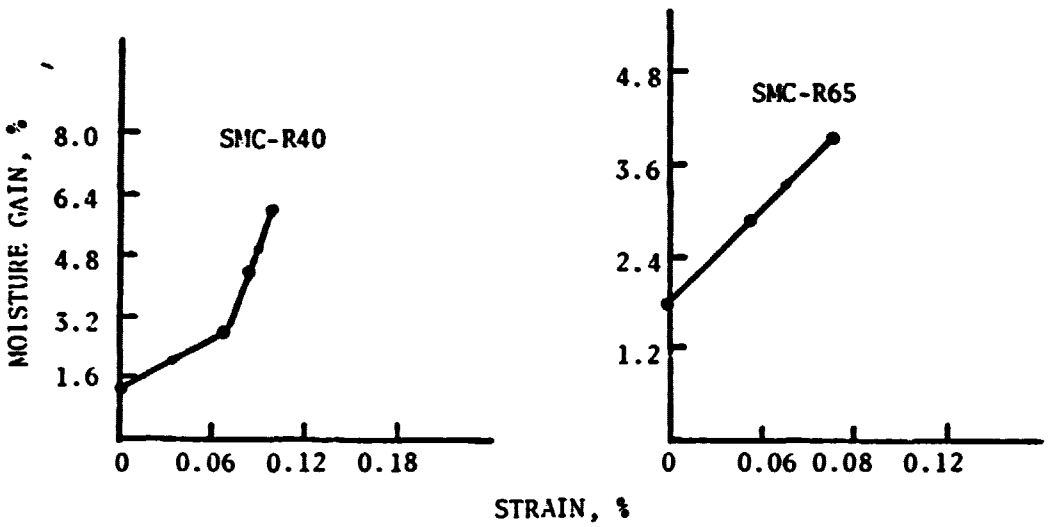

Fig. 26(g). Inplane swelling strains at 100/steam

R25 composite specimens swell in their plane also, Fig. 26. However, the in-plane strains of R40 and R60 composites can be positive or negative.

Part of the erratic swelling behavior in thickness direction is associated with blistering observed on specimen surfaces under the severe environments. Blisters resulted in apparent swelling during their growth stage. When they burst open, however, apparent contraction was measured. Yet the in-plane behavior cannot be explained by the blistering alone.

The bulk polyester did not show any noticeable change in dimensions until it reached maximum weight gain. Ashbee and Farrar [33] also reports negligible dimensional changes under water immersion for an ortho-phthalic polyester resin. Thus, the behavior of bulk polyester is in line with that of R40 and R60. However, R25 composites exhibit more swelling than expected.

4.3.4 Damage Development

Each time weight and dimensional measurements were taken, specimens were visually inspected for any sign of damage. Two types of changes were looked for on the specimen surface. The first change was in color and the second was the development of blisters and cracks.

(a) SMC-R25W (top), SMC-R25C (bottom)--from left, no exposure, 75°C/98% RH, RT/98% RH, RT/water

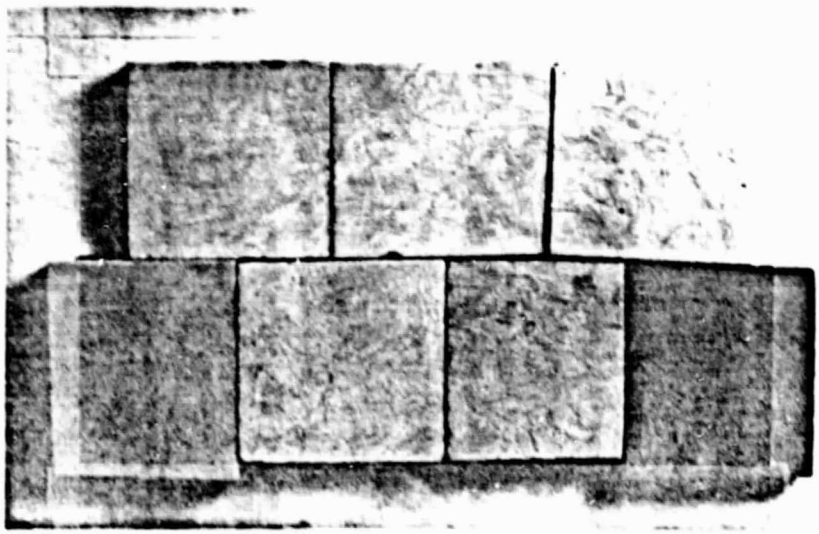

(b) SMC-R65--from left clockwise, RT/65% RH, RT/98% RH, RT/water, 100°C/steam, 75°C/water, 75°C/98% RH, 75°C/65% RH

Fig. 27. Color change on specimen surface

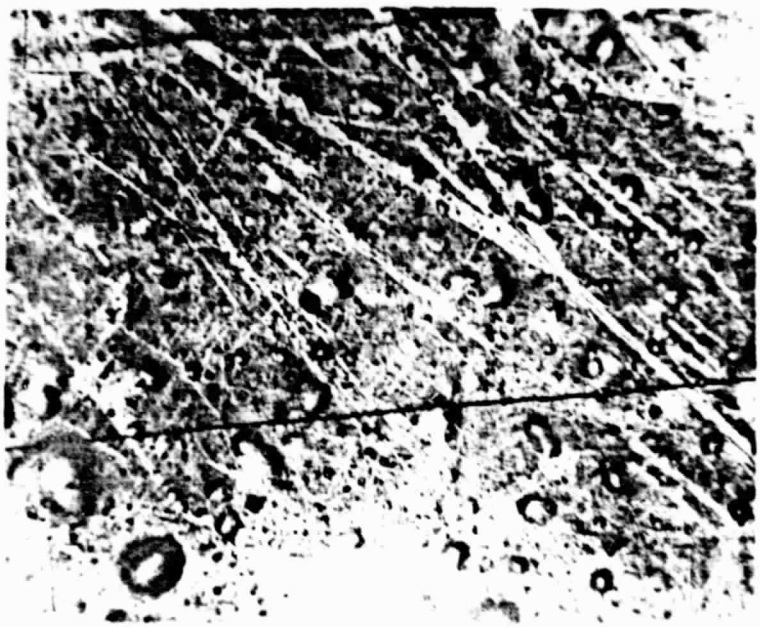

Fig. 28. Formation of small blisters, SMC-R65 at 100°C/steam

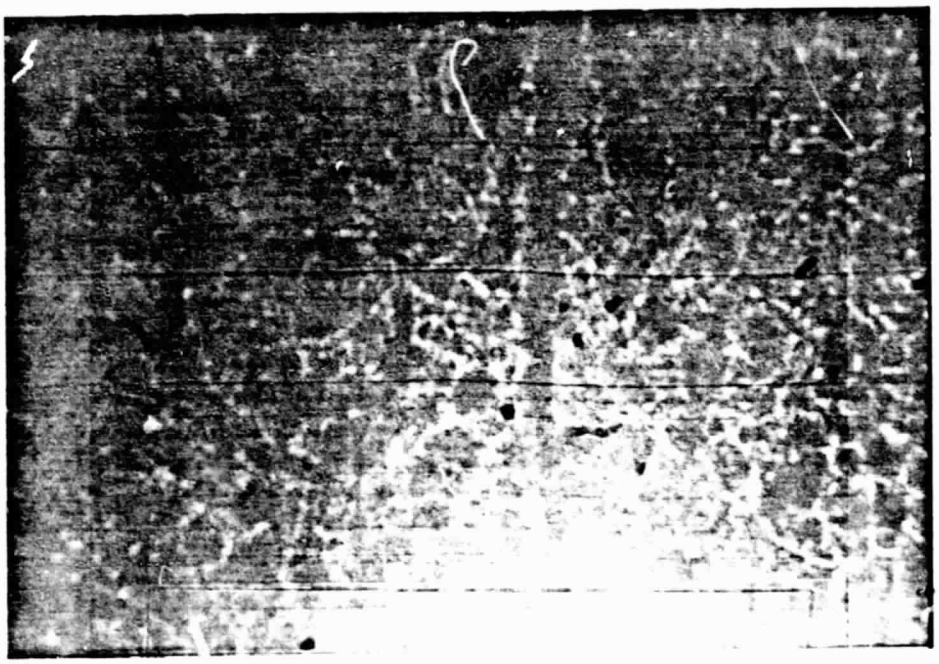

Fig. 29. Surface with many small blisters burst open, SMC-R65 at 75°C/98% RH

Fig. 30. Cracks on surface of bulk polyester specimen, 100°C/steam

There was not visibile sign of damage under all room temperature environments except for a slight change in color for R25 specimens immersed in water. However, all specimens changed color at 75°C, as described in Table 9. Pictures of specimens are shown in Fig. 27. Note the voids in SMC-R25 specimens. SMC specimens did not share the color of the bulk polyester counterparts under the same environment.

Small blisters about 100 μm in diameter were observed on specimen surface at 75°C regardless of relative humidity and also at 100°C/steam. These blisters were seen only on the composite specimens but not on the bulk polyester specimens. With time some of these blisters grew to 2-3 mm in diameter, as shown in Fig. 28, and burst open damaging the glossy appearance of the surface.

At 75°C/water and 100°C/steam large blisters formed. These blisters were clearly visible to the naked eye. Blistering was most severe at 75°C/water for all specimens. In bulk polyester blisters could be as large as 1 cm in diameter. When a blister was cut open, liquid was seen coming out. When the large blisters burst open, they left small craters.

The most severe damage in the form of surface cracks was seen in bulk polyester at 100°C/steam, Fig. 30. Although not clear in the figure, most of these cracks were fairly well aligned. The composite specimens rarely showed surface cracks even under the same environment.

Fibers seem effective in preventing surface cracks.

The blisters are certainly responsible for increased weight gain, as the experimental data indicate. The apparent temperature dependence of maximum weight gain in Fig. 23 can thus be explained at least partially by the blistering. Since no blistering was observed at 75°C/65% RH, both RT and 75°C weight gains would be expected to be equal to each other.

To investigate the internal damage in more detail, specimens were cut through the middle and cross sections were examined on an optical microscope. The color changes and damages observed are summarized in Table 11. The most drastic change in color was observed at 100°C/steam, Fig. 31. The specimens are the same as those in Table 10.

For many specimens which had been subjected to the severe environments the inside had different color than the outside. A thin surface layer could be easily observed from the color difference. The most drastic difference in color was observed in the bulk polyester specimen at 75°C/65% RH. Although the surfaces were dark silver, the inside was sienna brown, Fig. 32. However, all composite specimens did not show any change of color at this environment.

Photomicrographs of R25C specimens are shown in Fig. 33. This composite had voids visible to the naked eye even before any environmental exposure. These voids are clearly seen to be in resin-rich

Table 10. Color change and damage on specimen surface

Material	Environment	Period of exposure (days)	Color Before	Color After	Damage
R25C,	RT/98	220	white	white	none
R25W	RT/water	220	white	gray	none
	75/98	220	white	yellow	large blisters
R40,	RT/65	180	white	white	none
R65	RT/98	180	white	white	none
	RT/water	180	white	white	none
	75/65	180	white	cream	small blisters
	75/98	180	white	yellowish cream	small blisters
	75/water	180	white	whitish raw umber	small blisters large blisters
	100/steam	100	white	gray and raw umber	small blisters large blisters
Polyester	RT/65	150	opaque	opaque	none
	RT/98	150	opaque	opaque	none
	RT/water	150	opaque	opaque	none
	75/65	150	opaque	dark silver	none
	75/98	140	opaque	canary yellow	none
	75/water	140	opaque	light raw umber	large blisters
	100/steam	65	opaque	yellow ochre	cracks

Table 11. Color change and damage observed on cross section

Material	Environment	Period of exposure (days)	Color		Damage
			Before	After	
R25C	RT/98	220	white	white	large voids
	RT/water	220	white	white	large voids
	75/98	220	white	whitish canary yellow	large voids, cracks
R25W	RT/98	220	white	white	no damage
	RT/water	220	white	white	no damage
	75/98	220	white	whitish canary yellow	large voids, cracks
R40,	RT/65	180	white	white	no damage
R65	RT/98	180	white	white	no damage
	RT/water	180	white	white	no damage
	75/65	180	white	white	no damage
	75/98	180	white	brown, white	voids, cracks
	75/water	180	white	white, gray	voids, cracks
	100/steam	100	white	dark brown	voids, cracks
Polyester	RT/65	150	opaque	opaque	no damage
	RT/98	150	opaque	opaque	no damage
	RT/water	150	opaque	opaque	no damage
	75/65	150	opaque	sienna brown	no damage
	75/98	140	opaque	grayish canary yellow	no damage
	75/water	140	opaque	white	large cracks
	100/steam	65	opaque	grayish yellow ochre	cracks parallel to surface

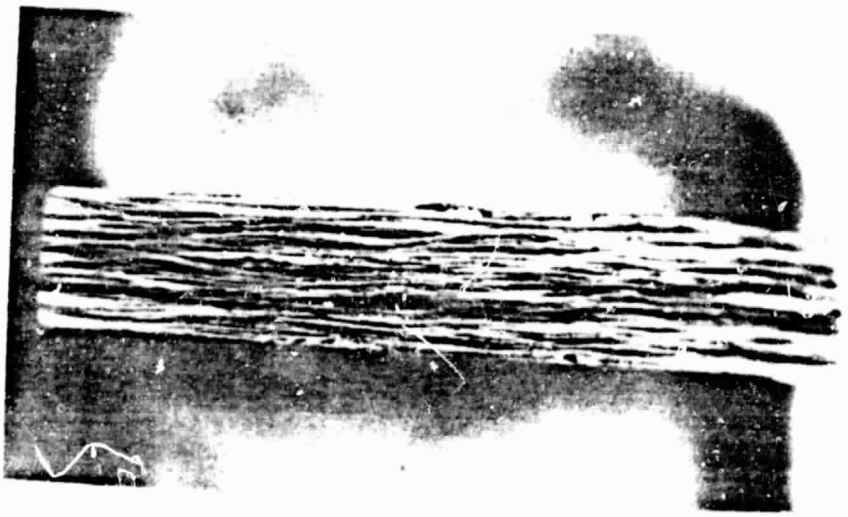

Fig. 31. Cross section of SMC-R65 at 100°C/steam

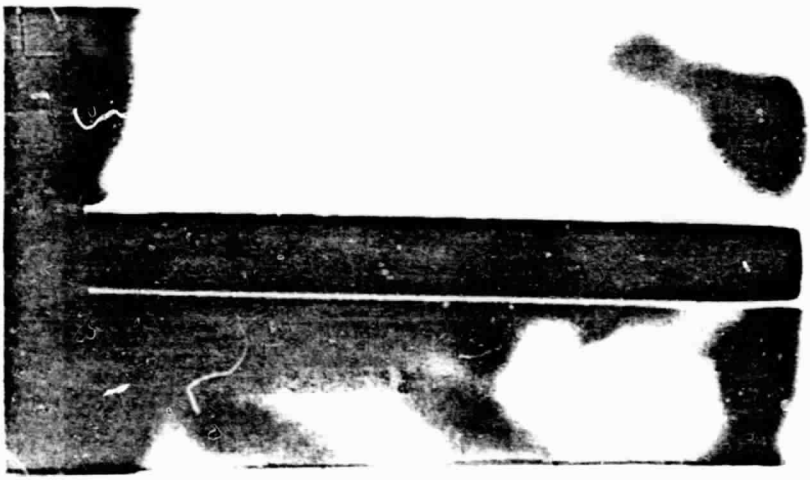

Fig. 32. Cross section of bulk polyester at 75°C/65% RH

(a)

(b)

Fig. 33. Photomicrographs of SMC-R25C: (a) no exposure; (b) RT/98% RH

(c)

(d)

Fig. 33 (cont.). Photomicrographs of SMC-R25C: (c) RT/water; (d) 75°C/98% RH

(a)

(b)

Fig. 34. Photomicrographs of SMC-R25W: (a) no exposure; (b) RT/98% RH

(c)

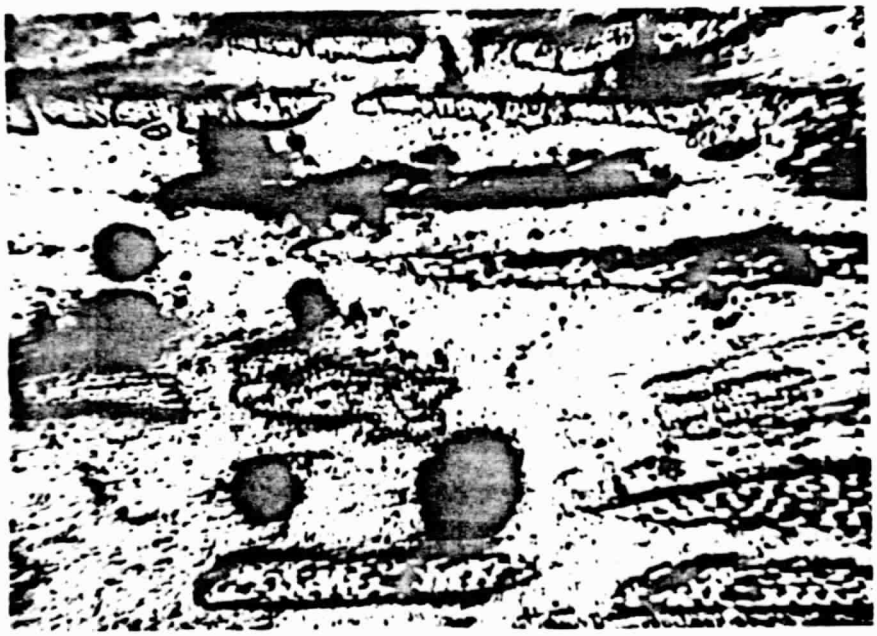

(d)

Fig. 34 (cont.). Photomicrographs of SMC-R25W: (c) RT/water; (d) 75°C/98% RH

(a)

(b)

Fig. 35. Photomicrographs of SMC-R40: (a) RT/65% RH; (b) RT/98% RH

(c)

(d)

Fig. 35 (cont.). Photomicrographs of SMC-R40: (c) RT/water; (d) 75°C/65% RH

(e)

(f)

Fig. 35 (cont.). Photomicrographs of SMC-R40: (e) 75°C/98% RH; (f) 75°C/water

(g)

Fig. 35 (cont.). Photomicrographs of SMC-R40: (g) 100°C/steam

(a)

(b)

Fig. 36. Photomicrographs of SMC-R65: (a) RT/65%; (b) RT/98% RH

(c)

(d)

Fig. 36 (cont.). Photomicrographs of SMC-R65: (c) RT/water; (d) 75°C/65% RH

(e)

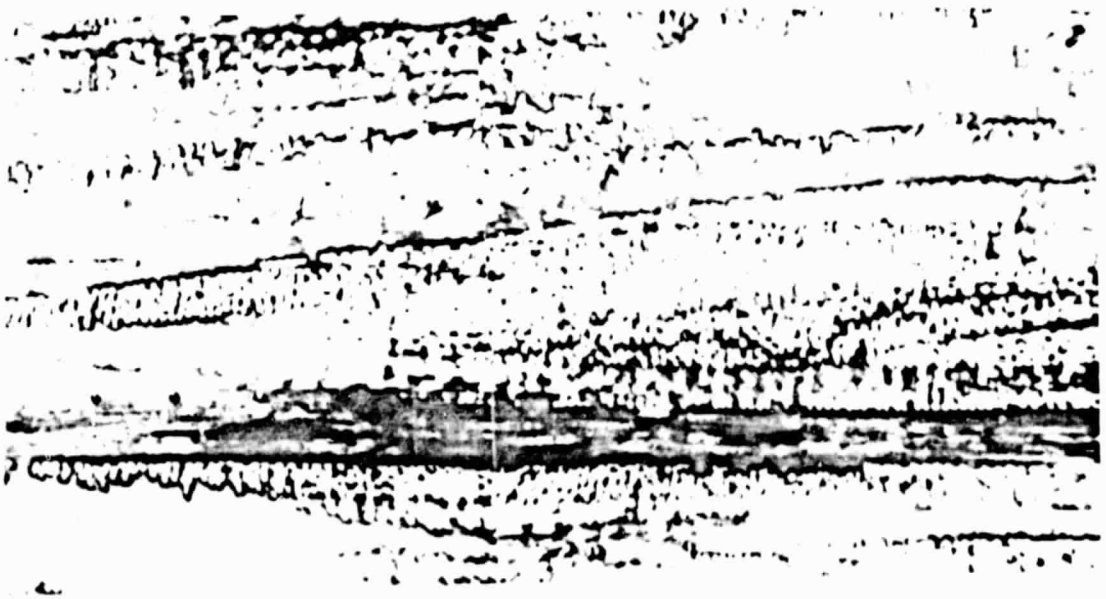

(f)

Fig. 36 (cont.). Photomicrograph of SMC-R65: (e) 75°C/98% RH; (f) 75°C/water

(g)

Fig. 36 (cont.). Photomicrographs of SMC-R65: (g) 100°C/steam

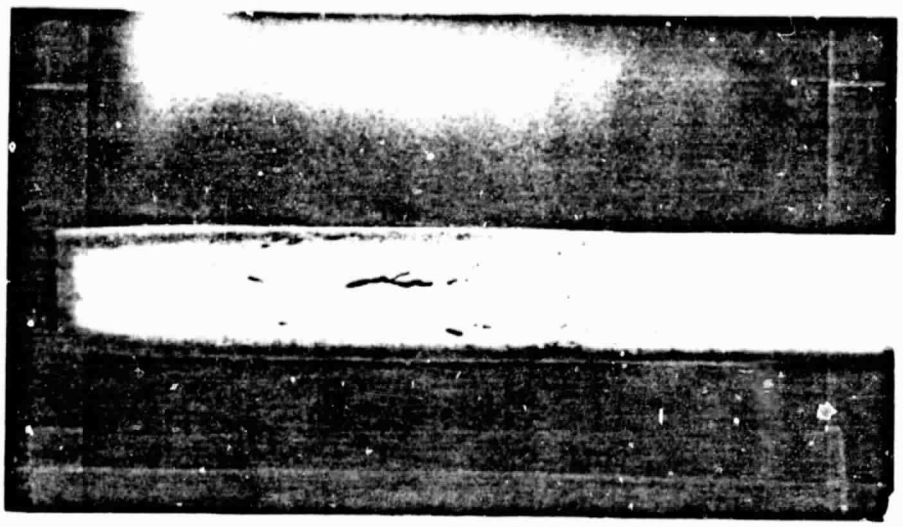

(a)

(b)

Fig. 37. Cracks in bulk polyester: (a) 75°C/water; (b) 100°C/steam

areas in Fig. 32. At 75°C/98% RH voids are larger, and, although not shown in the photomicrograph, delamination cracks developed and grew to blisters when they were rear the surface.

R25W composite is fairly void free, Fig. 34. Further formation of voids is not noticeable except at 75°C/98% RH.

Both R40 and R65 composites are also almost free of voids, Figs. 35 and 36. Voids are more frequently detected at 75°C environments. At 75°C/water delamination cracks are seen in resin-rich areas. Delamination cracks are larger at 100°C/steam.

In bulk polyester no voids or cracks are seen except at 75°C/water and 100°C/steam. At 75°C/water a large delamination crack developed near the mid plane, Fig. 37. Smaller cracks are almost parallel to the surface. It should be noted that no cracks were found in the planar surfaces.

Under 100°C/steam environment cracks developed everywhere although no crack grew big enough to cause delamination as observed at 75°C/water, Fig. 37. Again, all cracks on cross sections were almost parallel to the surface. The cracks on the surfaces were also fairly well aligned, indicating the possibility of an oriented structure.

From the observations described so far the following mechanism is

proposed for the development of damage under the environments studied. In composites moisture diffuses into voids and builds up pressure especially at elevated temperature. Cracks then develop from the voids and grow in the plane of the laminate. The fairly planar arrangement of fibers in SMC prevents crack growth normal to the plane. If the crack is near the surface, the pressure inside can push up the surface layer of polyester and a blister is seen on the surface.

Blistering was also reported by other investigators [47-50]. However, the observed blistering was between the gel coat and SMC substrate.

The observed damage agrees very well with the relative attenuation measured by the ultrasonic flaw detector, Fig. 38. In the figure environments are arranged in the increasing order of severity. The relative attenuation is defined as log A/A_o where A_o and A are the magnitudes of the reflected pulse in the specimens which have been subjected to RT/65% RH and any other environment, respectively. For SMC-R25 composites, specimens with no exposure were substituted for the reference data at RT/65% RH. The arrows in the figure indicate that the relative attenuation is higher than 40 db. Note that the damage at 100°C/steam is so severe that no composite exhibits a relative attenuation lower than 40 db.

4.3.5 Thermal Expansion

A typical thermal expansion curve for polyester is shown in Fig.

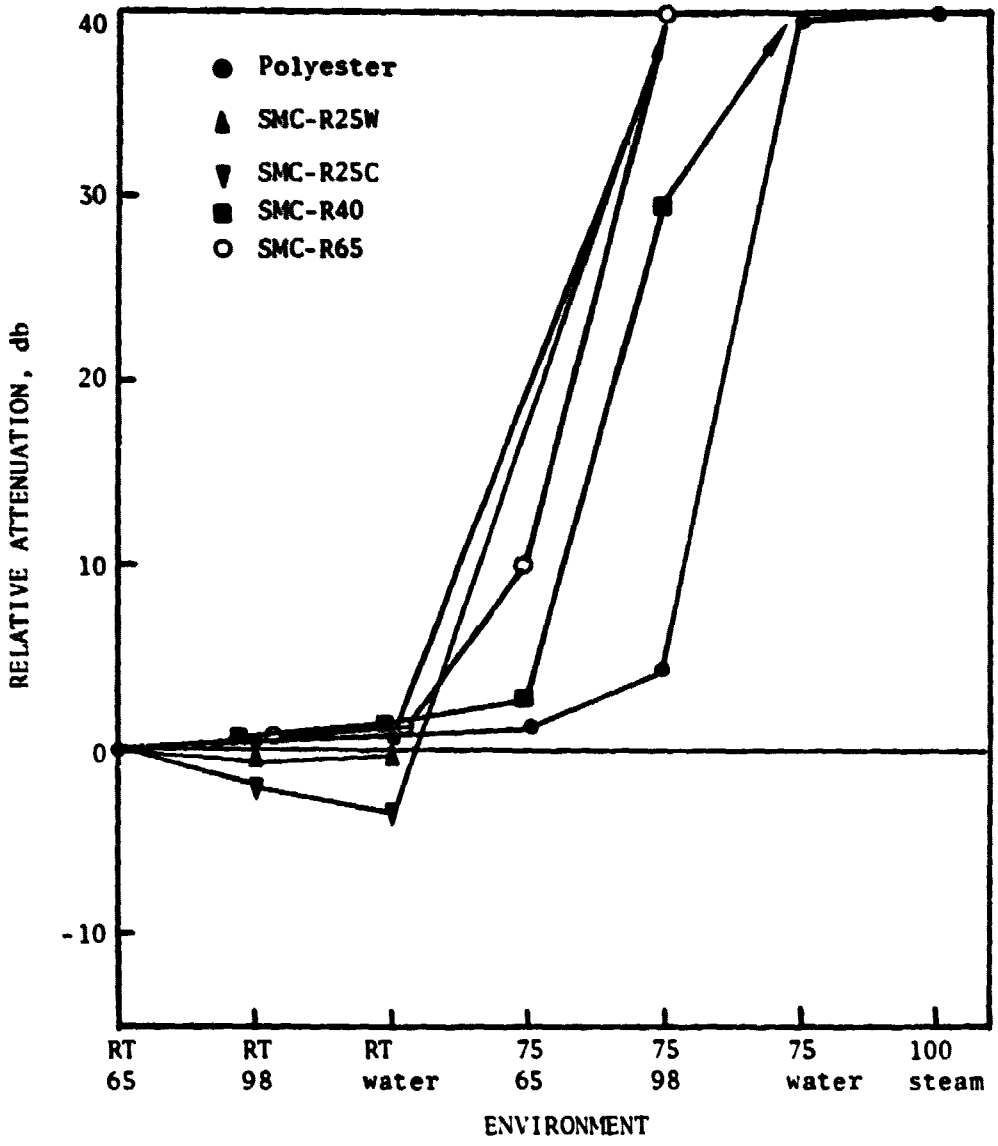

Fig. 38. Effect of environment on ultrasonic attenuation

39. The glass transition temperature is seen to be around 110°C.

For SMC-R40 and -R60 the thermal expansion behavior over the glass transition temperature is different from that of bulk polyester. Figure 40 is an in-plane thermal expansion curve for an SMC-R40 specimen. The slope above T_g remains fairly constant at a lower value than below T_g. However, in the thickness direction the thermal expansion curve of SMC composites is similar to that for amorphous polymers, Fig. 41.

The effect of fiber aspect ratio on the coefficients of thermal expansion of unidirectional composites is shown in Fig. 42. The prediction is based on Eqs. (1), (2), (10), (11), and (18). The predicted values of α_L and α_T at $\ell/d = 1$ are different from each other because the equations used are not valid in this case. The fiber aspect ratio is seen to have negligible effect when it is greater than ~100. The experimental results are all greater than the predictions.

The coefficients of thermal expansion for SMC composites are shown in Fig. 43, where the curves represent the predictions based on Eqs. (20) through (23). Note that the fiber aspect ratio of SMC composites is large enough to allow them to be treated as continuous fiber composites. The data for α_o show very little dependence on fiber volume content. The in-plane coefficient of thermal expansion α_I was measured in two normal directions, and both results are shown in the figure. Note the difference between these two points, indicating a slight anisotropy of

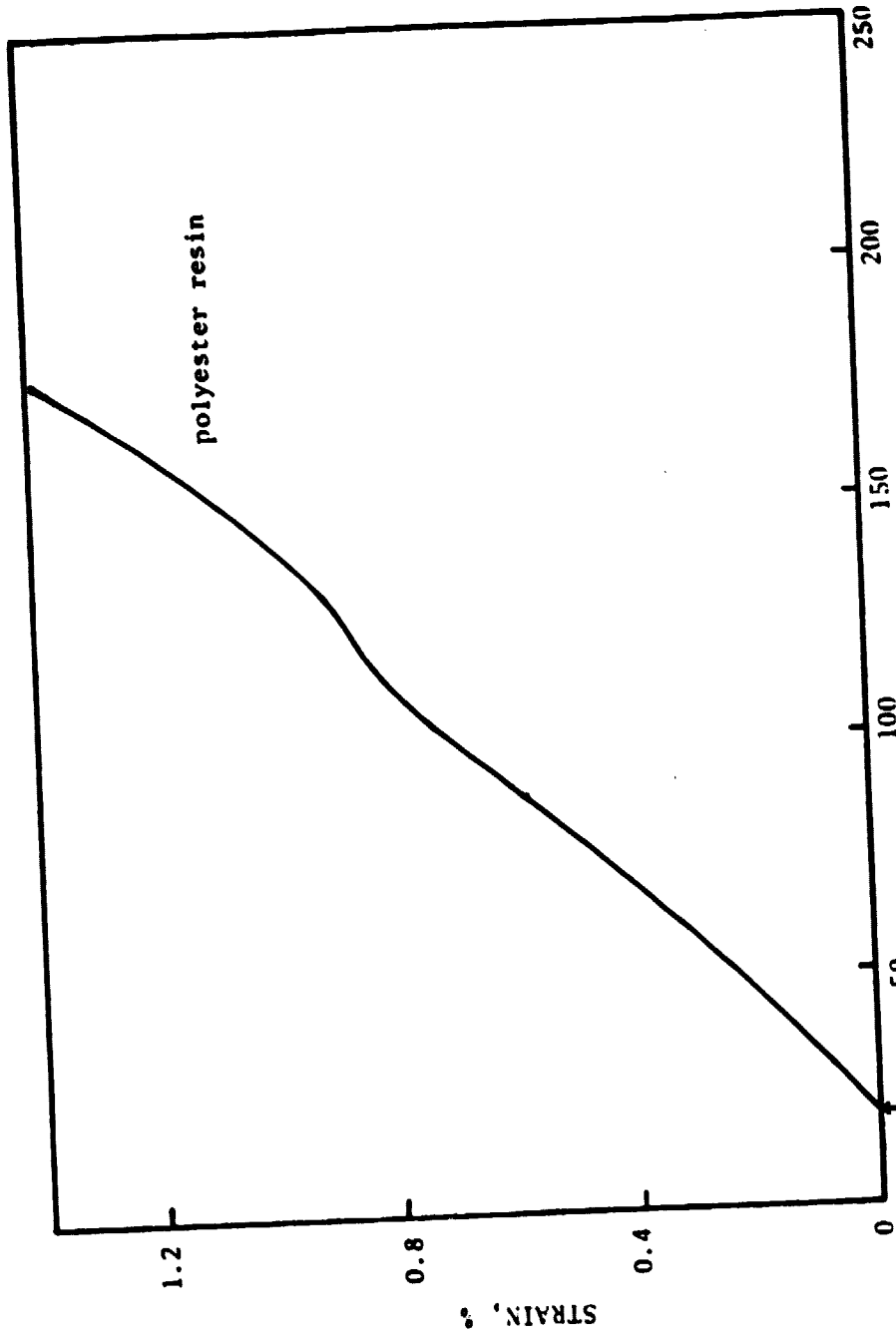

Fig. 39. Thermal expansion for polyester resin

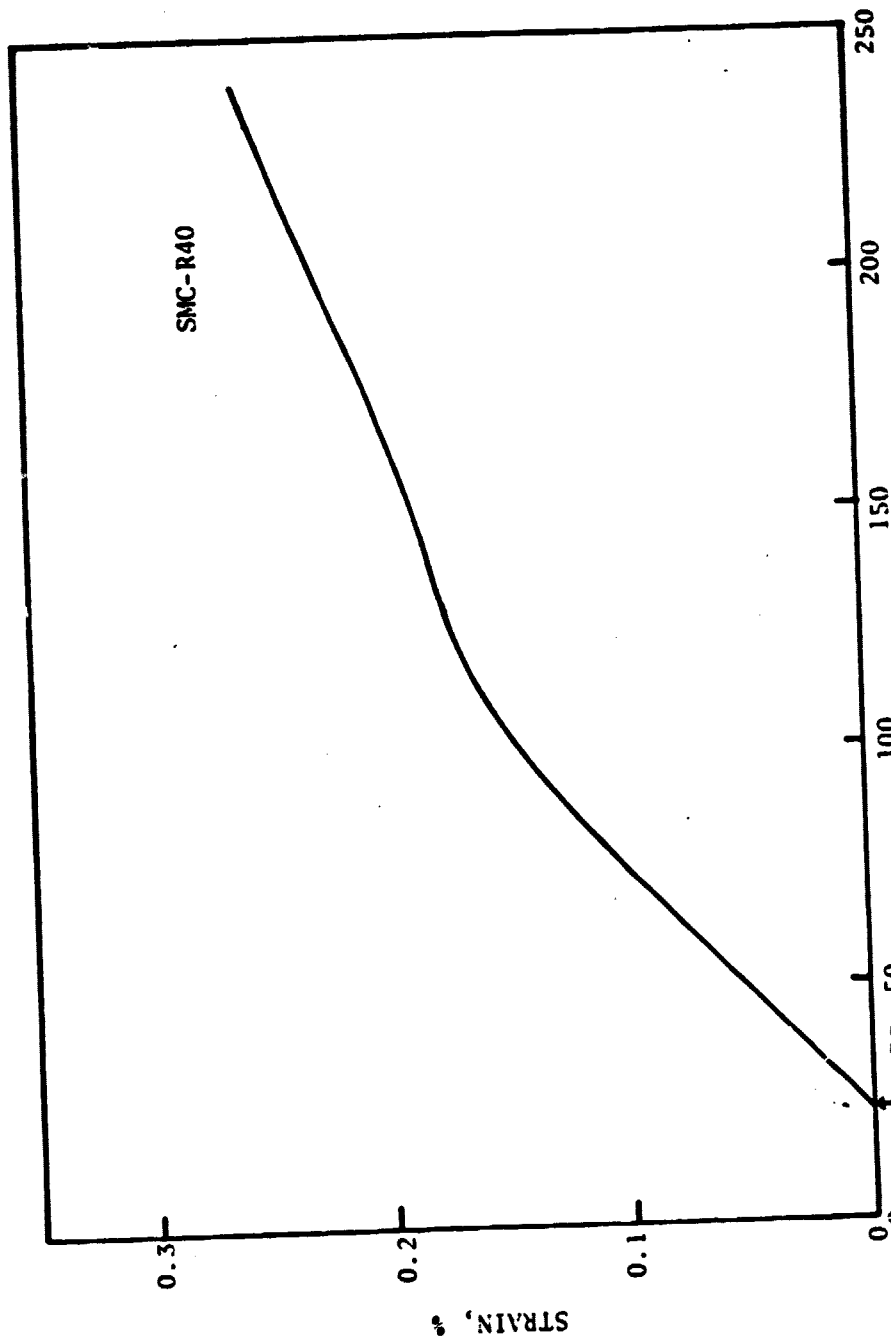

Fig. 40. Inplane linear thermal expansion for SMC-R40

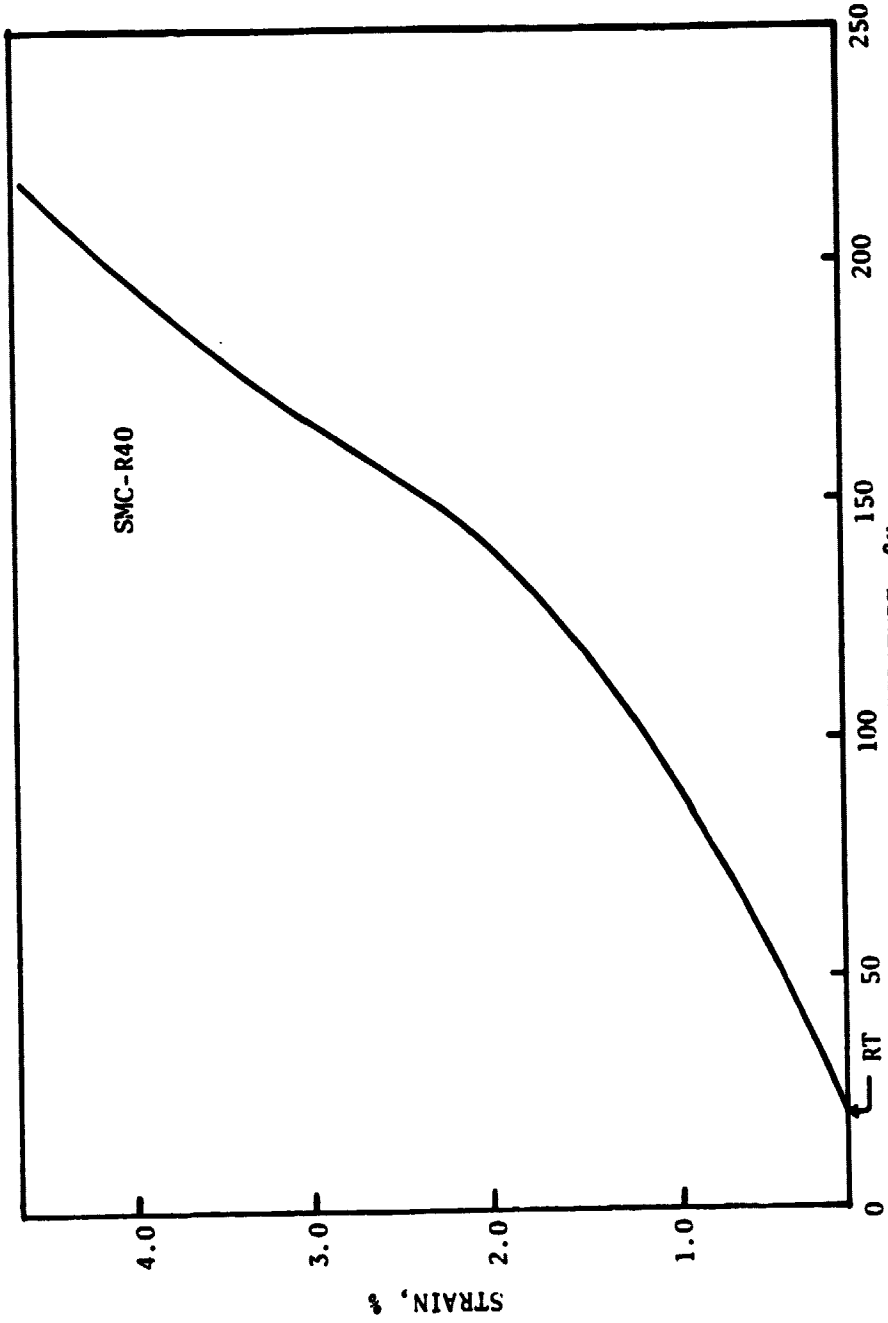

Fig. 41. Thermal expansion in thickness direction for SMC-R40

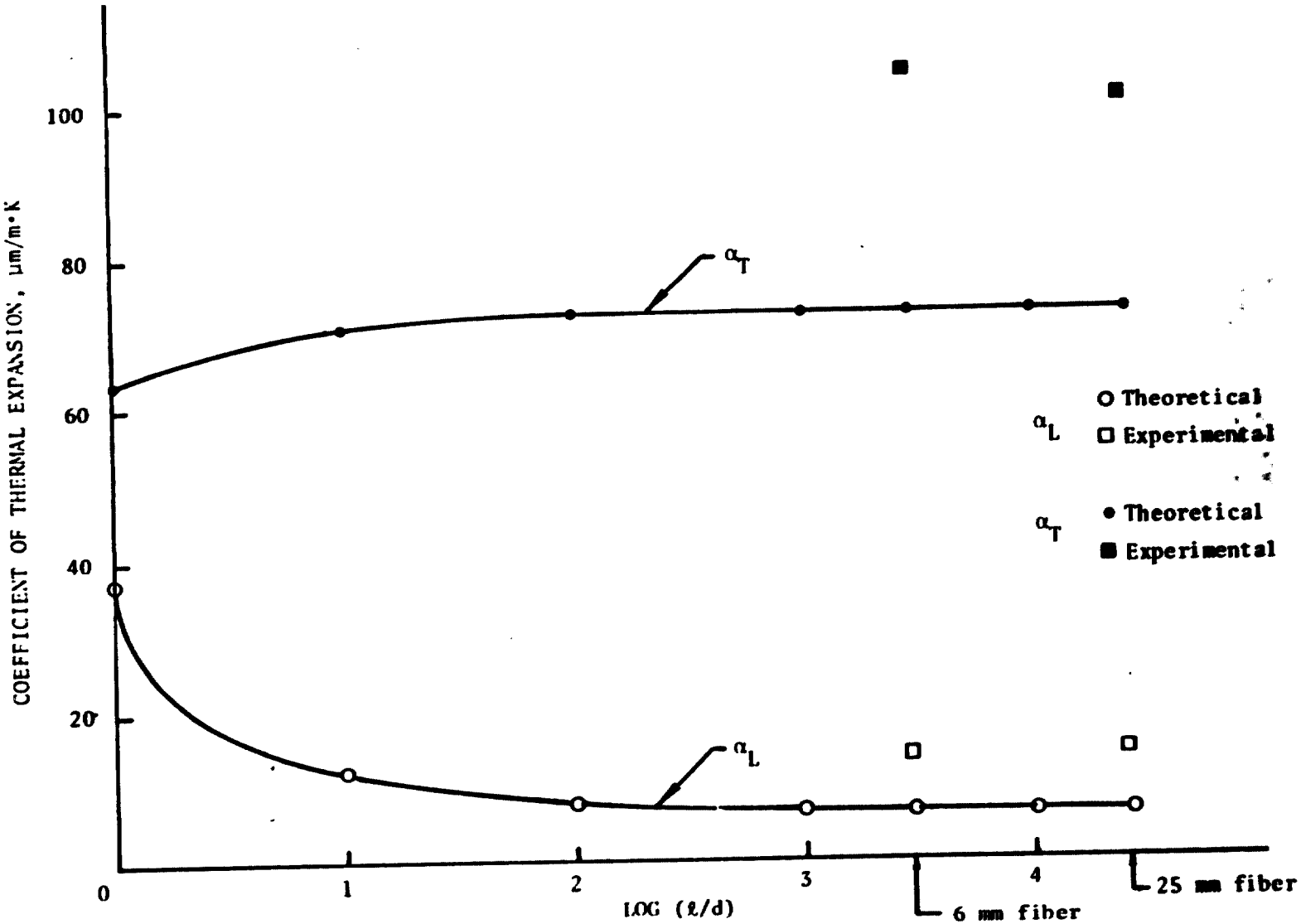

Fig. 42. Coefficient of thermal expansion vs. fiber aspect ratio for unidirectional composites

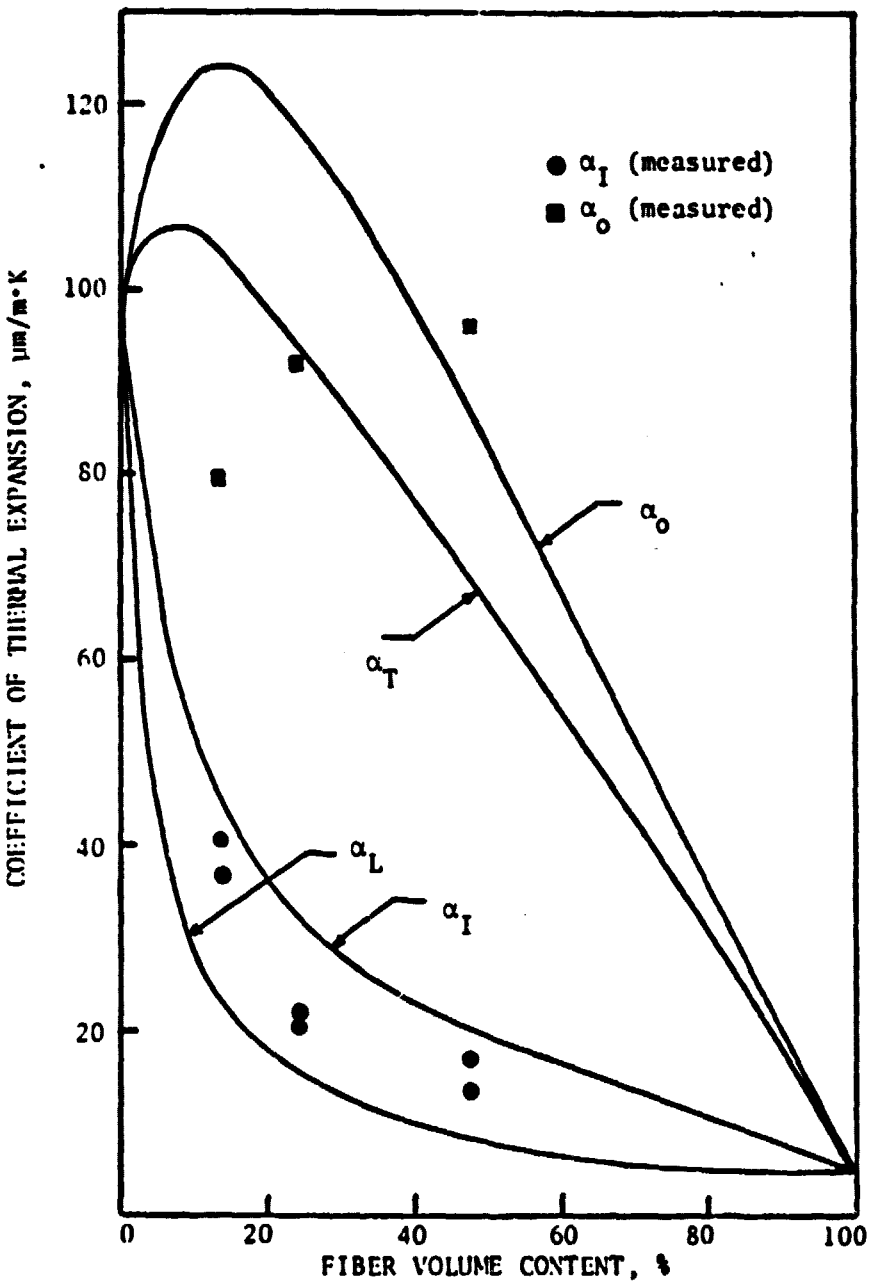

Fig. 43. Various coefficients of thermal expansion for SMC composites

the composite. The low values for SMC-R25 may be because of the presence of calcium carbonate in these composites. The best agreement between theory and data is observed for SMC-R65. For comparison purposes, Fig. 43 also includes the predictions for α_L and α_T.

In SMC composites fiber arrangement is not perfectly planar, and therefore, some effective stiffening in thickness direction is expected. Such stiffening will lead to a lower coefficient of thermal expansion. The stiffening effect is likely to be more severe in the case of low fiber volume content. This may be the reason why α_o remains almost the same for both R40 and R65.

4.4 Conclusions

The environmental effects studied in SMC composites and bulk polyester included moisture diffusion, swelling, thermal expansion, and damage growth. The fiber contents in the composites were 25, 40, and 65% by weight. Seven different environments were chosen for study: RT/65% RH, RT/98% RH, RT/water, 75°C/65% RH, 75°C/98% RH, 75°C/water, and 100°C/steam.

Moisture diffusion behavior of SMC composites and bulk polyesters depends very much on temperature and relative humidity. The maximum weight gain, which is usually taken as the equilibrium moisture content, was much higher at 75°C except under 65% RH. The diffusivity depended on relative humidity in an inconsistent manner perhaps because of the

material degradation observed under severe environments. Desorption took place at a slightly faster rate than absorption, and resulted in a permanent loss of material.

Swelling behavior was very erratic; no consistent relationship between weight gain and swelling strain could be established. Both in-plane and thickness strains could fluctuate between positive and negative values. Bulk polyester showed almost no dimensional changes until blistering became obvious. One exception was SMC-R25 composites; they showed swelling in the thickness direction as well as in the plane.

At 75°C both SMC composites and bulk polyester changed color. Furthermore, the composites showed blistering. There were two types of blisters: small and large. The small blisters were very thin and limited to the thin surface layer. They were also very small in diameter. These small blisters resulted in loss of glossy appearance on specimen surface when they burst open.

The large blisters were clearly visible to the naked eye, and were much thicker. The environments contributing to the development of large blisters were 75°C/98% RH, 75°C/water and 100°C/steam for the composites whereas only 75°C/water resulted in blistering for the bulk polyester. The blisters in the polyester were the result of large cracks inside. At 100°C/steam the polyester showed many cracks both inside and outside.

Some of these cracks are the result of blisters bursting open.

The fiber aspect ratio in the composites has been found to be so large that the theory for continuous fiber composites can be used to predict the coefficients of thermal expansion. The coefficients of thermal expansion of SMC-R25 were lower than predicted because of the presence of calcium carbonate.

5.0 SUMMARY AND RECOMMENDATIONS

A review has been made of various methods of predicting the expansion and diffusion properties of composite laminates. The analytical complexity and the lack of experimental data for short-fiber composites have been pointed out. However, it is concluded that the prediction equations for continuous-fiber composites can be applied to SMC composites as the effective fiber aspect ratio in the latter is large enough.

The effect of hygrothermal expansion on the dimensional stability of composite laminates has been demonstrated through the warping of unsymmetric graphite/epoxy laminates. The warping is very sensitive to the size of the panel, and to the moisture content which is in turn sensitive to the relative humidity in the environment. Thus, any long-term creep test must be carried out in a humidity-controlled environment.

Environmental effects in SMC composites and bulk polyester have been studied under seven different environments: RT/65% RH RT/98% RH, RT/water, 75°C/65% RH, 75°C/98% RH, 75°C/water, and 100°C/steam. The SMC composites chosen are SMC-R25, SMC-R40 and SMC-R65. The maximum weight gain depends on temperature under high humidity environments while the diffusivity depends on relative humidity. In many environments moisture diffusion is not Fickian probably because of the material damage. The most frequent damage at 75°C is blistering while no visible

damage occurs at room temperature. Small blisters are very thin and limited to the surface. When they burst open, the composite loses a glossy appearance on the surface. These small blisters develop under all environments at 75°C in SMC composites, but they do not form in bulk polyester. Large blisters are much thicker and clearly visible to the naked eye. They develop most frequently at 75°C/water and 100°C/steam. The cracking at 100°C/steam in bulk polyester is much more severe than in the composites perhaps because of the reinforcing effect of fibers.

Because of the limited scope of the present work some of the questions raised during the course of this study remain to be answered. The issues recommended for further investigation are listed below.

1. The water used for diffusion tests should be analyzed chemically to identify the mechanisms of material loss. The chemical species found in the water can then be compared with those in the specimens.

2. Mechanisms for blistering should be elucidated. Why are small blisters found only in SMC composites but not in bulk polyester?

3. Room-temperature environments seem fairly safe for SMC composites. However, the elevated temperature of 75°C is precarious especially under highly humid environments. The limiting environments should be identified for these composites.

4. Mechanisms for environmental degradation evidenced by color change should be identified.

5. Stability under environmental cycling should be investigated.

6.0 ACKNOWLEDGMENTS

The data on T300/5208 panels were obtained while the author (H. Thomas Hahn) was with the Materials Laboratory, Air Force Wright Aeronautical Laboratories. The T300/C69 panels were fabricated at the Institüt für Bauweisen-und Konstruktionsforschung, Deutsche Forschungs-und Versuchsanstalt für Luft-und Raumfart in West Germany while the author (HTH) was there as a visiting scientist. The help of D. G. Hwang in the preparation of Chapter 3 is gratefully acknowledged.

7.0 REFERENCES

1. Rosen, B. W. and Hashin, Z., "Effective Thermal Expansion Coefficients and Specific Heats of Composite Materials," Int. J. Eng. Sci., Vol. 8 (1970), p. 157.

2. Hashin, Z., Theory of Fiber Reinforced Materials, NASA CR-1944, 1972.

3. Christensen, R. M., Mechanics of Composite Materials, Wiley Interscience, 1979.

4. Eshelby, J. D., "The Determination of the Elastic Field on an Ellipsoidal Inclusion, and Related Problems," Proc. Roy. Soc. Lond., Vol. A241 (1957), p. 376.

5. Hill, R., "Theory of Mechanical Properties of Fibre-Strengthened Materials--III. Self-Consistent Model," M. Mech. Phys. Solids, Vol. 13 (1965), p. 189.

6. Hill, R., "A Self-Consistent Mechanics of Composite Materials," J. Mech. Phys. Solids, Vol. 13 (1965), p. 213.

7. Russel, W. B., "On the Effective Moduli of Composite Materials: Effect of Fiber Length and Geometry at Dilute Concentrations," Z. Angew. Math. Phys., Vol. 24 (1973), p. 581.

8. Wakashima, K., Otsuka, M. and Umekawa, S., "Thermal Expansion of Heterogeneous Solids Containing Aligned Ellipsoidal Inclusions," J. Composite Materials, Vol. 8 (1974), p. 391.

9. Laws, N. and McLaughlin, R., "The Effect of Fibre Length on the Overall Moduli of Composite Materials," J. Mech. Phys. Solids, Vol. 27 (1979), p. 1.

10. Takahashi, K., Harakawa, K., and Sakai, T., "Analysis of the Thermal Expansion Coefficients of Particle-Filled Polymers," J. Composite Materials, Vol. 14 (1980), p. 144.

11. Chou, T. W. and Nomura, S., "On the Thermomechanical Behavior of Short Fiber and Hybrid Composites," in Advances in Composite Materials, Vol. 1, R. Bunsell et al., Eds., Pergamon Press, 1980.

12. Ashton, J. E., Halpin, J. C., and Petit, P. H., Primer on Composite Analysis, Technomic Pub. Co., Westport, CT, 1969, Chapter 5.

13. Levin, V. M., "On the Coefficients of Thermal Expansion of Heterogeneous Materials," Mekh. Tverd. Tela (in Russian) (1967), p. 88.

14. Herman, J. J., "The Elastic Properties of Fibre Reinforced Materials When the Fibers are Aligned," Proc. Koninkl. Nederl. Akad. Wetenschappen, B70 (1967), p. 1.

15. Hahn, H. T., "Simplified Formulas for Elastic Moduli of Unidirectional Continuous Fiber Composites," Composites Technology Review, Vol. 2, No. 3 (1980), p. 5.

16. Schapery, R. A., "Thermal Expansion Coefficients of Composite Materials Based on Energy Principles," J. Composite Materials, Vol. 2 (1968), p. 380.

17. Tsai, S. W. and Hahn, H. T., "Introduction to Composite Materials, Technomic Pub. Co., Westport, CT, 1980.

18. Halpin, J. C. and Pagano, N. J., "The Laminate Approximation for Randomly Oriented Fibrous Composites," J. Composite Materials, Vol. 3 (1969), p. 720.

19. Craft, W. J. and Christensen, R. M., "Coefficient of Thermal Expansion for Composites with Randomly Oriented Fibers," J. Composite Materials, Vol. 15 (1981), p. 2.

20. Pagano, N. J., "Thickness Expansion Coefficients of Composite Laminates," J. Composite Materials, Vol. 8 (1974), p. 310.

21. Hahn, H. T. and Kim, R. Y., "Swelling of Composite Laminates," Advanced Composite Materials--Environmental Effects, ASTM STP 658, J. R. Vinson, Ed., ASTM, 1978, p. 98.

22. DeIasi, R. and Whiteside, J. B., "Effect of Moisture on Epoxy Resins and Composites," Advanced Composite Materials--Environmental Effects, ASTM STP 658, J. R. Vinson, Ed., ASTM, 1978, p. 2.

23. Crossman, F. W., Mauri, R. E., and Warren, W. J., "Moisture-Altered Viscoelastic Response of Graphite/Epoxy Composites," Advanced Composites--Environmental Effects, ASTM STP 658, J. R. Vinson, Ed., ASTM, 1978, p. 205.

24. Adamson, M. J., "Thermal Expansion and Swelling of Cured Epoxy Resin Used in Graphite/Epoxy Composite Materials," J. Mat. Sci., Vol. 15 (1980), p. 1736.

25. Springer, G. S. and Tsai, S. W., "Thermal Conductivities of Unidirectional Materials," J. Composite Materials, Vol. 1 (1967), p. 166.

26. Nomura, S. and Chou, T. W., "Bounds of Effective Thermal Conductivity of Short-Fiber Composites," J. Composite Materials, Vol. 14 (1980), p. 120.

27. Springer, G. S., Ed., Environmental Effects on Composite Materials, Technomic Pub. Co., Westport, CT, 1981.

28. Crank, J., The Mathematics of Diffusion, Oxford Univ. Press, 1956.

29. Crank, J. and Park, G. S., Diffusion in Polymers, Academic Press, 1968.

30. Shirrell, C. D., "Diffusion of Water Vapor in Graphite/Epoxy Composites," Advanced Composite Materials--Environmental Effects, ASTM STP 658, J. R. Vinson, Ed., ASTM, 1978, p. 21.

31. Augl, J. M. and Trabocco, R., "Environmental Studies on Carbon Fiber Reinforced Epoxies," Proc. AFOSR Workshop on Durability Characteristics of Resin Matrix Composites, Battelle Memorial Inst., 1975.

32. Whitney, J. M. and Browning, C. E., "Some Anomalies Associated with Moisture Diffusion in Epoxy Matrix Composite Materials," Advanced Composites--Environmental Effects, J. R. Vinson, Ed., ASTM, 1978, p. 43.

33. Ashbee, K. H. G. and Farrar, N., "Detection and Identification of Changes in the Physical Properties of Fibre/Matrix Interfaces," Proc. 1975 Int. Conf. on Composite Materials, E. Scala et al, Eds., AIME, 1975, p. 771.

34. Marom, G. S. and Broutman, L. J., "Moisture Penetration into Composites under External Stress," Polymer Composites, Vol. 2 (1981), p. 132.

35. McKague, E. L., Jr., Halkias, J. E., and Reynolds, J. D., "Moisture in Composites: The Effect of Supersonic Service on Diffusion," J. Composite Materials, Vol. 9 (1975), p. 2.

36. Browning, C. E., Husman, G. E., and Whitney, J. M., "Moisture Effects in Epoxy Matrix Composites," Composite Materials: Testing and Design (Fourth Conf.), ASTM STP 617, ASTM, 1977, p. 481.

37. Tsai, S. W., "Strength Characteristics of Composite Materials," NASA CR-224, April 1965.

38. Pagano, N. J. and Hahn, H. T., "Evaluation of Composite Curing Stresses," Composite Materials: Testing and Design (Fourth Conf.), ASTM STP 617, ASTM, p. 317.

39. Crossman, F. W., Mauri, R. E., and Warren, W. J., "Hygrothermal Damage Mechanisms in Graphite-Epoxy Composites," NASA CR-3189, Dec. 1979.

40. Lee, B. L., Lewis, R. W., and Sacher, R. E., "Environmental Effects on the Mechanical Properties of Glass Fiber/Epoxy Resin Composites. Part I. Effect of Static Immersion in Water on the Tensile Strength of Cross-Ply Laminates," AMMRC TR-78-18, Army Materials and Mechanics Research Center, Apr. 1978.

41. Hyer, M. W., "Calculations of the Room-Temperature Shapes of Unsymmetric Laminates," J. Composite Materials, Vol. 15 (1981), p. 296.

42. Kim, R. Y. and Hahn, H. T., "Effect of Curing Stresses on the First Ply-Failure in Composite Laminates," J. Composite Materials, Vol. 13 (1979), p. 2.

43. Hahn, H. T., "Residual Stresses in Polymer Matrix Composite Laminates," J. Composite Materials, Vol. 10 (1976), p. 266.

44. Wang, A. S. D. and Crossman, F. W., "Edge Effects on Thermally Induced Stresses in Composite Laminates," J. Composite Materials, Vol. 11 (1977), p. 300.

45. Carpenter, J. F., "Instrumental Techniques for Developing Epoxy Cure Cycles," presented at the 21st National SAMPE Symposium and Exhibition at Los Angeles, Apr. 1976.

46. Hahn, H. T. and Chin, W. K., "The Effect of Vacuum and Temperature on the Mechanical Properties of an Aramid/Epoxy Composite," Composites Technology Review, Vol. 3 (1981), p. 27.

47. Norwood, L. S., Edgell, D. W., and Hankin, A. B., "Blister Performance of GRP Systems in Aqueous Environments," Proc. 36th Ann. Conf., RP/C Inst., SPI, 1981, 23-F.

48. Edwards, D. B. and Sridharan, N. S., "Environmental Testing of High Strength Molding Compounds," presented at Press Molders Committee, SPI.

49. Adams, R. C., "Variables Influencing the Blister Resistance of Marine Laminates," Proc. 37th Ann. Conf., RP/C Inst., SPI, 1982, 21-B.

50. Brueggemann, W. H., "Blistering of Gel Coat Laminates," Proc. 34th Ann. Conf., PR/C Inst., SPI, 1979, 4-E.